FLIGHT CONTROL OF A TILT DUCT UAV WITH EMPHASIS ON THE OVER ACTUATED TRANSITION FLIGHT PHASE

A THESIS SUBMITTED TO
THE GRADUATE SCHOOL OF NATURAL AND APPLIED SCIENCES
OF
MIDDLE EAST TECHNICAL UNIVERSITY

BY

TUĞBA ÜNLÜ

IN PARTIAL FULFILLMENT OF THE REQUIREMENTS
FOR
THE DEGREE OF MASTER OF SCIENCE
IN
AEROSPACE ENGINEERING

SEPTEMBER 2009

Approval of the thesis:

FLIGHT CONTROL OF A TILT DUCT UAV WITH EMPHASIS ON THE OVER ACTUATED TRANSITION FLIGHT PHASE

submitted by **TUĞBA ÜNLÜ** in partial fulfillment of the requirements for the degree of **Master of Science in Aerospace Engineering Department, Middle East Technical University** by,

Prof. Dr. Canan Özgen _____
Dean, Graduate School of **Natural and Applied Sciences**

Prof. Dr. İsmail H. Tuncer _____
Head of Department, **Aerospace Engineering**

Prof. Dr. Ozan Tekinalp _____
Supervisor, **Aerospace Engineering Department, METU**

Dr. Ilkay Yavrucuk _____
Co-supervisor, **Aerospace Engineering Department, METU**

Examining Committee Members:

Prof. Dr. Cahit Çıray
Aerospace Engineering Dept., METU _____

Prof. Dr. Ozan Tekinalp
Aerospace Engineering Dept., METU _____

Dr. Ilkay Yavrucuk
Aerospace Engineering Dept., METU _____

Dr. Ali Türker Kutay
Aerospace Engineering Dept., METU _____

Dr. Tayfun Çimen
Roketsan A.Ş. _____

Date: _____

I hereby declare that all information in this document has been obtained and presented in accordance with academic rules and ethical conduct. I also declare that, as required by these rules and conduct, I have fully cited and referenced all material and results that are not original to this work.

Name, Last Name: TUĞBA ÜNLÜ

Signature :

ABSTRACT

FLIGHT CONTROL OF A TILT DUCT UAV WITH EMPHASIS ON THE OVER ACTUATED TRANSITION FLIGHT PHASE

Ünlü, Tuğba
M.S., Department of Aerospace Engineering
Supervisor : Prof. Dr. Ozan Tekinalp
Co-Supervisor : Dr. Ilkay Yavrucuk

September 2009, 143 pages

In the thesis, automatic flight control system is designed for Tilt Duct Unmanned Aerial Vehicle (UAV). The vehicle is a Vertical Take-Off Landing (VTOL) type with two symmetric rotors on the wings, one aft rotor on the aft body. It behaves like a helicopter but with higher speeds in forward flight. Transition flight of the aircraft from hover to cruise or take-off to forward flight is the primary concern of the thesis study with the nonlinearities and instabilities encountered, together with the over-actuated controls in this mode. A nonlinear simulation code is developed including nonlinear equations of motion together with the nonlinear aerodynamics, environmental effects, and rotor dynamics. Trim and linearization codes are also developed. Trim conditions for the transition flight phase are calculated for two different transition scenarios. Linear controllers are developed and nonlinear controller is designed for the transition mode. Nonlinear controller uses the state dependent Ricatti equation SDRE approach by using extended linearization. Two loop approach is used in order to increase controllability. In the inner loop, attitude rates are fed back and SDRE approach is used to calculate the feedback gain matrix online. In the outer loop, vehicle attitude is controlled using the eigenvalue assignment. Blended inverse algorithm based control allocation method

is used in control of the over-actuated transition phase. This algorithm is shown to be quite effective among different methods in not only generating necessary forces needed for the control, but also allocating with more control authority on the desired actuator.

Keywords: Tilt Rotor UAV, Modeling, Controller, Control Allocation, SDRE

ÖZ

YATAR ROTORLU İNSANSİZ HAVA ARACİNİN ARTİK EYLEYICILI GEÇIŞ FAZİNDA UÇUŞ KONTROLÜ

Ünlü, Tuğba
Yüksek Lisans, Havacılık ve Uzay Mühendisliği Bölümü
Tez Yöneticisi : Prof. Dr. Ozan Tekinalp
Ortak Tez Yöneticisi : Dr. İlkay Yavrucuk

Eylül 2009, 143 sayfa

Bu tezde Yatar Rotorlu Insansız Hava Aracı (IHA) için otomatik kontrolcü tasarımı yapılmıştır. IHA, kanatlardaki iki ve arka gövdedeki tek rotoruyla dikey iniş ve kalkış yapabilen, helikoptere benzeyen fakat ileri uçuşlarda yüksek hızlara ulaşabilen bir tasarımdır. Askı modundan seyir moduna veya kalkıştan ileri uçuşa geçişte doğrusal olmayan, kararsız davranışlar ve yedekli kontrol sistemleri, bu tez için öncelikli çalışma konusudur. Aerodinamik etkiler, çevresel etkiler, rotor modellemesi, ve doğrusal olmayan hareket denklemlerini içeren benzetim kodu geliştirilmiştir. Trim ve doğrusallaştırma kodları yaratılmıştır. Geçiş modundaki trim noktaları iki farklı seneryoda bulunmuştur. Doğrusal kontrol sistemleri ve özellikle geçiş modu için doğrusal olmayan kontrol sistemi tasarlanmıştır. Doğrusal olmayan kontrolcü, durumlara bağlı Ricatti denklemini içeren SDRE yaklaşımını kullanmaktadır. Kontrol edilebilirliği arttırabilmek için iki döngü kullanılmıştır. İç döngüde döngüsel türevlerin geri beslemesi yapılmıştır, SDRE metodu kullanılarak geri döngü matrisleri her zaman aralığında hesaplanmıştır. Dış döngüde eigenvalue atamasıyla aracın açısal durum kontrolü yapılmıştır. Artık eyleyicili geçiş modunda blended inverse algoritması tabanlı kontrol dağıtımı yapılmıtır. Bu metod diğer dağıtım metodları içinde gerekli kuvvetleri sağlamada ve istenilen kontroller

üzerinde otorite yaratmada oldukça etkili olmuştur.

Anahtar Kelimeler: Yatar Rotorlu IHA, Modelleme, Kontrolcü, Kontrol Dağıtımı, SDRE

To my mother

ACKNOWLEDGMENTS

I would like to express my sincere gratitude to my thesis supervisor Prof Dr. Ozan Tekinalp and co-supervisor Dr. İlkay Yavrucuk for their guidance, aid and support.

I would like to thank to my family for their endless trust and encouragements, especially to my mother for being always beside me.

I appreciate the very precious help and advices of Barış Timurkaynak, Hilal Ercin, Onur Tarımcı, Volkan Kargın, Deniz Karakaş, Umut Susuz and also support of all my other colleagues.

Finally special thanks to my dear friends in the Control Laboratory of the METU Aerospace Department, Sinem Isık, Zeynep Çakır, Batu Demir, Tugba Elmas, Mehmet Kılıç and also Miray Demir, Gönenç Gürsoy, Ece Sağol, Öznur Yemenici for their precious moral aid.

TABLE OF CONTENTS

LIST OF TABLES

TABLES

LIST OF FIGURES

FIGURES

LIST OF ABBREVIATIONS

A, B, C, D	Linearized system matrices
a_0	Rotor blade lift curve slope
b	Wing reference span
b	Number of rotor blades
c	Wing reference chord
C_{oeff}	Coefficient
F, M	Forces, Moments
g	Gravity
$h_d MSL$	Altitude with respect to MSL
I_{XX}	Inertia in body x-axis
I_{YY}	Inertia in body y-axis
I_{ZZ}	Inertia in body z-axis
I_{XZ}	Inertia on body x-z plane
I_{XY}	Inertia on body x-y plane
I_n	n-dimensional unit matrix
$\overline{J}$	Performance index
J	System jacobian matrix
K_{LQR}	LQR gain
K_P	Proportional gain
K_I	Integral gain
K_D	Derivative gain
K_{twist}	Rotor blade twist
L	Left
$L_{xcg_{Thm}}$	Longitudinal distance from CG to main rotor
$L_{ycg_{Thm}}$	Lateral distance from CG to main rotor
$L_{xcg_{Tha}}$	Longitudinal distance from CG to aft rotor
m	Mass
N_x, N_y, N_z	Normal accelerations in 3 axes
p, q, r	Body angular velocities
P	Ricatti solution matrix
Q, R	Weightings in performance index for state-error and controls
R	Right
R, M, N	Body-fixed roll, pitch, yaw moments
u_i	Vector of rates in steering law
ut, xt, xdt, yt	System trim inputs, states, state derivatives and outputs
u, v, w	Translational velocities in the body fixed frame
u, x, xd, y	System inputs, states, state derivatives and outputs
V	Velocity
v^i	Farfield velocity
v_b	Flow velocity past rotor
v_i	Flow velocity induced through rotor
X, Y, Z	Body-fixed drag, sideforce, lift forces

Greek

α	Angle of attack
$\dot{\alpha}$	Rate of angle of attack
β	Sideslip angle
$\dot{\beta}$	Rate of sideslip angle
δ_{ail}	Aileron input
δ_i	Vector of gimbal angles in steering law
δ_{elev}	Elevator input
δ_{rud}	Rudder input
δ_{ThML}	Main left throttle input
δ_{ThMR}	Main right throttle Input
$\delta_{ThMLlon}$	Main left throttle input longitudinal component
$\delta_{ThMLlat}$	Main left throttle input lateral component

$\delta_{ThMRlon}$	Main right throttle input longitudinal component
$\delta_{ThMRlat}$	Main right throttle input lateral component
δ_{ThAlon}	Aft throttle input longitudinal component
δ_{ThAlat}	Aft throttle input lateral component
η	Exit guide vane angle of the aft propeller
γ	Adiabatic index or flight path angle (FPA)
μ	Main engine tilt angle
ω	Body-fixed total angular rate
ω_r	Rotor angular speed
ω_n	Natural Frequency, Damping ratio
ϕ,θ, ψ	Bank - Heading - Pitch angle
ρ, ρ_0	Air density, in mean sea level
τ	Rotor thrust
θ_{coll}	Collective input
ζ	

Subscripts

$_A$	Denotes aerodynamics
$_{aero}$	Denotes aerodynamic coefficients
$_{body}$	Denotes in body-fixed axis
$_c$	Denotes commanded
$_C$	Denotes control
$_{cg}$	Denotes due to CG
$_{ref}$	Denotes reference input
$_{dyn}$	Denotes dynamic coefficients
$_{dr}$	Denotes Dutch roll mode
$_e$	Denotes error
$_{hor}$	Denotes horizontal
$_{lat}$	Denotes lateral-directional axis
$_{lon}$	Denotes longitudinal axis
$_{ph}$	Denotes phugoid mode
$_{req}$	Denotes required
$_{ref}$	Denotes referenced or used
$_{sp}$	Denotes short period mode
$_G$	Denotes gravity
$_r$	Denotes roll mode
$_s$	Denotes spiral mode
$_{static}$	Denotes static coefficients
$_T$	Denotes thrust
$_{un}$	Denotes unwanted
$_{ver}$	Denotes vertical
$_{WBT}$	Denotes wing-body-tail configuration

Abbreviations

AFCS	Automatic flight control system
BI	Blended inverse method
CG	Center of gravity
DATCOM	Data Compendium
DCM	Direction Cosine Matrix
DES	Desired
DOF	Degree of Freedom
EAS	Equivalent Airspeed
ISA	International Standard Atmosphere
LQ	Linear Quadratic
LQG	Linear Quadratic Gaussian
LQR	Linear Quadratic Regulator
MIMO	Multi Input-Multi Output
MP	Moore-pseudo
MSL	Mean sea level
NED	North-East-Down
PID	Proportional-Integral-Derivative
RPM	Revolution per Minute
SAS	Stability augmentation system
SISO	Single Input-Single Output
UAV	Unmanned Aerial Vehicle
USAF	United States Air Force
WGS	World Geodetic System
6-DOF	Six degrees of freedom

CHAPTER 1

INTRODUCTION

1.1 The Aim of the Thesis

The aim of the thesis is to work on a detailed analysis of dynamic modeling, trim, linearization, flight controller design, transition control and allocation of redundant controls for the design of tilt-duct vertical takeoff and landing (VTOL) unmanned aerial vehicle (UAV) concept. This design is part of a former research activity carried out in the research group, with members from the Department of Aerospace Engineering and the Department of Electrical and Electronics Engineering, Middle East Technical University. The main purpose of the design is to develop an autonomously controlled VTOL UAV, which can takeoff and land vertically similar to a helicopter, and convert to a propeller driven airplane in forward flight mode by tilting its ducted propellers forward. [30] During the control of the autonomous aircraft, the highly nonlinear dynamics during transition from hover to forward flight requires more complex algorithms such as gain scheduled-linear, or nonlinear controller systems. Therefore, besides the designed control systems for cruise or hover, a detailed controller design study is needed for transition mode. The thesis addresses the design of controllers for the transition mode of the aircraft and allocation of redundant controls with considerations on flight phase.

1.2 Literature Survey

1.2.1 Overview of Tilt-Rotor Concept and UAV Designs

In recent years, there has been an increased emphasis on the use of unmanned aerial vehicles for performing missions including surveillance, reconnaissance, target acquisition and/or des-

ignation, data acquisition, communications relay, or supply flights, where the use of manned flight vehicles is not appropriate or feasible. Under the current developments, there are generally three types of UAV configurations; a fixed-wing type configuration (a fuselage with wings and horizontally mounted engines for translational flight), helicopter type configuration (a fuselage with a rotor mounted above which provides lift and thrust) and hovering fixed-wing type configuration (a fuselage with a rotor system which provides hovering and level flight, as well as vertical take-off and landing) that may have a tilt rotor mechanism. Winged UAVs are widely used since they have considerably greater speeds and endurance and they can carry a larger mission payload and/or fuel supply. However, they require forward motion to maintain lift and therefore are not capable of hovering over a fixed spatial point. They are also incapable of delivering ordinance, laser designating targets and need a runway to take-off or land.

Due to the need for VTOL capability and hovering, the first type developed was the helicopter. Although, it proved to be quite useful in rescue operations and short range point-to-point transportation, it carries the disadvantages of limitations when operating in confined areas due to the exposed rotors rotating above the fuselage and having low speed and range. Also, helicopter UAVs tend to have a high center-of-gravity (CG) and therefore have limited ability when landing on sloped surfaces or pitching ship decks. At this point, non-rotary wing concept comes into view offering a compromise between helicopter-like vertical flight and efficient wing-borne cruise. [35]

The ability of tilt rotor-type UAVs to take-off and land vertically, combined with their ability to hover for extended periods of time over a point and operate in confined areas off steep slopes, make them ideally suited for real time tactical reconnaissance, target acquisition, surveillance, and ordnance delivery missions.

The history of non-rotary wing VTOL aircraft development has generally proceeded along separate paths with tail-sitter, tilt rotor or ducted rotor UAVs etc. Tilt Rotor (Prop-rotor) aircraft provide two or more very large propellers mounted on wingtips or wing pylons. The propellers rotate through 90 degrees of angle, from a horizontal axis for forward flight, through to a vertical axis for vertical lift thrust. Tilt-duct concept has some basic differences than the tilt-rotor concept. The propellers are located in the ducts attached to the tip of the wings. This brings an advantage due to `end-plate´effect and cause simplicity to obtain the thrust value di-

rectly. ``Ducted rotors, or ducted fans, are more efficient and quieter than exposed propellers of the same diameters´´[54]. They are also safer than exposed propellers on the ground. While the ducted fan provides greater lift than a simple unducted propeller, the same thing cannot be said for the drag, the drag produced by the duct shroud in forward flight limit the fidelity of the aircraft. Another difference is that, the propellers require no hinge or swash-plate design and manufacturing. Such details also lead to the main objective of this design, `cheap and easy manufacturing´. This design has also the purpose to combine the advantages of VTOL capability with a UAV.

As an overview on the tilt-rotor manned aircrafts in history, firstly in the 1940s The Transcendental Aircraft Co. designed and built the Transcendental Model 1-G which is the first tilt-rotor VTOL aircraft. It was a single place, research aircraft with a gross weight of 794 kg and two 5.2 m diameter, tilting rotors. In the 1970's, Bell's tiltrotor design, XV-3 and XV-15 was also built, and success on the design and analysis on these aircrafts leaded the V-22 Osprey world's first production tiltrotor supported by the United States government. This aircraft in figure 1.1 uses two widely spaced proprotors, similar to large propellers, but without ducts. The HV-609 / BA609 Civil Tiltrotor is then manufactured by using the technology gained from the V-22 project. Then the following designs like QTR - Quad Tilt Rotor, OSTR Optimum Speed Tilt Rotor, AMT - Air Maneuver Transport, ATT - Advanced Theater Transport can be given as other examples.[56] [30]

Figure 1.1: Bell-Boeing Tilt-Rotor design V-22 Osprey

As an autonomous aircraft, the Eagle Eye, shown in Figure 1.2 can be given as an example of a researched and manufactured tiltrotor UAV by Bell Helicopter. It has a maximum speed

of 200 kts (370 km/h) and an endurance of 5.5 hours, 200 Ib (90 kg) payload. Recently the American Dynamics Flight Systems is also researching on an aircraft named `AD-150´that has two ducted fan rotors on the wings with about 1020 kg maximum weight and 154 m/s (300 knots) maximum speed.

Figure 1.2: Bell Tilt-Rotor UAV design Eagle Eye

1.2.2 Recent Work on Hovering Fixed-Wing Aircraft Control

Hovering fixed-wing autonomous aircraft control is being researched by several research groups. For this aim, flight test studies are being developed for especially hovering and transition modes of the aircraft. The use of dynamic inversion with adaptation and hover-transition flight test results were performed by the research group of Gatech [65] for hovering and transition characteristics. Research at Aerovironment's SkyTote were carried out and flight tests also done for this UAV [61]. The autonomous flight tests are conducted by a group at the Drexel University [55] mainly concerning a linear controller for hovering. In addition, Aurora Flight Golden Eye design [63], Caltech Ducted Fan [37] and T-Wing design [33] of the University of Sydney can be given as the research subjects on controller designs including the works on different flight modes. Further studies were done on control or transition simulations as in [69] [60] [57]. A design of trajectory tracking controller for a similar tiltrotor unmanned aerial vehicle with a design objective of one fixed controller architecture for all flight modes using `Neural Network´was presented by Gyeongnam University, Korea in 2007 [59]. There are very few studies in the literature including especially nonlinear modeling and transition control of a similar tilt-duct UAV design.

1.2.3 Recent Work on Control Allocation

Redundant actuator system means a system with several combinations of actuator positions which give the same effects on the system behavior. The over-actuated control mechanism like the one of Tilt-Duct UAV has redundancies for different channels (in longitudinal or lateral sense like throttle - elevator effect in pitching or rudder- aft fan effect in yawing) and require a system distributing the given control command to available or demanded actuators. In recent years, the allocation problem has gained high importance since nonlinear controller systems which are based on the required control moments and forces also began to be preferred. To allocate the needed torques, forces or moments, two different approaches are generally used: dynamic and static approaches. The static approach is used as a separate allocator outside of the controller and dynamic one can be considered as an optimization of the decision on distribution inside the controller as in the linear quadratic optimal control problem [71].

The dynamic allocation is studied by many researchers in the literature. One of them is [42], which compares a direct allocation method ”preserves the directionality of the moment” and a mixed optimization method ”minimizes the error between the desired and the achieved moments as well as the control effort” and compares their computational accuracy. The work of the Harkegard [49] is also an important example for these studies in which ”the control allocation problem is posed as a constrained quadratic problem which provides automatic redistribution of the control effort when one actuator saturates in position or rate”. The static allocation of redundant mechanisms was originally addressed in the contest outside the control mechanism of robotic manipulators in order to avoid singularities. Two different allocation approaches are also compared in [50] in which ”two tools for distributing the control effort among a redundant set of actuators are optimal control design and control allocation are used”. For this comparison it is concluded that ”a benefit of using a separate control allocator is that actuator constraints can be considered”. Since the thesis works are mainly on the static type of allocation technique many literature researches and thesis will be addressed.

The control allocation methods are developed in different senses. One contribution is done by [41] which focuses on algorithms for solving redundant control allocation problems with their computational efficiency to meet four or more objectives with control effectors constrained by upper and lower limits. Another contribution is in [46] in which 2 algorithms are proposed based on classical active set methods as `active set algorithm´and `sequential-weighted least

squares´. The approaches and application of these methods are explained in [48].

Further contributions are done and used in the allocation of the redundant set of control moment gyroscope in the sense of using allocation statically [52]. The same works are done for dissimilar redundant actuators [70] and robotic manipulators [53]. In all these static allocation methods the general classifications that are shown schematically in figure 1.3 are referenced in the thesis, studied and compared. Then an improved allocation method called `Blended-Inverse´is used for satellite attitude control is mentioned as the most efficient way.

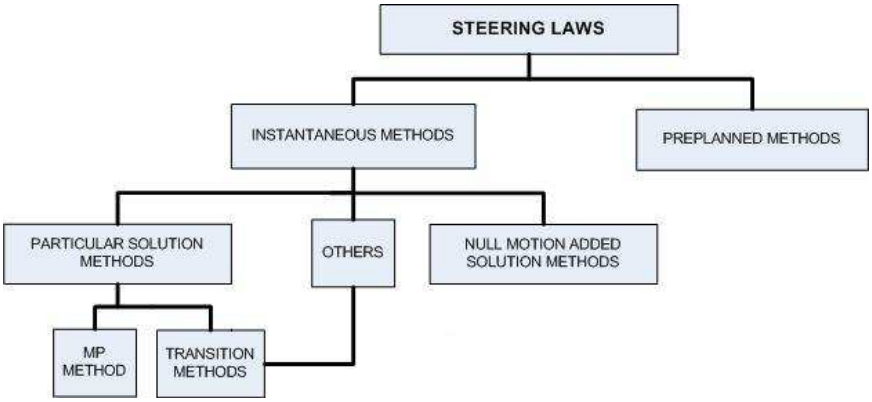

Figure 1.3: Classification and Branches of the Steering Law

In the thesis, the `Blended-Inverse´control allocation method is adapted to the UAV control mechanism as explained in Chapter 5.

1.2.4 Recent Work on Nonlinear SDRE Approach

Since early 1960's, the State-Dependent Ricatti Equation (SDRE) technique as the extension of linear quadratic regulator has attracted considerable attention with its effective control mechanism of nonlinear systems and its great design flexibility by the state-dependent coefficient (SDC) matrices. The earliest known proposal of using state feedback Ricatti based linear control methods on nonlinear systems appears in [3]. The solution to low-order systems is proposed with `arbitrary time-varying matrices´, `global asymptotic stability´is proven and `suboptimal controller performance´is shown to be more favorable than the corresponding optimal controllers. Various approaches are proposed in [5] and [8] which introduces SDRE solution for any location `traversed in the state-space´. In [12] conditions relating the suboptimal solution to the optimal solution are derived. State and control penalty matrices are

assumed to be variable in [3] and [5]. In [19] both SDRE matrices and nonlinear H_∞ control problems are proposed ,where weighting matrices are not restricted to be constant or functions of time but may be functions of states. Local asymptotic stability is proven for suboptimal state feedback. An additional also necessary condition that must be satisfied for optimality of the state feedback regulator is given. [18] proposes a Lyapunov function with limited class of weighting matrix definitin in order to establish global stability for suboptimal SDRE state feedback regulator. Lastly, [24] introduces the justification of controllability methods on nonlinear methods and gives examples to successful application of SDRE approach for each type of controllability. The iterative solution techniques are also used in the algebraic Ricatti equation (ARE) solutions [51] [68] and different approaches are defined for State Dependent Coefficient (SDC) matrices [44] [36]. A detailed survey on SDRE may be found in [67] and [24].

1.3 Contents of the Thesis

In the thesis, the analyses carried out for obtaining the properties and the geometry of the design are given in Chapter 2. The modeling of flight mechanics of the Tilt-Duct UAV with 6-DOF dynamic equations and nonlinear aerodynamic data is explained in Chapter 3. In Chapter 4, the trim and linearization analyses are presented. These works are all done in Matlab® and Simulink® environment. The stability characteristics are also analyzed and the linear model is validated with the nonlinear model by their dynamic responses to step input disturbance. The methods for the allocation of redundant control system are summarized in Chapter 5. The given methods are referenced in the controller analysis and the results are given in the results part of the corresponding studies. The linear controller analysis is given in Chapter 6 which includes the methodologies, the structure of the controller, results for different flight modes including control allocation in transition. Lastly in Chapter 7, the nonlinear SDRE method for the control of transition flight mode of the aircraft, the controller structure and the results are given.

1.4 Original Contributions of the Thesis

The thesis introduces new concepts to the area of automatic flight control analyses on the air vehicles of the same class. The related original contributions can be stated as follows:

- Development of the nonlinear dynamic model and simulation code for the Tilt-Duct VTOL UAV.
- Dynamic Model of the rotary motion for propellers.
- Application of control allocation algorithm `Blended Inverse´to the transition flight phase of the UAV.
- Development of a two loop nonlinear control method that is based on State-Dependent Ricatti equation approach in the inner loop and eigenvalue assignment to the nonlinear attitude equations in the outer loop for the Tilt-Duct UAV during its transition flight phase.

CHAPTER 2

SPECIFICATIONS OF THE TILT DUCT UAV

2.1 Introduction

In this chapter, the design and analyses carried out by Armuçuoğlu and Okan [30] [31] are summarized, further inspections and additional analyses on the characteristics of the aircraft are explained. Main design and performance characteristics which are critical for the simulation and control studies are given in the related subsections. Geometry and design characteristics are explained in detail in appendix A.

2.2 Basic Characteristics Considered in the Design

As described before, the first basic characteristic of the tilt duct UAV system which differs from the other conventional type UAVs, helicopters and tilt-rotor UAVs, is the moving ducts covering propellers that are located on the tip of the wings which leads to cancel out the effects of induced flow and brings the advantage of `end-plate effect´. The ducts have **`main propellers´** inside that are designed to provide the thrust necessary for both vertical and translational flight modes. Vertical motion of the UAV is provided by maintaining the ducts vertical so that the thrust (downwash) of the rotors provide the necessary lift for the aircraft. The ducts always have synchronized movement in horizontal direction; however the propellers inside may have different collective (blade pitch) settings in order to have differential thrust for rolling in hover regime or in low speed. The aft fan is also moved laterally to obtain a yawing moment similarly in hover regime or in low speed conditions.

The ducted UAV have the tendency to experience a nose-up pitching moment. That is, the

airflow over the airframe and through the rotor system produces a moment about the aircraft's center of gravity which causes the nose of the aircraft to pitch upward. At this point, the second basic characteristics of the UAV comes into picture with its **`aft propeller´** which is introduced to counter-act this pitch-up moment in transition flight mode.

The Tilt-Duct UAV design is an interesting research subject for control studies. The most challenging part is the control of the transition mode, since the effectiveness of the control surfaces and stability characteristics change with the flight condition, especially with speed and the transaction (movement) of the ducts.

2.3 Performance Characteristics

A mission profile requirement shown in figure 2.1 was considered in the design phase of the Tilt-Duct UAV.

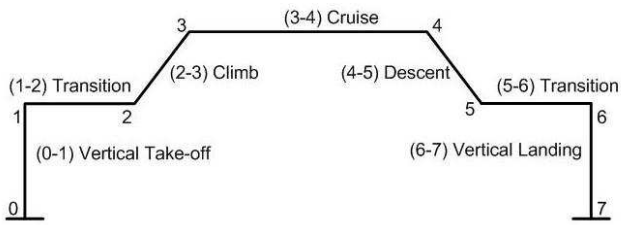

Figure 2.1: Mission profile for the Tilt-Duct UAV

The main performance requirements, which are the leading factors of the design, are given in table 2.1.

Table 2.1: Main performance requirements

Performance Criteria	Requirements	Unit
Operational Altitude	2000	m
Cruise Speed	≥38 ≥73.42	m/s knots
Stall Speed (at 1000m)	29 50	m/s knots
Payload Weight	10	kg
Max Range	1520	km

After the design phase of the aircraft, performance measures become apparent. The critical measures in table 2.2 characterizes the UAV which shall be considered during modeling studies of the aircraft dynamics and automatic control design in the thesis.

Table 2.2: Aircraft performance characteristics

Performance Criteria	Values	Unit
hp/W	0.0476	hp/N
W/S	574	N/m^2
Cd0	0.056	-
L/D_{max}	10.72	-
Best Range Speed	34.7 67.45	m/s knots
Maximum Allowable Speed	88.4 171.84	m/s knots
Cruise Speed	45 87.47	m/s knots

2.4 Aircraft Technical Design and Geometry

Aircraft design technical drawings for the METU project of Tilt-Duct UAV [31] are given in appendix A. The geometric properties of the aircraft are also included.

2.5 Aerodynamic Characteristics

In the content of the current study, additional work had been done to predict the aerodynamic characteristics of the aircraft. The most critical part of the aerodynamic design was characterized by the airfoil selection of wing and stabilizers. They were chosen from the Eppler series as being E-583 for wing and E-521 for horizontal-vertical stabilizers which are known to give high aerodynamic efficiency (high lift-low drag) for low speed regimes. The 3-Dimensional aerodynamic properties were obtained by stability derivatives of the aircraft obtained from AIAA [38] program, which uses empirical method by giving statistical values for competitor aircrafts.

In this thesis, the aerodynamic characteristic of the Tilt Duct UAV is studied by considering the Ducts and Conventional layout (as a fixed wing UAV) separately.

The body-wing-tail-control surfaces are studied assuming that it is a conventional type airplane and aerodynamic properties are obtained by Digital DATCOM [10] [17] which is a more realistic and widely-used empirical database program, giving nearly exact results especially for designs with conventional layouts and moderate aspect ratios. Since the Tilt-Duct UAV has a high wing configuration without dihedral or twist, the 3-dimensional, nonlinear aerodynamic coefficients obtained from DATCOM are more likely to be accurate. However since DATCOM database is more reliable for NACA airfoil series, a sufficiently matching NACA airfoil selection is made instead of using Eppler data, to be introduced in DATCOM Data Card.

Aerodynamic effects of the ducts with their connections to the wing are obtained by using research studies of Hoerner on Drag [4] which is a fundamental and reliable method to estimate drag coefficients of most shapes to be used in a drag equation or to estimate aerodynamic drag loads.

2.5.1 Assumptions

- **Mach Number Effect**: In forward flight, the Tilt-Duct UAV is rather low in speed. Since Mach number is low, the effect of it on aerodynamics is ignored. Aerodynamic coefficients are obtained for maximum operational speed in the operational altitude regime (150 m/s, 2000m).
- **Propulsion and Thrust Effect**: Since the engine and propellers are covered by the ducts, their slipstream effects are reduced. Instead, drag effect of the ducts are more pronounced. Their effects are integrated to the aerodynamics as `external drag due to ducts´. Direct effect of the thrust is not considered as the aerodynamic effect, their dynamic effects are considered as external Forces and Moments.
- **Ground Effect / Landing Gear Effect / Flap Effect**: Since the UAV is VTOL type, the flight conditions will not include high speed in a take-off or landing run, there is no forward velocity in these regimes. Therefore, aerodynamic characteristics will not be affected by any landing or take-off configuration change. In addition, ground effect on the rotors, as in the case for helicopter, will be canceled by the ducts.
- **Elasticity Effect**: Elasticity Effects are ignored since the UAV does not experience high speeds or high dynamic pressure values.

2.5.2 Aerodynamic Coefficients and Related Derivatives

A further study is done to define the aircraft aerodynamic properties. The tool DATCOM [10] is used, which gives empirical aerodynamic database which are all in stability axis for the specified Mach, Re number, reference center of gravity and areas. The prepared input data cards in which body and airfoil shapes, geometric properties are introduced to the tool and as a result, built-up aerodynamic properties for all the components of the aircraft are obtained.

Body and Section Profile

Body information which is introduced as frame stations at several sections is obtained from Catia drawings as in figure 2.2.

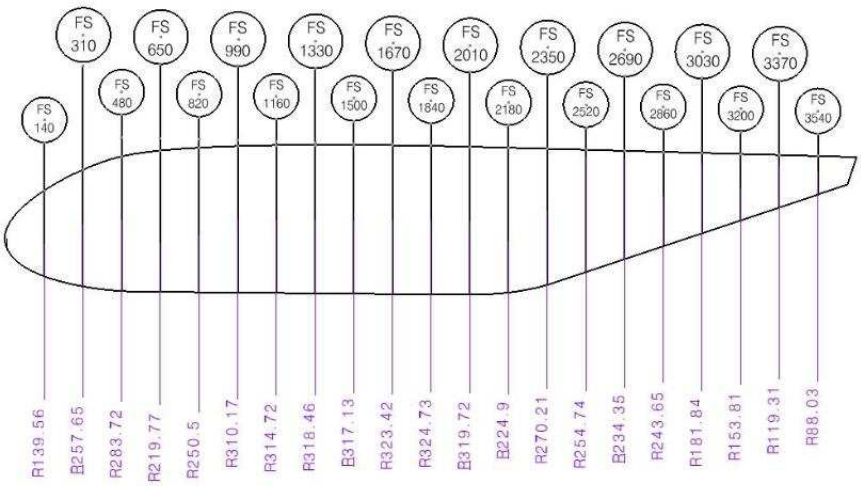

Figure 2.2: Information for frame stations of fuselage section radius

Airfoil section data for wing and horizontal-vertical tails which are integrated to the input data card are NACA profiles, NACA747a415 and NACA0015 (figures 2.3, 2.4).

Full Aircraft Aerodynamic Data

Full aircraft aerodynamic data is tabulated and plotted in appendix B.

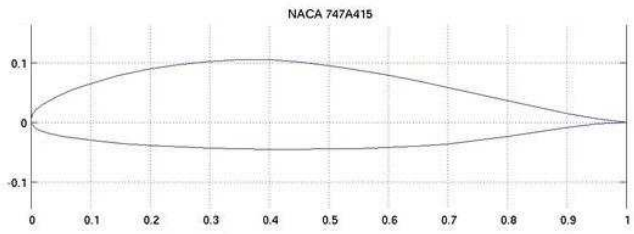

Figure 2.3: Wing airfoil section : NACA 747a415

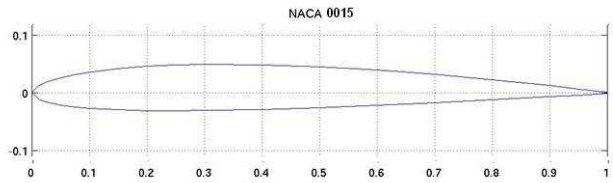

Figure 2.4: Horizontal - vertical tail symmetric airfoil section : NACA 0015

2.5.3 Aerodynamic Effect of the Ducts

The duct around the propellers can be assumed as a fairing or cowling around the engine, which reduces the total drag of the nacelle body. The ducts can be taken as a towning ring around the rotors, almost entirely hiding the engine. It may eliminate % 80 - 90 of the external drag caused by the protruding cylinders [4]. However their internal drag is included.
Drag forces created by the ducts can be studied individually depending on the flight modes of the aircraft, since in different regimes like cruise or hover, wing interference or aircraft speed affects will vary. Drag effects are obtained as drag coefficients from [4], which is a reliable source including results for various wind tunnel experiments implemented on various geometries. These coefficients are nondimensionalized by the exposed area of the surfaces and further corrected by the reference of wing area.

Drag of the Ducts in Horizontal

When the ducts are in horizontal direction, wing interference effects begin to be the most critical criteria. For a plump nacelle shape, Hoerner studies [4] give some mounting configurations of the nacelle on wings as in figure 2.5.

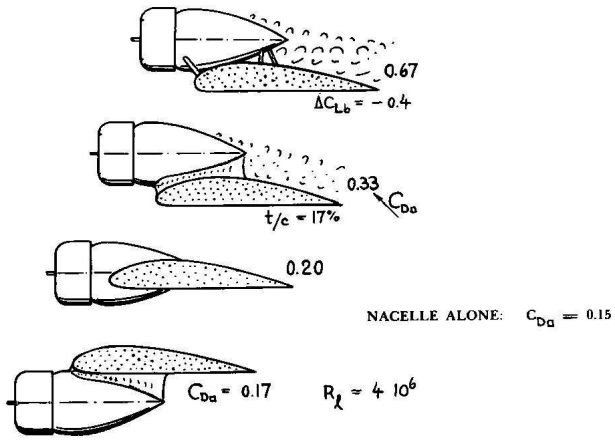

Figure 2.5: Drag of several radial-engine installations, demonstrating interference with wing [4]

The effect of the wing interference is also dependent on the lift characteristics of the wing as given in figure 2.6. The drag effect (C_{db}) corresponding to the lift is taken as the induced value and the subscript of `b´which is indicating the interference area is assumed to be the whole exposed area to obtain the largest drag value.

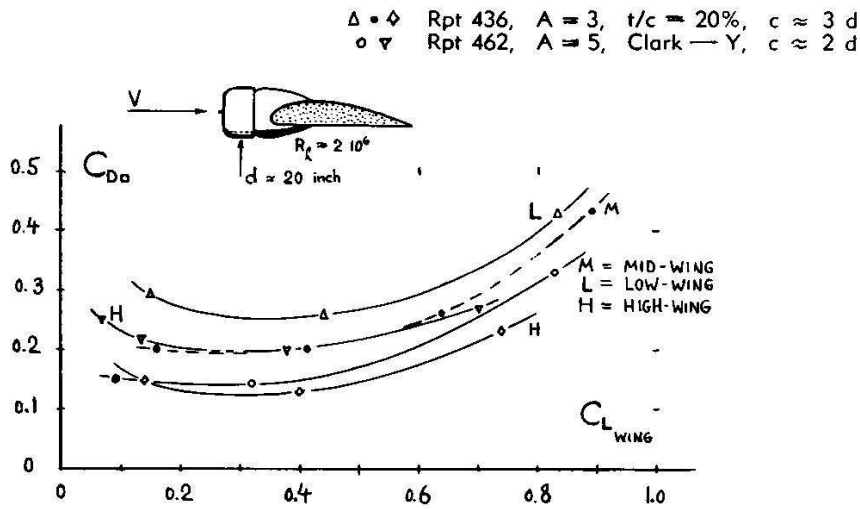

Figure 2.6: Drag coefficient of engine nacelle as a function of the lift coefficient of the wing on which they are installed [4]

Drag of the Ducts in Vertical

When the ducts are in vertical direction, the duct can be taken as a cylinder shape, considering the section view in the free-stream direction. The drag coefficient of the circular cylinders is given in figure 2.7.

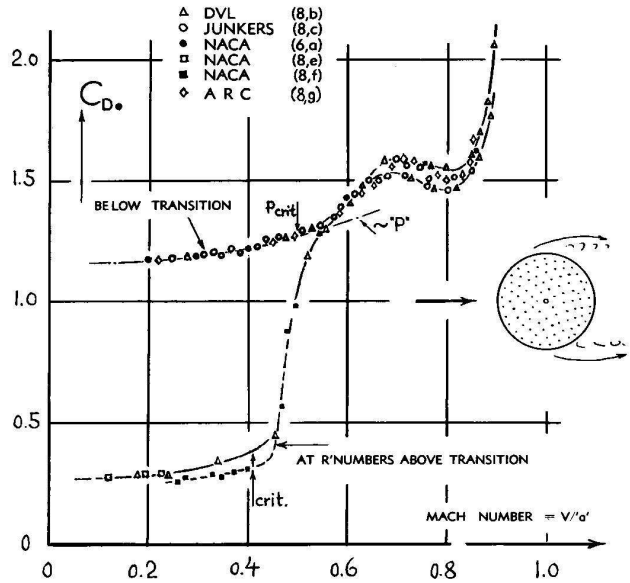

Figure 2.7: Drag coefficients of circular cylinders, tested between walls in various wind tunnels at subcritical Re and Re above transition [4]

Drag of the Ducts in Transition Mode

In transition, when the ducts are in intermediate condition, the drag of the ducts will be the combination of the drag caused by the horizontal or vertical condition of the ducts and will change with the duct angle (μ) which shall be defined by a sin - cosine correction. The drag equations considered in the study are equations 2.1 for interference drag due to lift on the wing and 2.2 to obtain drag coefficient corrected by the wing reference area. [4]

$$C_{db} = 0.035C_{lb}^2 \tag{2.1}$$

$$C_{d_{duct}} = C_{d_0} * S_{ref}/S_w \tag{2.2}$$

With these equations, cruise and hover drag values are obtained and for the transition mode,

the correlated equation can be defined as in 2.3.

$$C_{d_{duct}trans} = C_{d_{duct}cruise}cos(\mu) + C_{d_{duct}hover}sin(\mu) \tag{2.3}$$

Total Drag Effect of the Ducts for Full Operation

When the ducts are in horizontal, considering the configuration of duct mounting above the wing, drag coefficient due to wing lift in high angles of attack (for the highest drag) are as in table 2.3.

Table 2.3: Drag effect of the ducts for aircraft cruise mode

Criteria	C_{d0}	C_{lb}
Figure 2.5	0.67	-0.4
Figure 2.6	0.35	
total drag coefficient	1.02	
with %80 reduction (ducts)	0.21	

Equation defining the drag effect of the ducts in horizontal is then obtained as in equation 2.5.

$$C_{lb} = 0.035(-0.4)^2 = 0.0056 \tag{2.4}$$

$$Cd_{duct,cruise} = (0.21 + 0.0056)1.1458/(1.754) = 0.1736 forcruise \tag{2.5}$$

When the ducts are in vertical, for the subcritical Reynolds number when the Mach number is taken around 0.21 and drag values are obtained (table 2.4).

Table 2.4: Drag effect of the ducts for aircraft hover mode

Criteria	C_{d0}	C_{lb}
Figure 2.5	0.67	-0.4
Figure 2.7	1.2	
total drag coefficient	1.87	

Equation defining the drag affect of the ducts in vertical is then as in equation 2.7.

$$C_{lb} = 0.035(-0.4)^2 = 0.0056 \tag{2.6}$$

$$C_{d_{duct}hover} = (1.87 + 0.0056) * 1.1458/(1.754) = 1.226 forhover \tag{2.7}$$

Therefore, combining equations 2.5 and 2.7 for all the flight modes and considering these values will be twice since there are two propellers and ducts. The resulting equation can be defined as equation 2.8.

$$C_{d_{duct}trans} = 2 * 0.1736cos(\mu) + 2 * 1.226sin(\mu) \tag{2.8}$$

While the ducts are in vertical, the drag coefficient is considerably large. However since there will be no forward speed value in this regime, the drag effect is zero. While moving through the forward flight, the thrust effect will counteract the drag due to ducts.

2.6 Weight and Balance Characteristics

In this section mass-inertia and CG parameters of the aircraft are given. The inertias are checked and the missing information for these values are calculated with the geometry and weight information by build up method. Several components with their mass characteristics are given in table A.12.

The inertia values for the full aircraft are obtained as in table A.11. These values are combined with present weight-geometry data and simple assumptions.

2.7 Propulsion and Fuel System Characteristics

Propulsion and fuel system information of the aircraft includes the propellers, engines and fuel tanks with their technical qualifications, working principles and locations.

In the UAV design, two main propellers are two-blade type used with individual engines for each one. They are directly connected, housed in ducts, attached to the tips of the wings with a tilt mechanism. Tilting mechanism is done via a central shaft, driven with a single actuator.

Aft propeller is a four-blade type with inlet and exit guide vanes that are used for thrust vectoring. It is located at the aft of the fuselage. Guide vanes are closed during cruise flight. They are vectoring in vertical direction and fully open to be used as thrust supporters in hover mode.

Fuel Tanks are installed in the wing. Systems are selected for a low cost propulsion system

for a UAV with a low-weight combination. Engines are obtained from Limbach Flugmotoren GmbH company manufacturing four or two stroke piston engines for very light airplanes, powered gliders and UAVs.

All the properties due to propellers and fuel system are given in table 2.5.

Table 2.5: Propeller and fuel system geometric parameters

Parameter	Value	Unit
Main Propeller Diameter	1.2	m
Aft Propeller Diameter	0.44	m
Main Propeller Revolution Speed	500	rpm
Aft Propeller Revolution Speed	600	rpm
Main Propeller Blade Number	2	
Aft Propeller Blade Number	4	
Available Wing Fuel Volume	63.44	cm^3

2.7.1 Engine Properties

Engines for the main propulsion system are selected to be Limbach L-275-E, and the engine for the aft propulsion system is Limbach L-90-E which was an evolutionary step in developing the L-275-E. 2.6 and 2.7 show the engine qualifications. [27]

Table 2.6: Main engine qualifications and performance values

Performance	15 kW (20hp) at 7200 rpm
Displacement	274 cm^3 (16.72 cub. inches)
Cylinders	2 cylinder, horizontally opposed
Dry Weight Approximation	7,2 kg with magneto ignition Fuel
Fuel	AVGAS 100LL or 90RON mixed with a suitable oil to the ratio of 1:25 or 1:50 (with synthetic oil)
Ignition	Shielded ignition system

Table 2.7: Aft engine qualifications and performance values

Performance	6hp at 8500rpm
Cylinders	2 cylinder, horizontally opposed
Ignition	Single ignition system

CHAPTER 3

NONLINEAR 6-DOF DYNAMIC MODEL

3.1 Introduction

Dynamic simulation code for the Tilt-Duct VTOL UAV is created in Matlab® - Simulink® environment in order to use an interactive graphical tool and a set of block libraries that are useful for the control and visualization of complicated parameter interactions. Nonlinear dynamic model simulates 6-DOF equations of motion, ISA Atmosphere relations and Navigational transformations. It also simulates air vehicle aerodynamics and powerplant.

3.2 Nonlinear Dynamic Model Structure

A brief description of the subsystems in the simulation code are given below.
`Aerodynamics´ subsystem includes the aerodynamic static and dynamic coefficients and aerodynamic effect of the ducts.
`Main and aft propellers´ is the subsystem with estimated dynamics determining the required rpm set or collective inputs for the required throttle setting. The system is based on a basic momentum theory and blade element theory, an iterative solution method is used between the thrust, induced and farfield velocities [57]. The system inputs are introduced as percentage of the maximum rated engine thrust values, so that a linear relationship between the inputs and thrust vectors is obtained for simplicity of linearization and control studies.
The subsystem *`Environment´* or *`Atmosphere´* is the `ISA Atmosphere´model including FAA Standard system for gust winds. The altitude effects on pressure, temperature, density, and dynamic pressure are analyzed, and the angle of attack and sideslip angle are also introduced

here.

In *`6 DOF equations of motion´* block, the external forces and moments are introduced, the necessary transformations are done, and the body angular rates, velocities, translational and rotational motions are obtained by the related equations derived. Body and Earth Fixed Frame motions of the vehicle are obtained. Mass, inertia properties and the effects of gravitational acceleration are included in the subsystem.

`Controls´ subsystem introduces the control inputs to the system by saturating the related deflections, angles or thrust values. The actuator effects are ignored but can be modeled here.

`Autopilot´ subsystem includes the control design algorithms and control gains to calculate the required controls for usage in the dynamic model, which are sent to the control subsystem. Control allocation methods for the redundant control channel in transition flight are also added here. The explanations about the equations derived and solved for each subsystem are given in this chapter.

The general view of the dynamic model and the sub-blocks are as in figures 3.1, 3.2 and detailed model blocks for significant subsystems are given in appendix C.

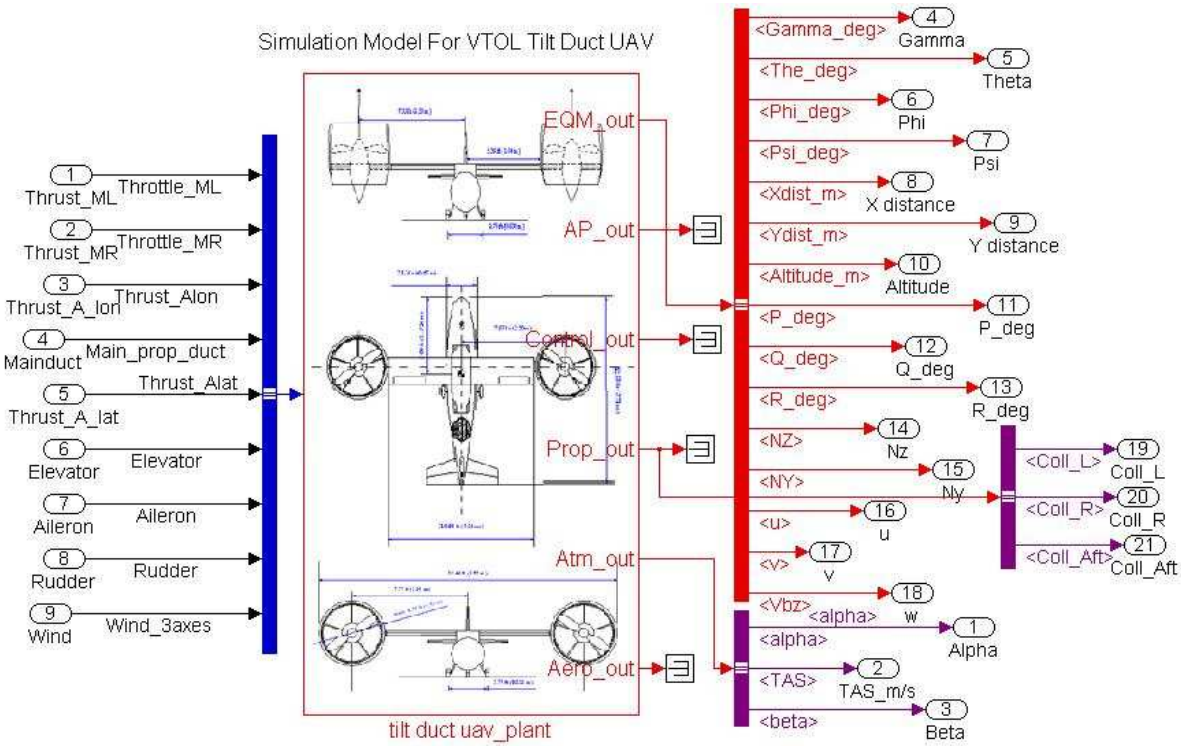

Figure 3.1: Dynamic simulation model : general view with input - output

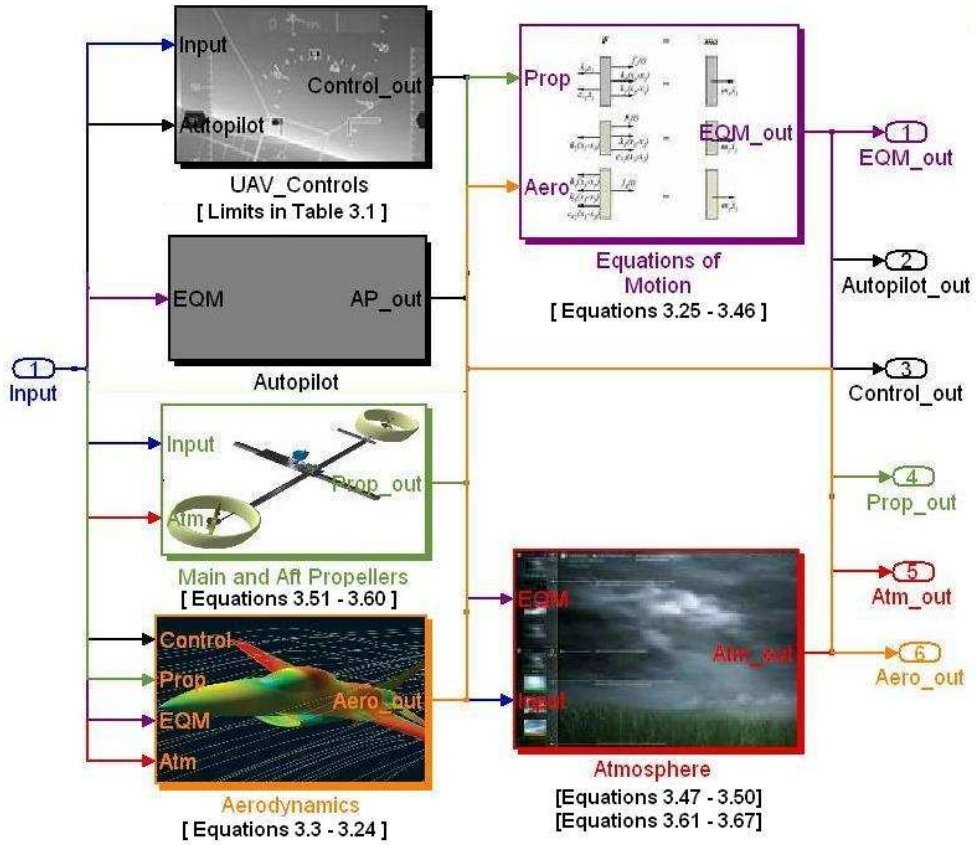

Figure 3.2: Dynamic simulation model : subsystems with input - output

3.3 Aerodynamics Subsystem

Aerodynamic static and dynamic forces are obtained by using component build - up method by resolving each component as in equation 3.1,then related transformations are done and the total coefficients are combined as in equation 3.2 to combine the aerodynamic properties in the model.

$$C_{oeff_{static}} = C_{oeff_{wbt}} + C_{oeff_{\delta elev}} + C_{oeff_{\delta ail}} + C_{oeff_{rud}} \tag{3.1}$$

$$C_{oeff_{tot}} = C_{oeff_{static}} + C_{oeff_{dynamic}} \tag{3.2}$$

Th empirical tool used for the Tilt-Duct UAV (when considered as a conventional type UAV) aerodynamic analysis, DATCOM [10], defines the aerodynamic coefficients in stability axis and at the defined point of the reference. Therefore they are translated to the body axis and

center of gravity where the aerodynamic forces and moments for the equations of motion are defined. Since the CG position of the aircraft may change, transformation to the center of gravity (CG) reference frame is carried out as in equations 3.16 - 3.18 .

$$C_L = C_{L_{WBT}}(\alpha) + C_{L_{\delta elev}}(\delta_{elev}) + (C_{L_q} q + C_{L_{\dot{\alpha}}} \dot{\alpha})\frac{c}{V} \tag{3.3}$$

$$C_D = C_{L_{WBT}}(\alpha) + C_{D_{\delta elev}}(\delta_{elev}) \tag{3.4}$$

$$C_{D_{\delta elev}}(\delta_{elev}) = C_{D0}(\delta_{elev}) + C_{D_\alpha}(\delta_{elev})\alpha \tag{3.5}$$

$$C_M = C_{M_{WBT}}(\alpha) + C_{M_{\delta elev}}(\delta_{elev}) + (C_{M_q} q + C_{M_{\dot{\alpha}}} \dot{\alpha})\frac{c}{V} \tag{3.6}$$

$$C_Y = C_{Y_{WBT,\beta}}\beta + C_{Y_{\delta rud}}(\delta_{rud}) + (C_{Y_p}(\alpha)p + C_{Y_r} r)\frac{b}{2V} \tag{3.7}$$

$$C_R = C_{R_{WBT}}(\alpha) + C_{R_{\delta ail}}(\delta_{ail}) + C_{R_{\delta rud}}(\delta_{rud}) + (C_{R_p}(\alpha)p + C_{R_r}(\alpha)r)\frac{b}{2V} \tag{3.8}$$

$$C_N = C_{N_{WBT,\beta}}\beta + C_{N_{\delta ail}}(\alpha, \delta_{ail}) + C_{N_{\delta rud}}(\alpha, \delta_{rud}) + (C_{N_p}(\alpha)p + C_{N_r}(\alpha)r)\frac{b}{2V} \tag{3.9}$$

$$C_{X_{cg}} = C_{X_{body}} \tag{3.10}$$

$$C_{Y_{cg}} = C_{Y_{body}} \tag{3.11}$$

$$C_{Z_{cg}} = C_{Z_{body}} \tag{3.12}$$

$$C_{R_{cg}} = C_{R_{body}} - (C_{Y_{body}}\Delta z_{cg} + C_{Z_{body}}\Delta_{cg})/b \tag{3.13}$$

$$C_{M_{cg}} = C_{M_{body}} + (C_{X_{body}}\Delta z_{cg} - C_{Z_{body}}\Delta x_{cg})/c \tag{3.14}$$

$$C_{N_{cg}} = C_{N_{body}} + (C_{Y_{body}}\Delta x_{cg} + C_{X_{body}}\Delta y_{cg})/c \tag{3.15}$$

$$\Delta x_{cg} = x_{cg} - x_{ref} \tag{3.16}$$

$$\Delta y_{cg} = y_{cg} - y_{ref} \tag{3.17}$$

$$\Delta z_{cg} = z_{cg} - z_{ref} \tag{3.18}$$

3.4 Equations of Motion Subsystem

In the subsystem where 6 - degrees of freedom (6DOF) equations of motion (EOM) are implemented, the external forces and moments, inertias, axes transformations are introduced to the system. The equations are represented by Euler angle transformations for the rotation of Body-fixed coordinate frame about the Earth-fixed reference frame [40]. The general dynamics are mathematical representations of the motion in the Body-axis system.

3.4.1 Total Forces and Moments

Total forces and moments on the aircraft are due to the aerodynamic effects, thrust and weight (gravity). These are all combined in the `Equations of Motion´subsystem to be added to the dynamics of the aircraft in order to be considered in the motion.

3.4.1.1 Aerodynamic Effect

Due to the aerodynamic coefficients obtained as described in Chapter 2, the combined effects in equations 3.3 - 3.15 are obtained in the `Aerodynamics´block. Here, dimensional aerodynamic forces and moments are derived as follows to be added to the total effects for the motion of the aircraft.

$$X_A = C_{X_{cg}} qS \tag{3.19}$$

$$Y_A = C_{Y_{cg}} qS \tag{3.20}$$

$$Z_A = C_{Z_{cg}} qS \tag{3.21}$$

$$R_A = C_{R_{cg}} qSb \tag{3.22}$$

$$M_A = C_{M_{cg}} qSc \tag{3.23}$$

$$N_A = C_{N_{cg}} qSb \tag{3.24}$$

3.4.1.2 Gravitational Forces

In this part, gravity (g) effect is transformed to the body axis frame by equation 3.25.

$$X_G = -mgsin\theta, \quad Y_G = mgcos\theta sin\phi, \quad Z_G = mgcos\theta cos\phi \tag{3.25}$$

3.4.1.3 Geodetic Frame Effect for Gravitational Forces

The turn rate of the local geographic frame with respect to the Earth fixed frame can be shown by the associated quantity expressed in terms of the rate of change of latitude and longitude.[40] [29]

$$\begin{bmatrix} \dot{\lambda}cosL & -\dot{L} & -\dot{\lambda}sinL \end{bmatrix} \tag{3.26}$$

$$\dot{\lambda} = \frac{v_E}{R_0 + h} \tag{3.27}$$

$$\dot{L} = \frac{v_N}{R_0 + h} \tag{3.28}$$

Latitude, longitude and height above the surface of the Earth are given by equations 3.29, 3.30, 3.31.

$$\dot{L} = \frac{v_N}{R_N + h} \tag{3.29}$$

$$\dot{\lambda} = \frac{v_E secL}{R_E + h} \tag{3.30}$$

$$\dot{h} = -v_D \tag{3.31}$$

$$R_N = R(1 - e^2)/(1 - e^2 sin^2 L)^{3/2} \tag{3.32}$$

$$R_E = R/\sqrt{1 - e^2 sin^2 L} \tag{3.33}$$

where, Length of the semi-major axis, R = 6378137.0 m

Length of the semi-minor axis, r=R(1-f) = 6356752.3142 m

Flattening of the ellipsoid, f=(R-r)/R = 1/298.257223563

Major eccentricity of the ellipsoid, $e = [f(2 - f)]^{1/2}$ = 0.0818191908426

Earth‘s rate, Ω = 7.292115x 10^{-5} rad/s (15.041067 deg/hour)

3.4.1.4 Thrust Forces-Moments

The forces and moments due to the thrust system is taken as equated in the related block of *’Main and Aft Propellers’* subsystem.

3.4.2 Implementation of Mass of Inertias

Estimated inertia values of the aircraft are introduced to the model in this block. Alternatively, a changing inertia model is also produced. By the help of a switch, the selection of one of two models can be done. During trimming and control studies, the fixed inertia model is generally used for the usage of trim - control analyses.

3.4.3 Axes Transformations

The dynamic model is created in the way to make it possible to be executed with the real-time data from navigation sensors and data units. Therefore, all the associated co-ordinate systems, their transformations and relations are added to the model.

3.4.3.1 Definition of Axes Systems

Inertial Axis System : Defined by the axes ($OXiOYiOZi$), is a non rotating reference system that has the origin at the center of the Earth (defined in figure 3.3).

Earth-Fixed Axis system : Defined by the axes ($OXeOYeOZe$) along the Eart‘s polar axis. The Earth axis is rotating due to the Inertial frame with the rotational speed of the Earth, Ω about OZi axis (defined in figure 3.3).

Navigational System (NED) : Has the origin at OX OY OZ and located on the surface of the Earth such that the OZe axis is directed towards the center of the spherical Earth. Axes are all aligned with the directions of north, east and local vertical (down) (defined in figure 3.3).

Body-Fixed Axis System : Is an orthogonal axis system centered at ($OXbOYbOZb$) (generally the CG) fixed to the vehicle and aligned with the roll, pitch, yaw axes of the vehicle in which the navigation system is installed (defined in figure 3.3).

Wind or Flight Path Coordinate System : Has the origin ($OXwOYwOZw$) at the CG of the aircraft, where the x-axis is aligned with the velocity vector. The horizontal and lateral axes are defined in the directions of the horizontal and lateral wind. Angle of attack and slip-stream angle defines the orientation of the wind coordinate system (defined in figure 3.3).

Wander Azimuth Frame : By this frame, the singularities in the poles of the navigation system is avoided. It is a level axis like navigation frame, however is rotated through the wander angle about the local vertical.[23]

3.4.3.2 Body-Fixed to Earth Axis

The transformation from body fixed axis system to Earth axis system is done by the transpose of the Direction Cosine Matrix (DCM) which is a 3x3 matrix, the columns of which represent unit vectors in body axes projected along the reference axis. In DCM approach the transformation from one co-ordinate frame to another is defined by three rotations about different axes taken in turn. The Euler angles usage for the transformation is the most popular and simple technique to define the airplane motion relative to the Earth.[38]

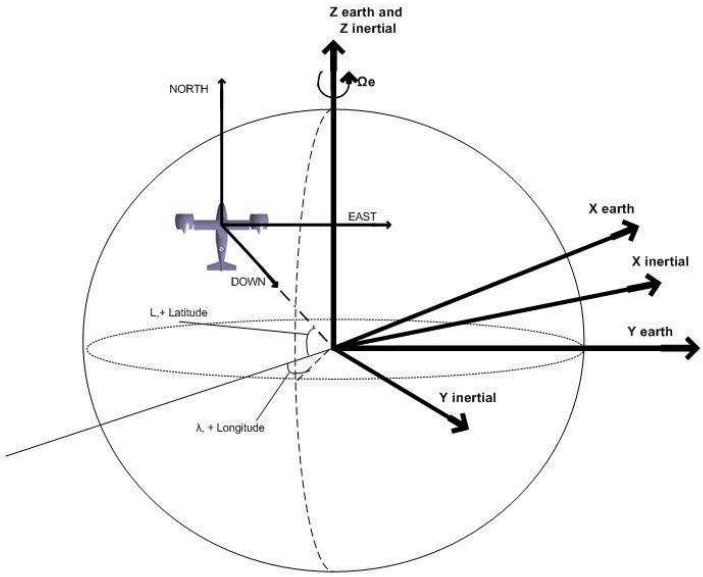

Figure 3.3: Inertial - Earth - NED axes systems

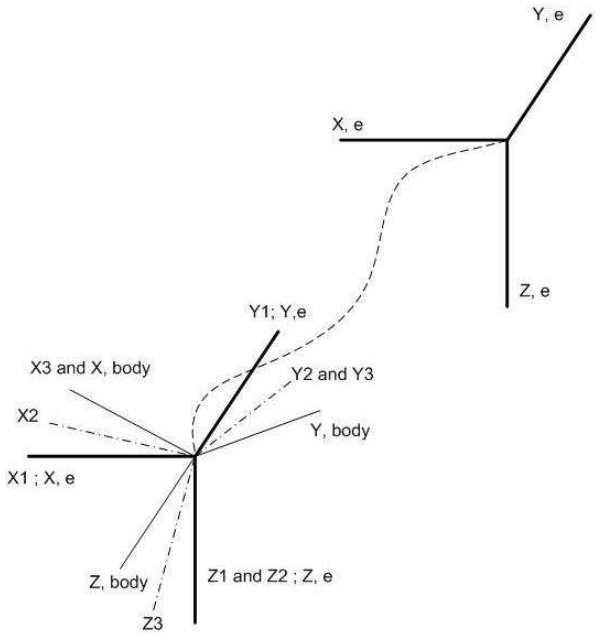

Figure 3.4: Euler transformation

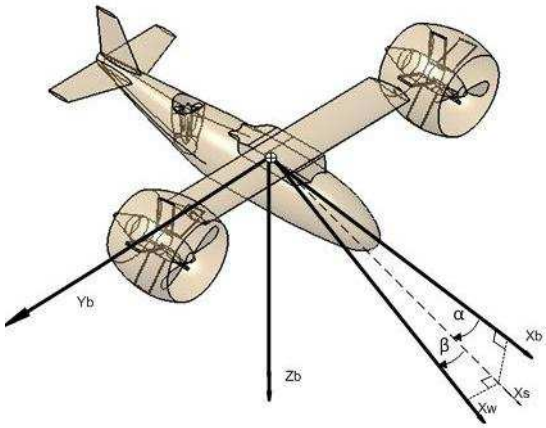

Figure 3.5: Stability - Wind - Body-Fixed axes transformation

$$\begin{bmatrix} u_1 \\ v_1 \\ w_1 \end{bmatrix} = \begin{bmatrix} cos\psi & sin\psi & 0 \\ -sin\psi & cos\psi & 0 \\ 0 & 0 & 1 \end{bmatrix} \begin{bmatrix} cos\theta & 0 & -sin\theta \\ 0 & 1 & 0 \\ sin\theta & 0 & cos\theta \end{bmatrix} \begin{bmatrix} 1 & 0 & 0 \\ 0 & cos\phi & sin\phi \\ 0 & -sin\phi & cos\phi \end{bmatrix} \begin{bmatrix} u \\ v \\ w \end{bmatrix} \tag{3.34}$$

The $(DCM)^T$ matrix used for transformation of Body to Earth Axis is given in terms of Euler angles as in equation 3.35 which is the multiplied form of equation 3.34

$$V^E = \begin{bmatrix} cos\theta cos\psi & -cos\phi sin\psi + sin\phi sin\theta cos\psi & sin\phi sin\psi + cos\phi sin\theta cos\psi \\ cos\theta sin\psi & cos\phi cos\psi + sin\phi sin\theta sin\psi & sin\phi cos\psi + sin\phi sin\theta sin\psi \\ -sin\theta & sin\phi cos\theta & cos\phi cos\theta \end{bmatrix} V^b \tag{3.35}$$

3.4.3.3 Wind and Stability Axis to Body-Fixed Axis

Since the angle of attack and sideslip angle define the orientation of the wind coordinate system with respect to the body-fixed axis system, the transformation can be done with these angles directly. Additionally, stability axis can also be defined by the angle of attack orientation as shown in figure 3.5.

The transformations can be expressed as equations 3.36 and 3.37.

$$V^b = \begin{bmatrix} u_1 \\ v_1 \\ w_1 \end{bmatrix} = \begin{bmatrix} cos\alpha cos\beta & -cos\alpha sin\beta & -sin\alpha \\ sin\beta & cos\beta & 0 \\ sin\alpha cos\beta & -sin\alpha sin\beta & cos\alpha \end{bmatrix} V^w \tag{3.36}$$

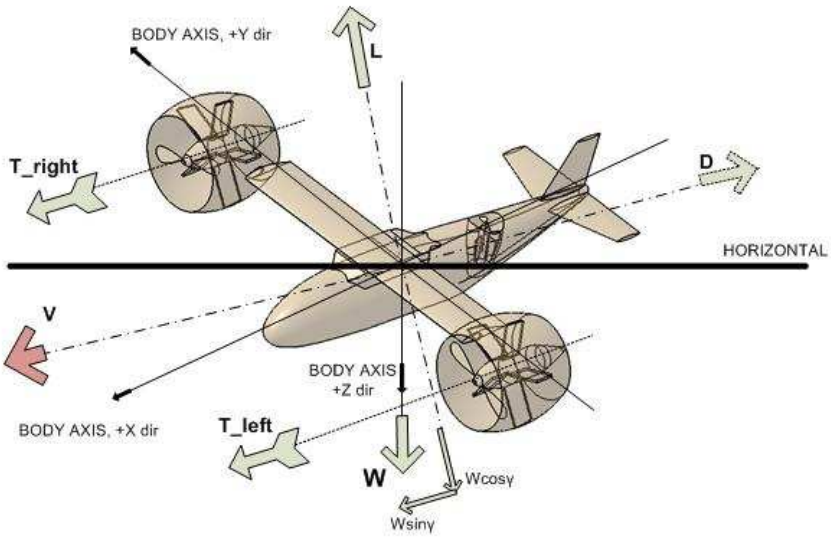

Figure 3.6: Body Axis - Wind axes system and forces on the aircraft

$$V^b = \begin{bmatrix} cos\alpha & 0 & -sin\alpha \\ 0 & 1 & 0 \\ sin\alpha & 0 & cos\alpha \end{bmatrix} V^{stab} \tag{3.37}$$

3.4.4 6-DOF General Equations of Motion

3.4.4.1 Force-Moment Equations in Body Axis

Force - Moment Equations in Body Axis is defined as equations follow [38]:

$$m\dot{u} + wq - vr + gsin\theta = X_A + X_T \tag{3.38}$$

$$m\dot{v} + ur - wp - gcos\theta sin\phi = Y_A + Y_T \tag{3.39}$$

$$m\dot{w} + vp - uq - gcos\theta cos\phi = Z_A + Z_T \tag{3.40}$$

$$I_{xx}\dot{p} - I_{xz}\dot{r} + I_{xz}pq + (I_{zz} - I_{yy})rq = R_A + R_T \tag{3.41}$$

$$I_{yy}\dot{q} + (I_{xx} - I_{zz})pr + I_{xz}(p^2 - r^2) = M_A + M_T \tag{3.42}$$

$$I_{zz}\dot{r} - I_{xz}\dot{p} + (I_{yy} - I_{xx})pq + I_{xz}rq = N_A + N_T \tag{3.43}$$

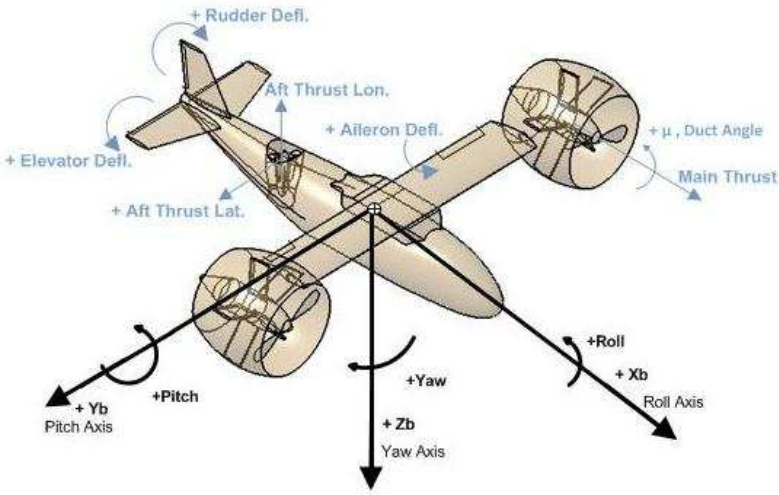

Figure 3.7: Sign convention for the translational-angular motion and controls of the aircraft

3.4.4.2 Kinematic Equations

Kinematic Equations are given as equations follow [38]:

$$\dot{\phi} = p + qsin\phi tan\theta + rcos\phi tan\theta \tag{3.44}$$

$$\dot{\theta} = qcos\phi - rsin\phi \tag{3.45}$$

$$\dot{\psi} = qsin\phi sec\theta + rcos\phi sec\theta \tag{3.46}$$

The sign convention for the forces, moments, velocity or rates used in these equations is in the same manner with the body axis, and is shown in figure 3.7.

3.5 Atmosphere(Environment) Subsystem

3.5.1 ISA Atmospheric Effects

The Atmosphere block uses the geopotential height and international standard atmosphere (ISA) condition to evaluate temperature, speed of sound, air pressure, and air density using mathematical representation for the ISA values. Density and speed of sound are calculated using a perfect gas relationship , below which the geopotential altitude of 0 km and above

the geopotential altitude of 20 km, temperature and pressure values are held. The standard atmophere values are referenced from the 1976 Standard Atmosphere to 86 kilometers [9]. Critical values defining the atmosphere are :

Ambient temperature at sea level, T_b = 288.15K

Lapse rate, L =0.0065 K/m

Specific gas constant, R = 287.0531 J/Kkg, 8.31432 J/Kmol

Within an atmospheric layer, the temperature difference is linear with the difference in geopotential altitude.

$$T = T_b + L(H - H_b) \tag{3.47}$$

Speed of sound [m/s] equation is as : $a = \sqrt{\gamma RT}$ By the hydrostatic equation, air pressure [Pa] can be defined as equation 3.48.

$$\frac{P}{P_b} = \left(\frac{T_b + L(H - H_b)}{T_b}\right)^{\frac{g}{RL}} e^{\frac{(Htroposphere-H)g}{RT}} \tag{3.48}$$

Here, $e^{\frac{(Htroposphere-H)g}{RT}}$ is the stratosphere model. Air density [kg/mˆ3] can be defined as equation 3.49

$$\frac{\rho}{\rho_b} = \left(\frac{(\frac{T}{T_b})^{\frac{g}{RL}}}{(\frac{T}{T_b})}\right) e^{\frac{(Htroposphere-H)g}{RT}} \tag{3.49}$$

3.5.2 Wind Gust Model

The external wind effect can be implemented to the model as input to the system, which can be defined in 3-axis as in 3.50. In this block, the wind inputs are translated to the body axis and added to the velocity components in body-axis. If desired, MATLAB® gust and turbulence models can be implemented.

$$V_{Wind} = \begin{bmatrix} V_{wx} & V_{wy} & V_{wz} \end{bmatrix}^T \tag{3.50}$$

3.6 Propulsion and Engine Effects Subsystem

The input for propulsion system to the model is done by introducing the percentage of the maximum thrust capability of main propulsion system and aft propulsion system. In addition,

the positions of the main ducts and position of the aft throttle fan are also given as inputs to the dynamic model through the propulsion system model.

The maximum thrust capabilities of the engines are assumed and taken as;

Max Thrust Main Left - Right = 640 N
Max Thrust Aft = 196 N

As an alternative, a subsystem is also added to the model in order to compute the necessary collective settings for the propellers.

3.6.1 Propulsion and Rotor Dynamics

In order to obtain linearity during analyses, maximum thrust percentages are defined as inputs to the model. However, the model also includes an algorithm that uses collective inputs to obtain the thrust of rotors. The Rpm settings are taken to be constant. Since the model is using percentage inputs, required collectives are given as outputs of the system.
The equations governing the rotor model are based on basic momentum theory and blade element theory. The concept is like a helicopter rotor. However, since the ducts are decreasing rotor flow intake and the rotor is not hinged, a simplified approach is sufficient.[13] [57]
The airspeed through the rotor is caused by the airspeed on the z-axis (v_z), the rotary motion and geometry of the blades. It can be expressed as in equation 3.51.[57]

$$v_b = v_z + \frac{2}{3}\omega_r r(\theta_{coll} + \frac{3}{4}K_{twist}) \tag{3.51}$$

Here, K_{twist} is the twist of the blades. The equation for rotor flow is simplified by taking an average effect of twist of the blades instead of integrating the blade sections. The thrust can be expressed as in equation 3.52.

$$\tau = \frac{1}{4}(v_b - v_i)\omega_r r^2 \rho_\infty a_0 b c_r \tag{3.52}$$

where, vi :induced velocity of the rotor
a_0: rotor lift curve slope
b: number of the blades
c_r: rotor blade chord
The far field velocity can be expressed as in equation 3.53.

$$v' = \sqrt{v_x^2 + v_y^2 + (v_z - v_i)^2} \tag{3.53}$$

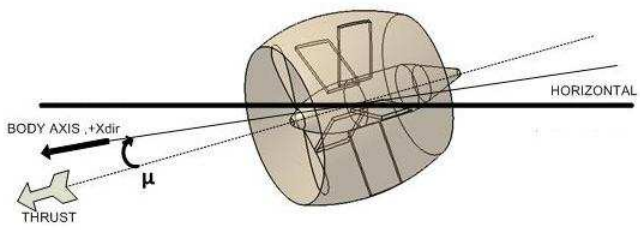

Figure 3.8: Thrust line axis of duct

The induced velocity is now expressed as in equation 3.54.

$$v_i = \frac{\tau}{2\pi r^2 \rho_\infty v'} \tag{3.54}$$

The duct effects are integrated as the drag forces of the ducts.

3.6.2 Engine Thrust Effects

Since the thrust line of the main engine is changing, this moving line is defined by the angle that the ducts do with the body x-axis (μ), for the transformation of the forces and moments this angle is used with the convention given in figure 3.8. Similarly the angle of the aft fan is due to its the lateral movement about the vertical axis and defined by the angle it does with the body x-y plane (ν).

Forces and Moments due to the Propulsion System are defined directly as:

$$X_T = (T_{MainL} + T_{MainR})cos\mu \tag{3.55}$$

$$Y_T = (T_{Aft})cos\eta \tag{3.56}$$

$$Z_T = (T_{MainL} + T_{MainR})sin\mu + (T_{Aft})sin\eta \tag{3.57}$$

$$L_T = L_{ycg_{Thm}}(T_{MainL} + T_{MainR})sin\mu \tag{3.58}$$

$$M_T = L_{xcg_{Thm}}(T_{MainL} + T_{MainR})sin\mu - L_{xcg_{Tha}}(T_{Aft})sin\eta \tag{3.59}$$

$$N_T = L_{xcg_{Tha}}(T_{MainL} + T_{MainR})cos\mu + L_{xcg_{Thm}}(T_{Aft_{max}})cos\eta \tag{3.60}$$

3.7 Control Surfaces and Inputs Block

Preferably, actuator dynamics for the main control surfaces are used in the model. In other words, it is present in the model but usually not used with the assumption that the control surface actuators work without a time delay or damping after the input is introduced to the model. The saturations are implemented as `limiters´to the controls including the throttle settings. The delimiter values used are as in table 3.1.

Table 3.1: Control surface deflections and input limits

Control	Unit	Limit
Throttle-Main-Left (ThML), Throttle-Main-Right (ThMR)	%	0 ~ 100 (Max 640 N)
Mainduct	deg	0 ~ 90
Throttle-Aft-Longitudinal (ThALon)	%	0 ~ 100 (Max 196 N)
Throttle-Aft-Lateral (ThALat)	%	0 ~ 100 (Max 196 N)
Elevator	deg	(-20) ~ (20)
Aileron	deg	(-15) ~ (10)
Rudder	deg	(-25) ~ (25)

The sign convention for the control surfaces and inputs to the model are given in figure 3.7.

3.8 Main Flight Parameter Calculations

In the simulation model of the Tilt-Duct UAV, basic flight parameters are calculated as their general descriptions and these values are usually the general inputs to the various subsystems. These parameters are typically; angle of attack [rad] (3.62), airspeed or TAS [m/s] (3.61), sideslip angle [rad] (3.63), derivative of angle of attack [rad/s] (3.65), derivative of sideslip angle [rad/s] (3.65), dynamic pressure [Ps](3.67), and equivalent airspeed [m/s] (3.68). The wind velocity effects are also included in these equations.

$$V = \sqrt{(u - u_w)^2 + (v - v_w)^2 + (w - w_w)^2} \tag{3.61}$$

$$\alpha = tan^{-1}\left(\frac{w - w_w}{u - u_w}\right) \tag{3.62}$$

$$\beta = sin^{-1}\left(\frac{w - w_w}{u - u_w}\right) \tag{3.63}$$

$$\gamma = tan^{-1}\left(\frac{V_{Ez}}{V_E}\right) \tag{3.64}$$

$$\dot{\alpha} = \frac{-F_x sin\alpha + F_z cos\alpha}{mVcos\beta} - tan\beta(pcos\alpha + rsin\alpha) + q \tag{3.65}$$

$$\dot{\beta} = \frac{-F_x cos\alpha sin\beta + F_y cos\beta + -F_z sin\alpha sin\beta}{mV} + psin\alpha - rcos\alpha \tag{3.66}$$

$$\overline{q} = \frac{1}{2}\rho V^2 \tag{3.67}$$

$$EAS = \frac{TAS\, a_0 \sqrt{\gamma}}{a} \tag{3.68}$$

γ : Relative pressure ratio at the flight altitude

a_0 : Speed of sound in mean sea level, 340.294 m/s

In addition, altitude wrt the Mean Sea Level (MSL) which is also known as 'Pressure Altitude' is one of the important parameters used in the model. It is the indicated altitude of an altimeter that is usually set to an agreed baseline pressure setting that is the air pressure at mean sea level (MSL) in the International Standard Atmosphere (ISA). It is a specified pressure value around 101,325 Pa. Mean Sea Level Altitude is calculated with a linear approach dependent on the temperature and associated altitude changes and the static and the relationship between static pressure and pressure altitude is defined in terms of the properties of the International Standard Atmosphere (up to 36,090 ft) equation 3.69. As explained in 1976 COESA, apart from the pressure values of 0.3961 Pa (about 0.00006 psi) and 101325 Pa (about 14.7 psi), altitude values are extrapolated logarithmically and air is assumed to be dry and an ideal gas. [40] [66]

$$h_d MSL(ft) = (1 - (\frac{P}{101.325})^{0.190255})\frac{288.15}{0.00199074} \tag{3.69}$$

3.9 Model Reference Acronyms

Inputs to the model :

- Throttle rate for the maximum allowable thrust of main left-right propeller [%] : *Throttle-ML (ThML) , Throttle-MR (ThMR)*
- Duct angles for the left-right main propellers [deg] :*Mainduct*

- Throttle rate for the maximum allowable thrust of aft propeller vertical component [%]: *Throttle-ALon (ThALon)*
- Throttle rate for the maximum allowable thrust of aft propeller lateral component [%] : *Throttle-ALat (ThALat)*
- Deflection of the elevator [deg] :*Elevator*
- Deflection of the aileron [deg] :*Aileron*
- Deflection of the rudder [deg] :*Rudder*
- Inputs for the wind model :*Wind-3D as Horizontal, Lateral, Vertical Components*

States :

- Positions in Body Frame : *X position-m, Y position-m, Z position-m*
- Velocities in Earth Frame : *U, V, W*
- Euler angles :*Phi, Theta, Psi*
- Altitude due to pressure difference :$h_d MSL$
- Rates of rotation : *P, Q, R*
- Rates of variation in angles of attack and sideslip : *Alphadot, Betadot*

Outputs of the model :

- Collective needed for the main rotors [deg]: *Left-collective, Right-collective*
- Collective needed fot the aft rotor [deg] : *Aft-collective*
- Velocity : *Speed (TAS-m/s), Mach, U, V, W*
- Position : *X position-m, Y position-m, Altitude,* $h_d MSL$
- Flight Attitude : *Alpha, Beta, Gamma, Theta, Phi, Psi*
- Rate of rotation : *P, Q, R*
- Load factor : *Nz, Ny, Nz*

CHAPTER 4

LINEAR MODEL ANALYSIS

4.1 Introduction

The linear representations of the nonlinear systems about an equilibrium is needed to determine stability characteristics of a system as well as improving the stability characteristics and designing the automatic flight control systems. These representations can be state-space, discrete-time or time-invariant in terms of transfer functions, linearized matrices and other state-space representations of single input-single output or multi input-multi output configurations.

The linearization processes are usually done around specific local equilibrium points by using the equations of motion of the dynamic system. These steady-state equilibrium points, about which the linearizations of related equations are done, are found by the process called `trimming´.

In this chapter linearization method for the nonlinear tilt duct UAV model is explained. Trimming methods and trim points of the system, which are mainly used in linear model analyses and control studies, are also explained and the results are given for both hover, cruise and transition regimes of the aircraft. In addition, the defined linearized models are compared with the nonlinear dynamic model in terms of their response characteristics to the various control disturbances and by this approach, linearization studies are verified.

4.2 Trim Analyses

Trim, stability and response characteristics are the main aspects characterizing the flight behavior of an aircraft. In addition, trim condition defines many important characteristics of a system and is of primary importance in stability and control studies. Especially, the analysis of conditions at unstable points, like the transition regime of the Tilt-Duct UAV, trimming plays an important role.

A trim point, also known as an equilibrium point, is a steady state point of a dynamic system. Mathematically, a trim point is a point where the system's rotational-translational derivatives are equal to zero or a fixed value. For an aircraft, the trim problem concerns the required inputs to hold the aircraft in equilibrium which means generally to fly straight and level. ``It can also be climbing, turning and maybe subjected to high angle of attack or sideslip, but if the translational velocity components are constant with the fixed inputs, then the aircraft can said to be in trim´´[62]. In the simulation model of the Tilt-Duct UAV, when the aircraft maintains a static balance in pitch, roll, yaw and a fixed attitude with regard to all wind axes components it is said to be in trim. Trim works to balance the aircraft at a specific point that is defined by the fixed parameters found by adjusting the inputs, states and outputs until the steady-state point is found.

4.2.1 Trimmer Methodology

In the thesis, trimming is done by a simulation-based optimization. This optimization is done by solving a system of linear equations at the initiated equilibrium points. The non-linear simulation model is linearized around an initial trim point and a converging loop is solved until the trim condition is calculated where the points of the required states, inputs and outputs are reached. After this iterative approach, unknown inputs, states and outputs are obtained. This approach is chosen as opposed to other alternative methods since it allows the model to give trim conditions with different requirements for input controls which is useful to investigate an aircraft system with redundant controls. Trim code computes a steady-state operating point before the simulation is executed in the open loop dynamic system.

The trimmer algorithm that is written in MATLAB® uses a search algorithm by mainly using the function `feval´and the function `linmod´to linearize the dynamic model. The linearization

method is explained in detail in Section 4.3. A formulation is done to obtain the general matrix representation as in equation 4.1 of the system that is described by equation 4.9 and equation 4.12.

$$\begin{bmatrix} A & B \\ C & D \end{bmatrix} \begin{bmatrix} \Delta x \\ \Delta u \end{bmatrix} = \begin{bmatrix} \dot{x} \\ y \end{bmatrix} \quad or \quad [G] \begin{bmatrix} \Delta x \\ \Delta u \end{bmatrix} = \begin{bmatrix} \dot{x} \\ y \end{bmatrix} \tag{4.1}$$

Here, G matrix represents the linearized form of the nonlinear model around the states obtained at each iteration. This matrix is obtained by using linearization code on the compile mode of the dynamic model. Inputs, states, state derivatives and outputs can have constrained or required terms as well as unconstrained or unknown terms as stated in equation 4.2. The G matrix can be reduced by using the corresponding raws of the required state derivatives ($\dot{x}$) and outputs (y) and columns of unknown inputs (u) and states (x) for simplicity.

$$\begin{aligned} u &= \left[u_{unknown}(size : un_u) \quad u_{required}(size : req_u) \right] \\ x &= \left[x_{unknown}(size : un_x) \quad x_{required}(size : req_x) \right] \\ \dot{x} &= \left[\dot{x}_{unknown}(size : un_{\dot{x}}) \quad \dot{x}_{required}(size : req_{\dot{x}}) \right] \\ y &= \left[y_{unknown}(size : un_y) \quad y_{required}(size : req_y) \right] \end{aligned} \tag{4.2}$$

The new reduced matrix is with dimension $(req_{\dot{x}} + req_{ny}, un_u + un_x)$ and can be symbolized as $\hat{G}$. It is important here to supply constrained value number higher than number of unknowns.

Trim Iteration

In order to explain the trim algorithm, equation 4.1 may be written as in equation 4.3. Iteration is carried out to obtain zeroes of the left hand side of the equation by running the model in compile mode (by using function `feval´of Matlab) at each step with new u_{i+1} and x_{i+1}. Convergence is achieved when $[\dot{x} - \dot{x}_i, y - y_i]$ is sufficiently close to zero.

$$\left[\hat{G}\right] \begin{bmatrix} x_{i+1} - x_i \\ u_{i+1} - u_i \end{bmatrix} = \begin{bmatrix} \dot{x} - \dot{x}_i \\ y - y_i \end{bmatrix} \tag{4.3}$$

Step by step, the iteration process starts with the initial guesses for x and u, the linearizaton is made around these guesses and by compiling the model, state derivatives and outputs are

obtained. At each iteration step, the new $[\Delta_x, \Delta_u]$ pair is obtained by taking inverse of the G matrix (if not full-rank, Q-R decomposition is used), it is added to the old $[x, u]$ values and the model is compiled again to find the new $[\dot{x}_i, y_i]$ pair. The iteration is stopped when the norm of the solution matrix $[\Delta\dot{x}, \Delta y]$ goes to zero. Finally the trim state and output pair $[x, u]$ are obtained.

Trim Main Constraints

A trimmed flight is defined to have angular and translational rates (accelerations) equal to 0 and control inputs should be constant. In both of the trim modules (cruise, transition), the flight path angle (γ) is required to be zero, in other words, the aircraft is required to be horizontal in the flight path. The trimmed steady conditions are given in equation 4.4 - equation 4.8. [38] [14]

For steady wing-level flight:

$$\phi = \dot{\phi} = \dot{\theta} = \dot{\psi} = 0 \tag{4.4}$$

For steady pitching flight:

$$\phi = \dot{\phi} = \dot{\psi} = 0 \qquad \dot{\theta} = fixed\ rate \tag{4.5}$$

For steady rolling flight:

$$\dot{\psi} = \dot{\theta} = 0 \qquad \dot{\phi} = fixed\ rate \tag{4.6}$$

For steady turning flight:

$$\dot{\phi} = \dot{\theta} = 0 \qquad \dot{\psi} = fixed\ rate \tag{4.7}$$

General Condition :

$$\dot{p} = \dot{q} = \dot{r} = \dot{u} = \dot{v} = \dot{w} = 0 \tag{4.8}$$

4.2.2 Trim Results for Hover

Regardless of the altitude of the aircraft, trim conditions for wing-level hover are listed in table 4.1.

Table 4.1: Hover trim results - zero pitch attitude at 305 m altitude

Speed [m/s]	$\delta_{Tmain}[\%]$	$\delta_{Taft}[\%]$	μ[deg]	η[deg]
0	67.6757	71.9761	90	90

4.2.3 Trim Results for Cruise

The trim results in cruise regime are obtained for different speeds starting from the most suitable one which does not show stall characteristics. Figure 4.1 shows the cruise regime trim results for 305 m (1000 ft) altitude from stall speed to the maximum allowable speed, with the information of attitudes and required control inputs. Figure 4.2 also show the needed collective inputs for the throttle control inputs.

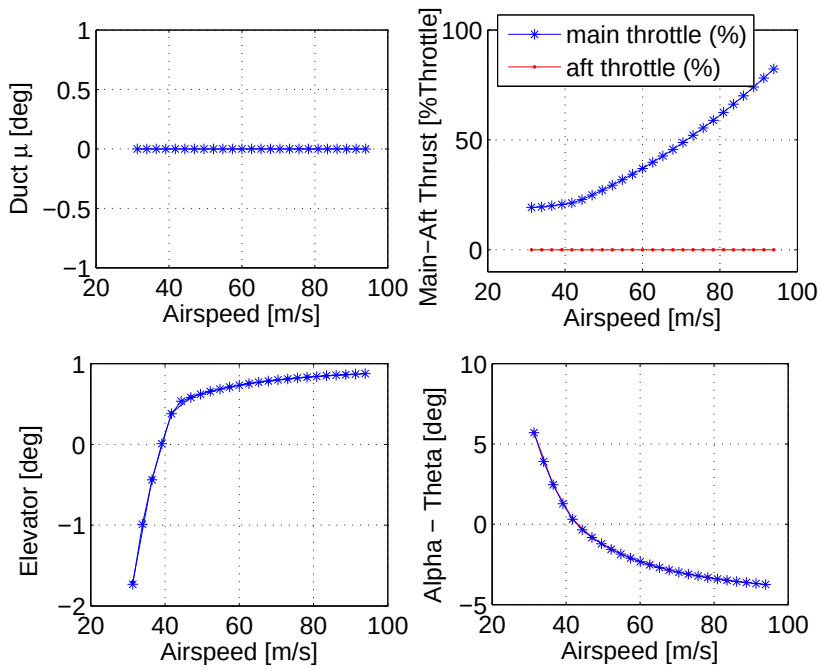

Figure 4.1: Cruise regime trim results at 305 m altitude from stall speed to maximum allowable speed

4.2.4 Trim Results for Transition

In this thesis, instead of investigating all the possible transition points, 2 different transition scenarios are studied and for the speed of entering the cruise mode, 3 different operational speeds are selected which are defined as the `Best Cruise Speed´, `Cruise Speed´and `Maxi-

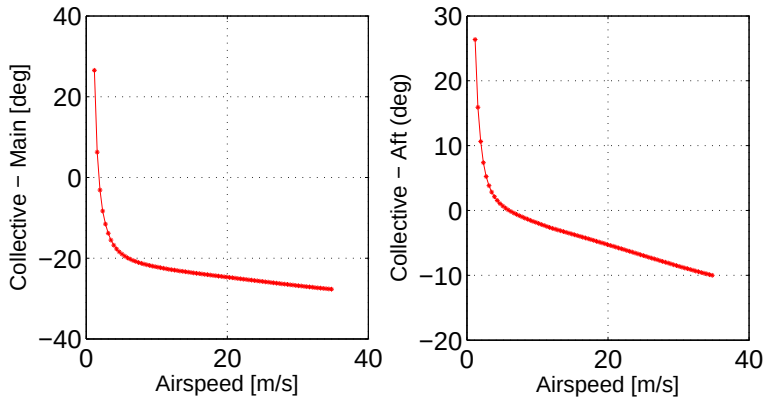

Figure 4.2: Example of the needed collective inputs (RPM Fixed) for main throttle in cruise for an intermediate speed range

mum Speed´. Transition scenarios are defined as follows:

1. While moving the ducts from vertical to horizontal, the change of the speed is linear with this motion. Therefore, the pitch attitude and angle of attack of the aircraft will be changing with duct motion due to the need to satisfy the horizontal speed requirement while counteracting the aircraft weight.

2. While moving the ducts linearly from vertical to horizontal, the pitch attitude or the nose motion of the aircraft is selected to be zero. Therefore, the overall speed changes in a nonlinear fashion with duct motion due to the need to satisfy the vertical force(weight). Conversely, if a linear change of the speed is maintained, the duct motion will not be linear. As expected, at lower speed regions the duct angle change should have a low gradient since forward thrust need is much less than the need of its vertical component.

4.2.4.1 Level Flight Trim Results for Transition

The trim results for the two scenarios presented above are given in figures 4.3 - 4.8. By comparing these results, the 2nd approach is seen to be more reliable, as expected for a smooth transition. Two different trim conditions are tried for this transition scenario. Since the pitching moment values are small enough to use only the aft throttle as a pitching control authority , firstly, elevator is not integrated to the results in figure 4.7, secondly elevator deflections are added to the system after a certain and sufficient (for elevator effectiveness) speed as shown

in figure 4.8. Figure 4.6 also show the example of the needed collective inputs for the throttle input controls for the first transition scenario.

These trim results again may not maintain in their equilibrium points for some conditions and need to be stabilized or controlled by some controller mechanisms. Both different scenario approaches and trim results for each states can further be used by the control studies for tracking the transition flight regime.

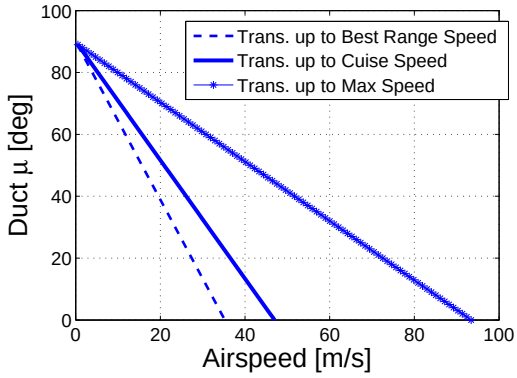

Figure 4.3: Transition scenario-1: Duct angle deflection change with speed

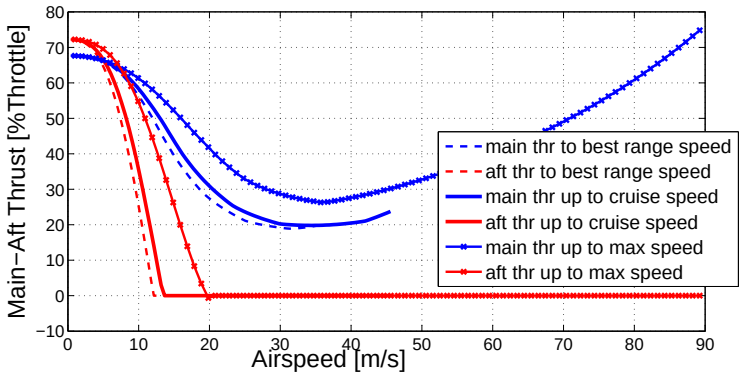

Figure 4.4: Transition scenario-1: Throttle settings change with speed

The sample of a trend in these trim results for cruise and transition are tabulated in appendix E.

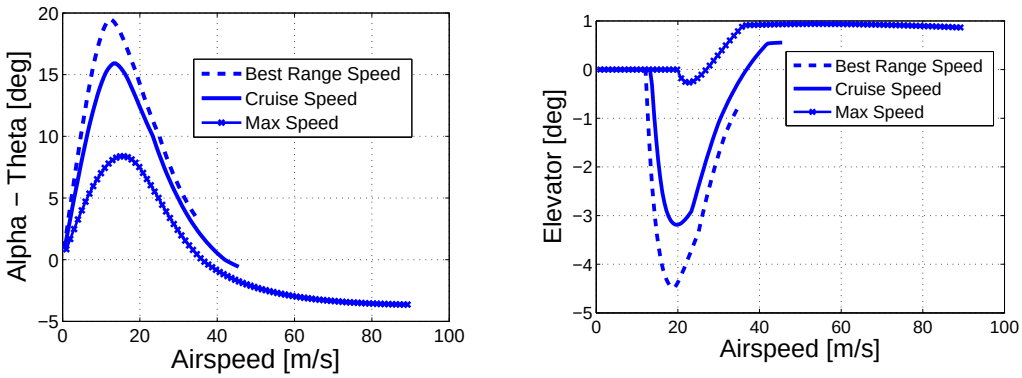

Figure 4.5: Transition scenario-1 : Pitch angle - angle of attack - elevator deflection change with speed [activated after sufficient speed]

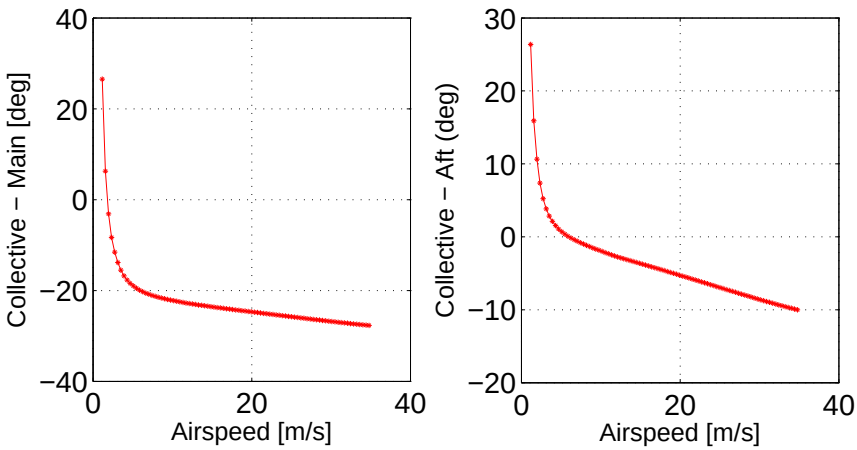

Figure 4.6: Example of the needed collective inputs (RPM Fixed) for main-aft throttle in transition scenerio-1 up to best range speed

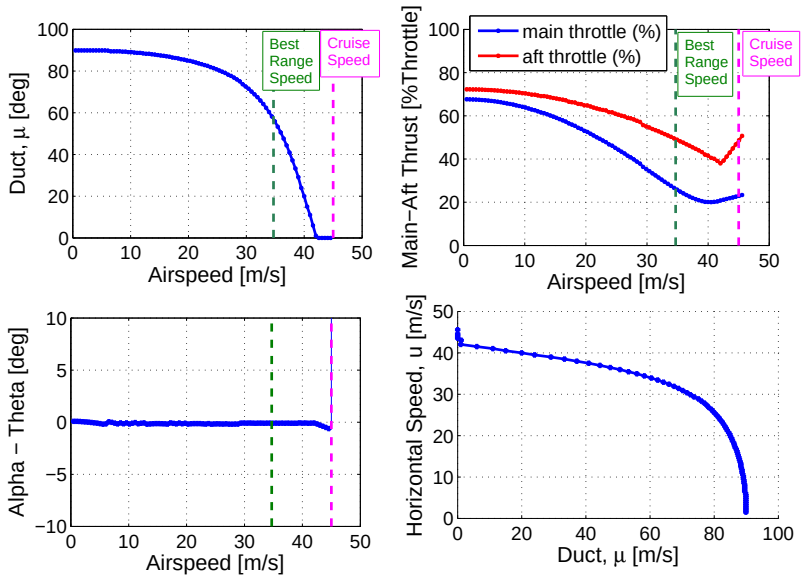

Figure 4.7: Transition scenario-2 : Change in major characterizing parameters for zero pitch attitude [No elevator deflection is integrated]

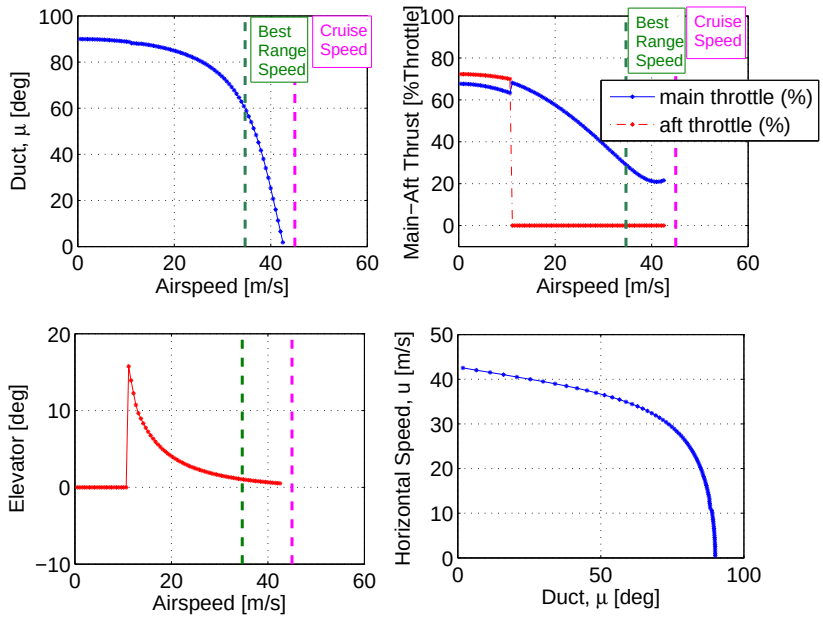

Figure 4.8: Transition scenario-2 : Change in major characterizing parameters for zero pitching [Elevator is activated after 12 m/s]

4.2.4.2 Level - Coordinated Turn Trim Results for Transition

While the aircraft is in a trimmed flight for a coordinated turn condition, the aircraft is maintained in a fixed bank angle and roll attitude as defined in equation 4.6 with no lateral acceleration. A coordinated turn trim study is done in order to see the response behavior of the aircraft in lateral maneuvers and the need for lateral controls. The trim conditions are found for different speed conditions and for all the input controls free. The results are as shown in figures 4.9 and 4.10.

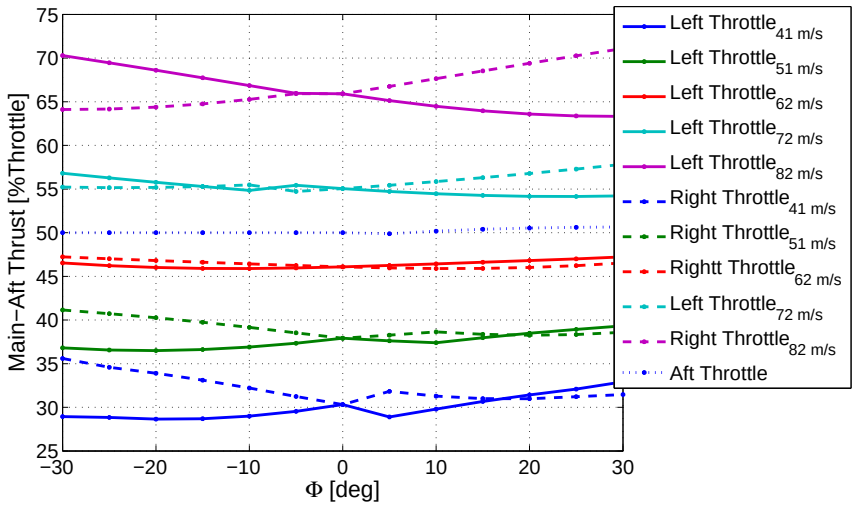

Figure 4.9: Throttle inputs for level - coordinated turn trim at 305 m altitude for different airspeed values

Simulation results for an example of a trim condition at 82 m/s and 10 degrees bank angle are given in terms of the position of the aircraft in figure 4.11.

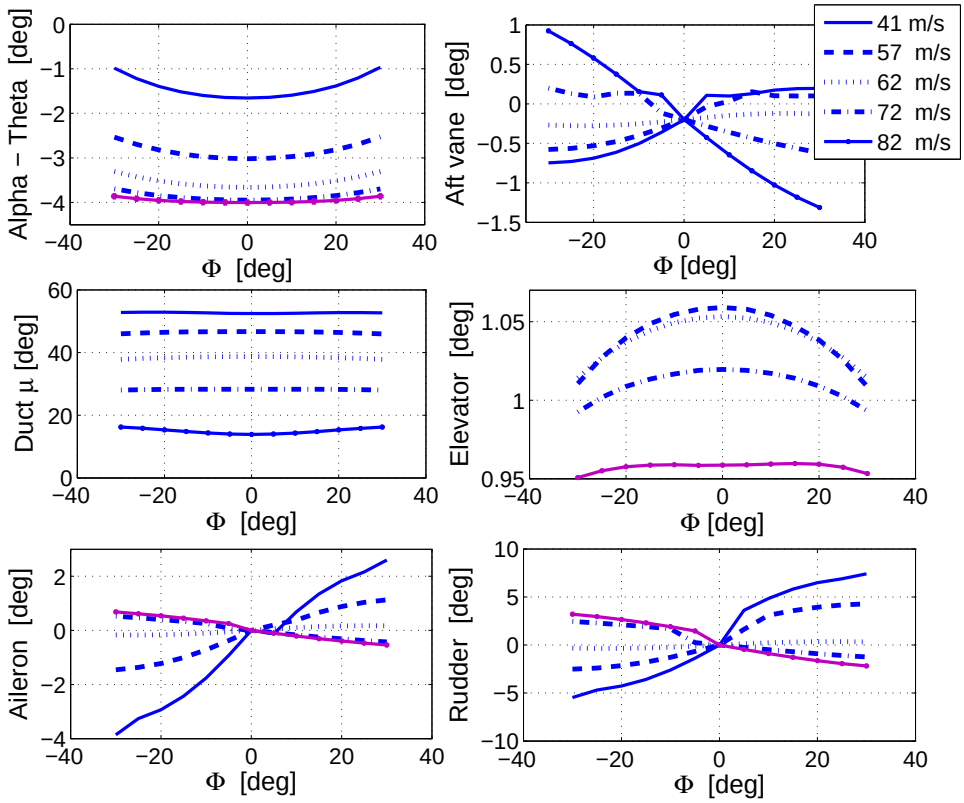

Figure 4.10: Level - coordinated turn trim results at 305 m altitude for different airspeed values

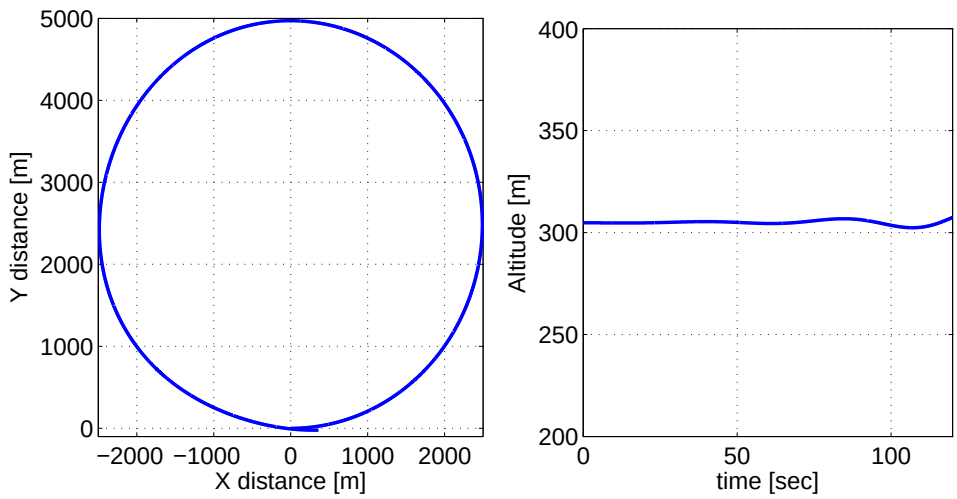

Figure 4.11: Level - coordinated turn trim simulation result for altitude 305 m Speed 82 m/s and bank angle 10 degrees

4.3 Linearization

As described before, linearization is the main step for a system to be identified with its stability, control characteristics, and handling quality classifications. The nonlinear systems are usually complicated systems and hard to analyze, most of the control or stability analyses techniques are developed for linear systems.

4.3.1 Linearization Tools and Algorithm

For the linearization of the model, MATLAB® code named `linmod´is used. Apart from the usual linearization codes in MATLAB, `linmod2´is also tried which computes a linear state-space model by perturbing the model inputs and model states and uses an advanced algorithm to reduce truncation error. However the results are very similar for both algorithms and `linmod´is used for the analyses.

State and the input vectors which are the trim or equilibrium points set the operating point at which the linear model is to be extracted. So the equilibrium point data and the dynamic system model are the main inputs to the linearization algorithm.

A classical Taylor series expansion approach can be used for the linearization representation. The 6-DOF equations of motion for the nonlinear systems are linearized to obtain a simple representation as given in equation 4.9, which has linearization form description as in equations 4.10 and 4.11 around steady - state equilibrium (trim) points.

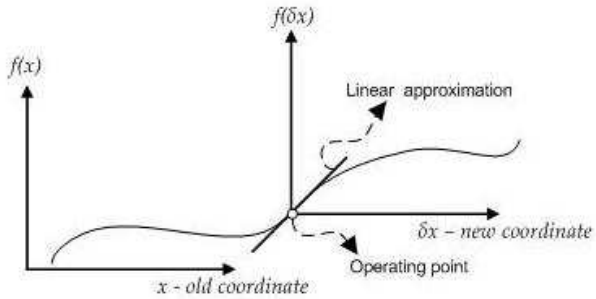

Figure 4.12: Taylor series approach for the representation of linearized equations in terms of equilibrium and perturbations

$$\dot{\bar{x}} \triangleq \bar{A}\bar{x} + \bar{B}\bar{u} \tag{4.9}$$

where $\tilde{x} = x - x_e$ or $\tilde{x} = x - x_{trim}$

$$\bar{A} = \begin{bmatrix} \left.\frac{\partial \bar{F}_1}{\partial \bar{x}_1}\right|_{\bar{x}_e,\bar{u}_e} & \left.\frac{\partial \bar{F}_1}{\partial \bar{x}_2}\right|_{\bar{x}_e,\bar{u}} & \cdots & \left.\frac{\partial \bar{F}_1}{\partial \bar{x}_n}\right|_{\bar{x}_e,\bar{u}} \\ \left.\frac{\partial \bar{F}_2}{\partial \bar{x}_1}\right|_{\bar{x}_e,\bar{u}} & \left.\frac{\partial \bar{F}_2}{\partial \bar{x}_2}\right|_{\bar{x}_e,\bar{u}} & \cdots & \left.\frac{\partial \bar{F}_2}{\partial \bar{x}_n}\right|_{\bar{x}_e,\bar{u}} \\ \vdots & \vdots & \vdots & \vdots \\ \left.\frac{\partial \bar{F}_n}{\partial \bar{x}_1}\right|_{\bar{x}_e,\bar{u}} & \left.\frac{\partial \bar{F}_n}{\partial \bar{x}_2}\right|_{\bar{x}_e,\bar{u}} & \cdots & \left.\frac{\partial \bar{F}_n}{\partial \bar{x}_n}\right|_{\bar{x}_e,\bar{u}} \end{bmatrix} \tag{4.10}$$

$$\bar{B} = \begin{bmatrix} \left.\frac{\partial \bar{F}_1}{\partial \bar{u}_1}\right|_{\bar{x}_e,\bar{u}} & \cdots & \left.\frac{\partial \bar{F}_1}{\partial \bar{u}_n}\right|_{\bar{x}_e,\bar{u}} \\ \left.\frac{\partial \bar{F}_2}{\partial \bar{u}_1}\right|_{\bar{x}_e,\bar{u}} & \cdots & \left.\frac{\partial \bar{F}_2}{\partial \bar{u}_n}\right|_{\bar{x}_e,\bar{u}} \\ \vdots & \vdots & \vdots \\ \left.\frac{\partial \bar{F}_n}{\partial \bar{u}_1}\right|_{\bar{x}_e,\bar{u}} & \cdots & \left.\frac{\partial \bar{F}_n}{\partial \bar{u}_n}\right|_{\bar{x}_e,\bar{u}} \end{bmatrix} \tag{4.11}$$

With the same approach the linearized system for outputs can also be written as in equation 4.12.

$$\tilde{y} \triangleq \bar{C}\bar{x} + \bar{D}\bar{u} \tag{4.12}$$

4.3.2 Model States-Inputs-Outputs used for Linearization

Since the coupling effects between longitudinal and lateral modes are weak, they are linearized separately and Tilt-Duct UAV state - input - output matrices are defined as follows:

$$x_{long} = \begin{bmatrix} u(m/s) \\ w(m/s) \\ Q(deg/s) \\ \theta(deg) \end{bmatrix} \tag{4.13}$$

$$u_{long} = \begin{bmatrix} \delta_{ThML}(\%max) \\ \delta_{ThMR}(\%max) \\ \delta_{ThAlon}(\%max) \\ \delta_{Duct}\mu(deg) \\ \delta_{Elev}(deg) \end{bmatrix} \tag{4.14}$$

$$y_{long} = \begin{bmatrix} \gamma(deg) \\ w(m/s) \\ Q(deg) \\ \theta(deg) \\ .... \end{bmatrix} \tag{4.15}$$

$$x_{lat} = \begin{bmatrix} w(m/s) \\ P(deg/s) \\ R(deg/s) \\ \phi(deg) \\ \psi(deg) \end{bmatrix} \quad (4.16) \qquad u_{lat} = \begin{bmatrix} \delta_{ThML}(\%max) \\ \delta_{ThMR}(\%max) \\ \delta_{ThAlat}(\%max) \\ \delta_{Ail}(deg) \\ \delta_{Rud}(deg) \end{bmatrix} \quad (4.17) \qquad y_{lat} = \begin{bmatrix} v(m/s) \\ P(deg/s) \\ R(deg/s) \\ \phi(deg) \\ \psi(deg) \\ ... \end{bmatrix} \quad (4.18)$$

Only few of the controls are used for hover and cruise modes as in 4.19 and 4.20. In transition mode all the control inputs can be used.

$$u_{hover,lon} = \begin{bmatrix} \delta_{ThML} & \delta_{ThMR} & \delta_{ThAlon} \end{bmatrix}^T \qquad u_{hover,lat} = \begin{bmatrix} \delta_{ThML} & \delta_{ThMR} & \delta_{ThAlat} \end{bmatrix}^T \quad (4.19)$$

$$u_{cruise,lon} = \begin{bmatrix} \delta_{ThML} & \delta_{ThMR} & \delta_{Elev} \end{bmatrix}^T \qquad u_{cruise,lat} = \begin{bmatrix} \delta_{Ail} & \delta_{Rud} \end{bmatrix}^T \quad (4.20)$$

4.3.3 Linearization Results

4.3.3.1 Linearized Hover Mode Matrix

Linearized hover mode matrices are given in appendix D equations D.17 - D.23 and the system eigenvalues in equations D.20 and D.24 indicate that the hover condition is unstable.

4.3.3.2 Linearized Cruise Mode Matrices

An example of the linearized longitudinal-lateral cruise matrices in appendix D are obtained at 305 m altitude for 60 m/s speed. Eigenvalues of the system in equation D.4 shows the airplane is stable in longitudinal axis for this flight regime.

The longitudinal eigenvalues may be identified as the classical short period and phugoid mode.

Table 4.2: Short period and phugoid mode characteristics for cruise mode at 305 m altitude and 60 m/s speed

Mode	Roots	Natural Frequencyω_n[rad/s]	Damping Ratio ζ
Short Period	-1.789± 1.283i	2.2	0.813
Phugoid	-0.044±0.260i	0.264	0.165

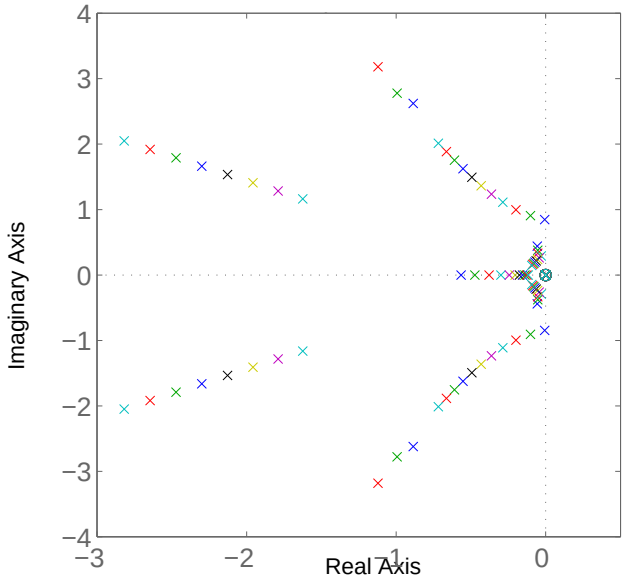

Figure 4.13: Root locus of the longitudal-lateral modes at altitude 305 m, speed 30-88 m/s

These eigenvalues of the system given in table 4.2 shows the airplane is stable in longitudinal axis for this flight regime.

The lateral modes are also examined and shown as in tables 4.3 and 4.4. In addition, the classical stable dutch roll mode and roll modes as well as slightly divergent spiral modes may be observed.

Table 4.3: Dutch roll mode characteristics for cruise mode at 305 m altitude and 60 m/s speed

Mode	Roots	Natural Frequency ω_n [rad/s]	Damping Ratio ζ
Dutch Roll	-1.789 ± 1.284i	1.29	0.282

Table 4.4: Roll and spiral mode characteristics for cruise mode at 305 m altitude and 60 m/s speed

Mode	Roots	Time Constant [s]	Time to Half Amplitude [s]
Roll	-0.244	4.105	2.845
Spiral	0.0006	1666.7	1155

The root locus of the longitudinal-lateral modes as a function of the forward speed is shown in figure 4.13. The system is observed to be stable for cruise mode for full operational flight speed regimes and eigenvalues move to the left as the speed increases.

4.3.3.3 Linearized Transition Mode Matrices

The longitudinal and lateral linearized system matrices for transition mode of the aircraft are obtained, as an example the condition with 40 degrees duct angle at 45 m/s speed linearized system matrices and associated eigenvalues are given in appendix D.

The first couple eigenvalues in equation D.12 are associated with short period, and second couple with the phugoid mode with faster and less damped characteristics with roots closer to zero.

Table 4.5: Short period and phugoid mode characteristics for transition mode 40 degrees duct angle at 45 m/s speed

Mode	Roots	Natural Frequency ω_n [rad/s]	Damping Ratio ζ
Short Period	-1.6030 ∓ 1.1640i	1.98	0.809
Phugoid	-0.0458 ∓ 0.1082i	0.118	0.39

The eigenvalues of the lateral modes given in equation D.16 are associated with dutch-roll, roll and spiral modes and characteristics are tabulated as in 4.6 and 4.7.

Table 4.6: Dutch roll mode characteristics for transition mode 40 degrees Duct Angle at 45 m/s speed

Mode	Roots	Natural Frequency ω_n [rad/s]	Damping Ratioζ
Dutch Roll	-0.3057 ± 1.1113i	1.15	0.265

Mode	Roots	Time Constant [s]	Time to Half Amplitude [s]
Roll	-0.2617	3.821	2.648
Spiral	0.0005	2000	1386

Table 4.7: Spiral and Roll Mode Characteristics for Transition Mode 40 degrees Duct Angle at 45 m/s Speed

Dynamic analyses show that in longitudinal mode short period and phugoid characteristics show the aircraft denotes Level -1 qualifications due to Military standards in Mil-F-8785C. In lateral-directional modes, for Dutch Roll and Spiral modes the aircraft is in Level-1 and Roll Mode characteristics are beyond the limits [21].

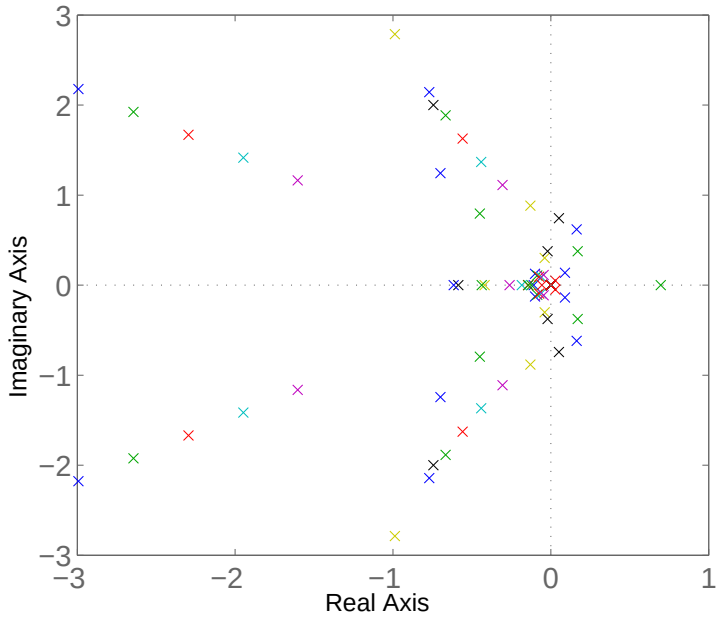

Figure 4.14: Root locus of the longitudal-lateral modes in transition obtained at altitude 305 m, when elevator deflection is activated at low speed regime

4.4 Linear Model Validation

The linearized system validation with the nonlinear systems plays an important role to show that the linearization has been carried out properly and to prove the linear system is reliable for the further linear control analysis. To verify linearization, a linearized system around the trimmed state at 305 m altitude and a low airspeed around 40 m/s is perturbed from the equilibrium with different ramp, step or doublet inputs and the results are compared with the responses obtained from the nonlinear simulation. The results in figures 4.15, 4.16, and 4.17 shows that the expected responses are obtained and the linear system reflects the nonlinear characteristics.

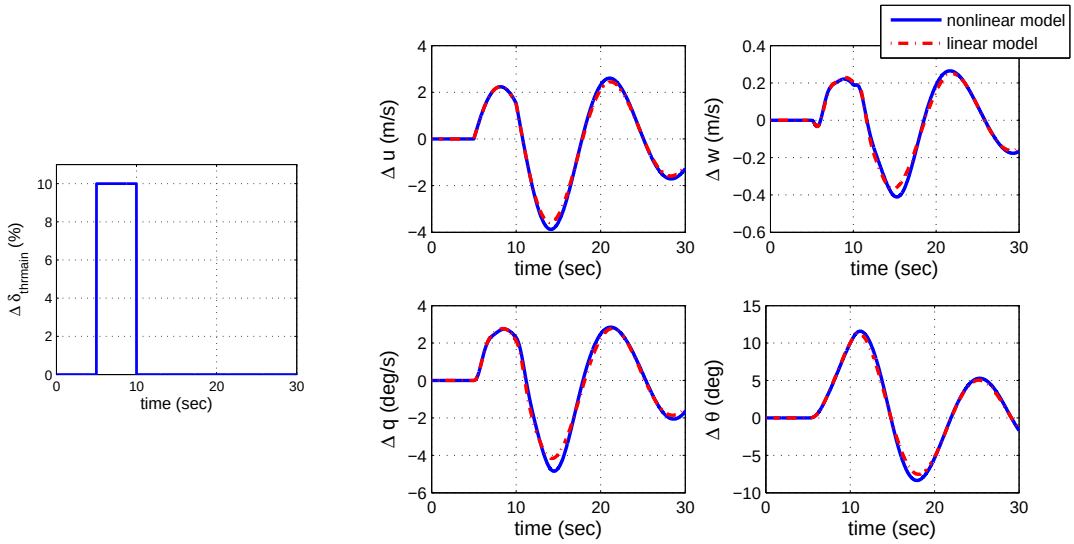

Figure 4.15: Nonlinear-linear model response to throttle input

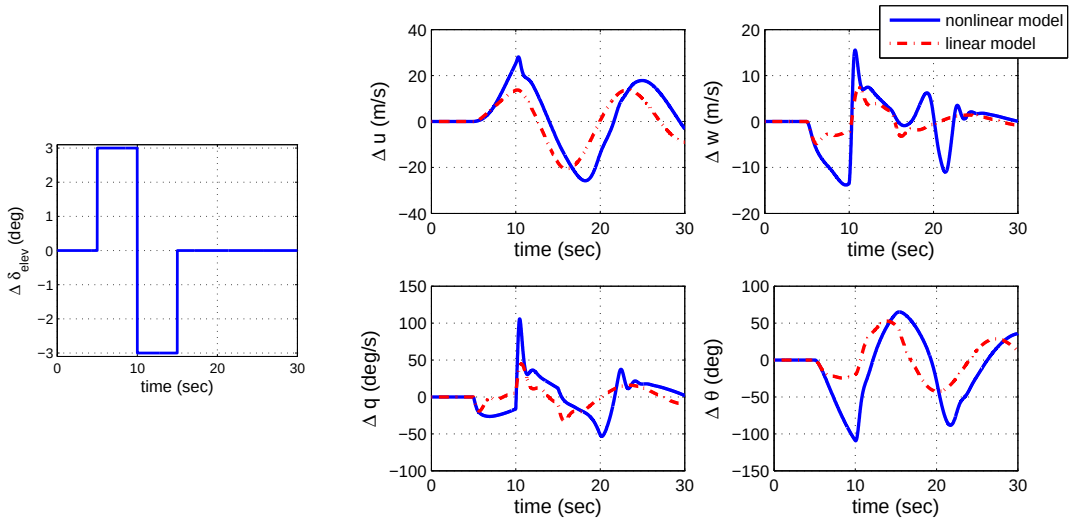

Figure 4.16: Nonlinear-linear model response to elevator doublet input

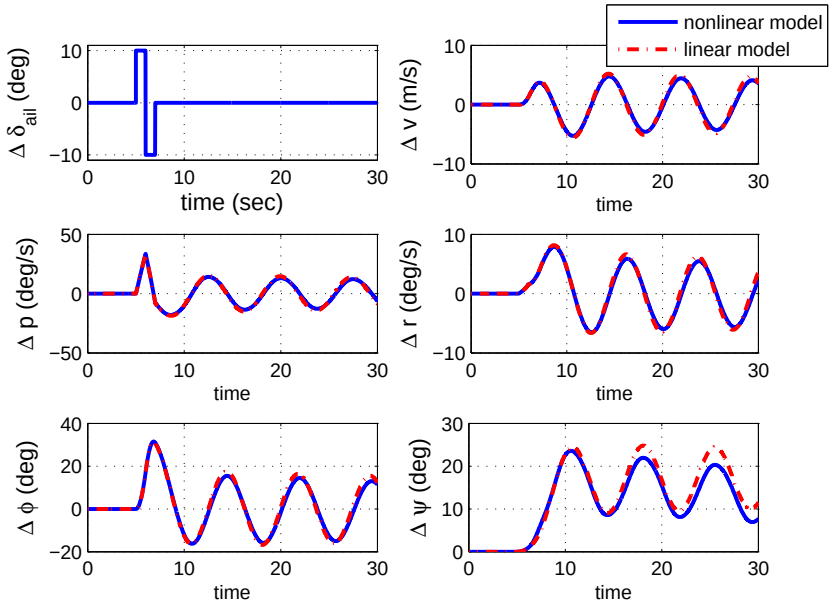

Figure 4.17: Nonlinear-linear model response to aileron doublet input

CHAPTER 5

CONTROL ALLOCATION

5.1 Introduction

In the thesis, one of the main scope is to address the allocation of the redundant controls mechanism of the tilt duct UAV in the transition mode. Since there are control surfaces and thrust systems that are interchangeable, the control system can be defined as redundant. The system is over actuated when all the controls are turned on which is the general case especially in the transition flight mode. Therefore, in addition to the feedback control system design, the control allocation problem shall also be addressed in the transition mode.

In this chapter, the redundant control system of tilt duct UAV is studied with a control allocation system which defines a relation between the control forces, moments and actual physical controls. Different allocation approaches are tried by the common aim to convert the required acceleration or forces input to propulsion, duct and control system input in the limit of the system capabilities.

The allocation methods tried in the thesis shall be defined as static solutions that are applied apart from the control system which are also used as particular solutions of instantaneous steering law techniques for control moment gyroscopes and robotic manipulators [45] [53]. For these mechanisms, static allocation techniques are preferable in the sense of avoiding singularities (gimbal angles at [-90°180°90°0°]) and they can be applied in aircraft systems in order to supply an authority on the controls to be within the surface or throttle limits and to behave in the desired way while allocating the redundant controls.

In this chapter, some control allocation methodologies are briefly described from the literature

with the general classifications and theories. After the control system of the UAV is explained, the approach of the allocation method in the transition control of the Tilt-Duct UAV is introduced. The comparison of the methodologies and related results are given in the following chapters with control analyses results.

5.2 Allocation Methodology

The control allocation methods in static sense are schematically shown in figure 1.3 for attitude control [45] [11]. These methods are developed for multilinkage robot arms and satellite attitude control with considerations to singularity transition avoidance. These approaches are also carried out in the control allocation of tilt duct UAV.

The methods given for the allocation are defined for a system with many physical controls serving same purposes to meet the requirements of the control forces and moments. The relation between the forces and moments and actual physical controls can be defined as in 5.1

$$u_1 = F\delta \tag{5.1}$$

5.2.1 Exact Solution Methods

5.2.1.1 Moore-Penrose Pseudo (MP) Inverse

Moore-Penrose Pseudo (MP) Inverse steering law is the basic method among the available steering laws. It is a simple algorithm but requires the Jacobian matrix to be non-singular. Therefore, this is a limiting factor for the usage of the system. In addition, with MP-inverse the allocation is not controllable.

$$\delta_{mp} = F^T[FF^T]^{-1}u_1 \tag{5.2}$$

5.2.1.2 Weighted Moore-Penrose Pseudo Inverse

Weighted form of the Moore-Penrose Pseudo(MP) Inverse helps to give weighings (by a defined 'Q') to each control surfaces. This approach allows to improve the authority on the allocation, however is still ineffective in passing or avoiding the singularities as in the case of MP method.

$$\delta_{wp} = Q^{-1}F^T[FQ^{-1}F^T]^{-1}u_1 \tag{5.3}$$

5.2.2 Transition Methods

5.2.2.1 Singular Robust (SR) Inverse

Singularity Robust (SR) steering law is developed for robotic manipulators to transit through certain type of singularities. Hence this method is used just for the singularity avoidance by the weight `S´in 5.4, not to supply an authority on the controls, it is not suitable for the control allocation on the over-actuated system.

$$\delta_{SR} = F^T[S + FF^T]^{-1}u_1 \tag{5.4}$$

5.2.2.2 Blended Inverse Method

This steering law blends the desired control surfaces satisfying the desired system accelerations and the required accelerations and leads an optimum selection for control inputs. By the weightings given to desired or the required input values, a reliable authority or control on the allocation system may be defined.

$$\delta_{Bi} = [qI_n + F^TRF]^{-1}[q\delta_{des} + F^TRu_1] \tag{5.5}$$

The blending coefficient `q´in 5.5 is usually taken as a scalar. In this manuscript the desired controls are taken as trim values at the given flight condition. To help controls stay in the

neighborhood of the trim values, and prevent them from saturating, the blending coefficient may be increased exponentially as the controls wander away from their desire values.

$$q = K_1 e^{\delta_{ierror}} \tag{5.6}$$

$$\delta_{i_{error}} = \frac{\delta_{i_{des}} - \delta_{i_{real}}}{\delta_{i_{des}}} \qquad R = Identity \tag{5.7}$$

The diagonal matrix q is a dynamically changed weighting according to the error between the desired and actual controls. The `R´weighting related to the required torque or force- moment values is taken as identity in this study.

5.3 Control Allocation for Tilt-Duct VTOL UAV

5.3.1 Over-Actuated Mechanism of the Controls

There are 8 main controls as input to the system which can be defined as equation 5.8.

$$u_{total} = \begin{bmatrix} \delta_{ThML}(\%max) \\ \delta_{ThMR}(\%max) \\ \delta_{ThAlon}(\%max) \\ \delta_{Duct}, \mu(deg) \\ \delta_{ThAlat}(\%max) \\ \delta_{Elev}(deg) \\ \delta_{Ail}(deg) \\ \delta_{Rud}(deg) \end{bmatrix} \tag{5.8}$$

However only few of them are used as main controls for hover and cruise as in equations 4.19 and 4.20. In transition, all these controls are switched on, except for the aerodynamic surfaces in very low speed conditions and aft throttle in high speed conditions. Translation control matrices are as in equations 4.14 and 4.17.

5.3.2 Control Allocation in Transition Mode

For the allocation mechanism in transition flight mode, first there is a need of defining the needed control accelerations (or forces) which are expected that the control surfaces will satisfy. The relation between these accelerations and control inputs can be defined by using 5.1 as 5.9.

$$Bu = B^{'} v \tag{5.9}$$

Here the vector v can be defined as the specific forces and moments on translational and rotational accelerations that are needed from the control surfaces as described in equation 5.10 and the $B^{'}$ matrix can be defined as identity. This is the main approach of the linear control system analyses.

$$v = \begin{bmatrix} a_x & a_y & a_z & \alpha_x & \alpha_y & \alpha_z \end{bmatrix} \tag{5.10}$$

Alternatively, as in the nonlinear control mechanism of the UAV, if the vector v is defined as forces that the control surfaces should satisfy, then the $B^{'}$ matrix can be referred as the one defined in chapter 7.

In line with these descriptions, the allocation algorithms can be rewritten as following equations.

$$u_{mp} = B^T [BB^T]^{-1} v \tag{5.11}$$

$$u_{wp} = Q^{-1} B^T [BQ^{-1} B^T]^{-1} v \tag{5.12}$$

$$u_{Bi} = [qI_n + B^T RB]^{-1} [qI_n u_{des} + B^T RB' v] \tag{5.13}$$

5.3.3 Determination of the Weightings in Allocation

The `Q matrix´in the weighted pseudo inverse method need to be determined. The **q weight** for blended inverse method can be identified as in equation 5.6. However a study to define the constant K_1 in equation 5.6 is needed here.

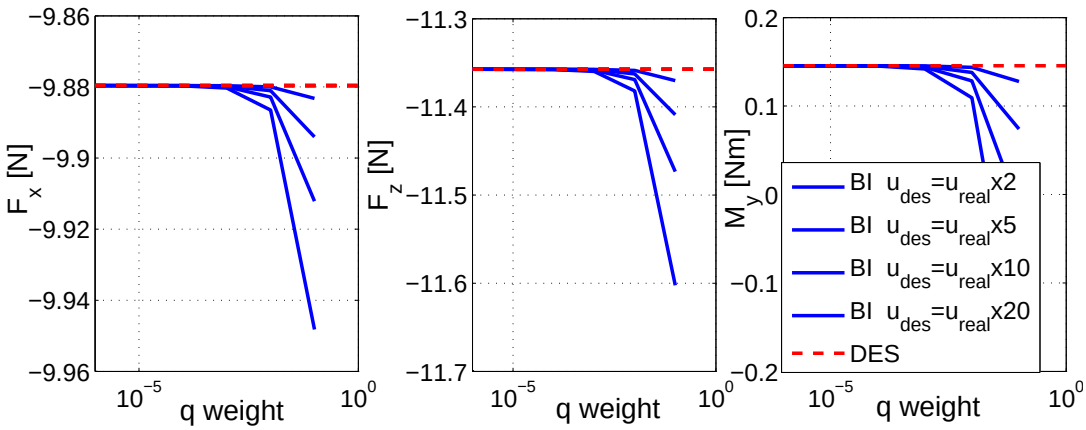

Figure 5.1: Study for estimation of blended inverse method q weighting in longitudinal

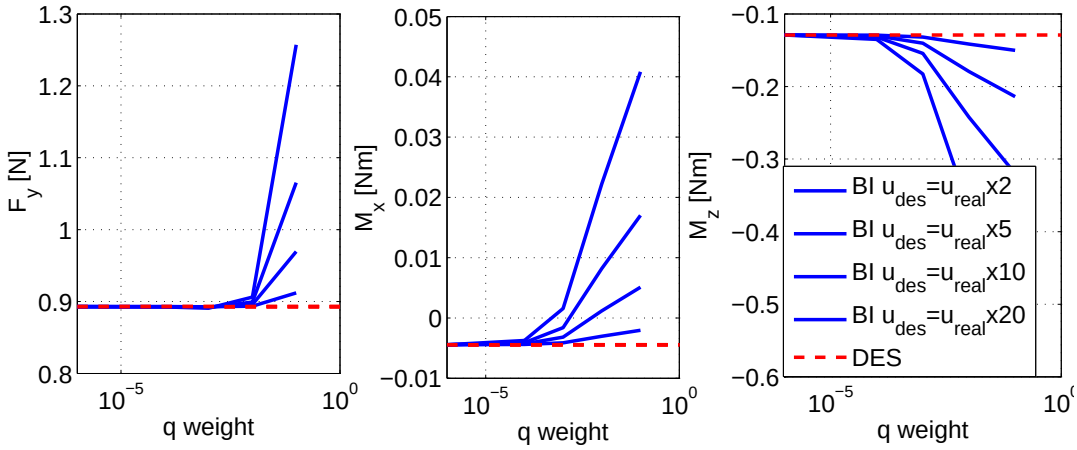

Figure 5.2: Study for estimation of blended inverse method q Weighting in lateral-directional

The example of a study to specify the q value in the allocation of longitudinal and lateral-directional controls can be given as in figures 5.1 and 5.2. Here the associated B, u_{des} (or u_{trim}), and F_{des} (or F_{trim}) around a trim condition in transition with 80 degrees duct and 5 m/s speed, are obtained. Then different desired values deviated by x2, x5, x10, x20 from the trim or desired input vectors are given to the allocation formulation to obtain the most suitable q value that gives back the actual or desired forces-moments.

As seen in the figures 5.1 5.2, the most convenient value for q is obtained to be around 10^{-4}, since for different values of the defined inputs to the system, this order of magnitude for q lets to obtain the actual forces or moments. This value can be taken as the K_1 term defined in 5.6. In case of the variation of the reference inputs deviated from actual ones, the term regarding

to the error is used as defined in equation 5.7.

Here since the weighting of required input is taken as a diagonal matrix consisting of the same value q in all the raws, then the element defined by the index i shall be chosen as one unique element of the control vector (for example the most critical one), or the norm of the errors for all elements of the control vector shall be used. In this thesis, during the transition control, this unique control input is selected to be the duct angle as a critical term that should be followed during transition and errors on this control is checked for allocation to be used in equation 5.7.

Another remark on the control allocation of the transition control is about the controller mechanism working for longitudinal and lateral both. Since the main throttle input (with differential effect) are effective for both longitudinal - lateral controls, the allocation is done separately to distribute the control authority on lateral controls and longitudinal controls and they are added to obtain the general control matrix 5.8.

CHAPTER 6

LINEAR CONTROLLER DESIGN

6.1 Introduction

Most of the control system theories revolve around linear systems, usually based on an assumption that the plant to be controlled and the controller itself are linear time-invariant (LTI) systems. Further they may be used for nonlinear systems through gain scheduling. This can be done by developing a transition scheme for the different operating points which are treated as equilibrium points around which the linearization is done before and validated to show the same response behavior as the nonlinear model.

In this chapter, first the linear controller is explained, the general system model structure is described with the inner and outer loop algorithms,the results are given for various controller modes of the linear automatic flight controller and results for different allocation types are also added for transition mode.

6.2 Linear Controller Methodology

Linear Controller Model is composed of an LQR control system in the inner loop and a classical control method designed as PID in the outer loop. A negative linear feedback is used. The control allocation is carried out in the inner loop with optional block changes due to different control allocation techniques.

6.2.1 Controllability and Observability

The controllability of a system is a necessary condition for the existence of a solution, since the goal is to transfer a system from an arbitrary initial state to the origin which is the main requirement of a controllable system [6].

In the thesis, controllability is always checked especially for the LQR approach (MIMO system).

The concept of observability is due to observing the output during a finite time interval and being able to determine the initial state.

In the thesis, observability is guaranteed since all the states are assumed to be physically measured and have a corresponding output.

6.2.2 PID Classical Control Method

A proportional-integral-derivative controller (PID) is a widely used method for the classical control approach with three separate gain parameters; the proportional, the integral and derivative terms as in 6.1 that are tried to be scheduled as a primary concern.

$$K_{PID}(s) = K_p + \frac{K_i}{s} + K_d s \tag{6.1}$$

The proportional term responds to the current error and provides instantaneous response. The integral term responds to the accumulation of errors and provides a slow response driving the steady-state error through 0. However it slows the response since the error must accumulate before the significant response of the controller. The derivative term responds to the rate at which the error is changing and provides some anticipatory and fast action as opposed to the integral action. It cannot accommodate constant errors, since they have nonzero error derivative as 0. [32]

In the thesis, while choosing the right poles or gains of the controller, trial - error approach and MATLAB© Simulink 'Optimization Technique : Signal Constraint' is used to obtain the desired time response characteristics like rise time, settling time (or time to peak), overshoot-undershoot behaviors as in Figure 6.1. [28]. The controller gains are also chosen to make

the system dynamics damped and fast enough, which also help to design where the general standards are not applicable or not sufficient.

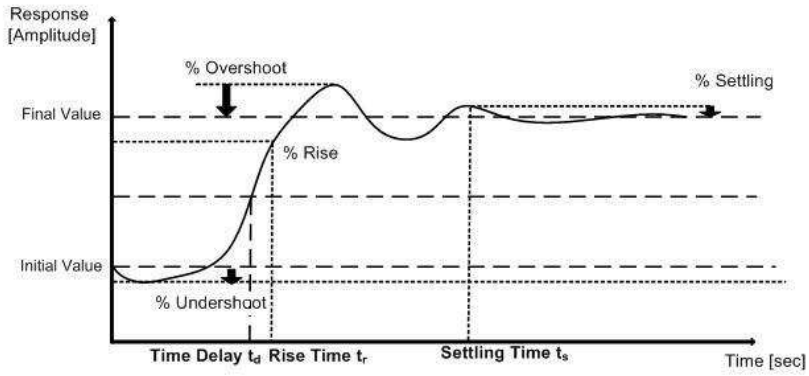

Figure 6.1: General time response characteristics for a step input

6.2.3 Linear Quadratic Regulator Problem

The case where the system dynamics are described by a set of linear differential equations as in 4.9 and the cost is described by a quadratic function is called ”LQ problem”. [47]. For a tracking control problem, system states are required to follow some desired state time history. This is also a generalization of the regulator control problem when the system is initiated from equilibrium and return to the equilibrium in such a manner so as to minimize a given performance cost.

6.2.3.1 Performance Measure

By defining a best applicable performance measure, the main aim is to determine an optimal control u, which leads to minimize the performance, $\bar{J}$ 6.2. [14] [64]

$$\bar{J} = \frac{1}{2}\int_0^\infty (x(t)^T Qx(t) + u(t)^T Ru(t))dt \tag{6.2}$$

The quadratic performance cost is required to characterize the system variables to perform in the desired way when minimized. Here Q (related with the energy of the states) and R

(related with the energy of the controls) are the diagonal positive semidefinite state penalty and positive semidefinite control penalty weighting matrices which are used for making the best choice for the way in keeping the state errors x(t) and respectively control corrections u(t) small. As an example, keeping state deviation penalty Q large means to obtain small state deviations at the expense of high control input values while minimizing $\bar{J}$.

6.2.3.2 Penalty Matrices

Q and R matrices can be determined by a simple approach as described by the `Bryson's Inverse Square Method' as defined in 6.3. By this method each state deviation or control is weighted by its possible maximum value. Therefore, by this rule, the cost J is scaled and maximum possible value for each term is taken as unit which is really important to bring the component of controls and state deviations to the same order.

$$Q = \left\{ q_{ii} = \frac{1}{q_{iMAX}^2} \right\}^n \qquad R = \left\{ u_{ii} = \frac{1}{u_{iMAX}^2} \right\} \tag{6.3}$$

6.2.3.3 Gain Matrix Determination

Optimal K matrix is obtained by 6.4 which is obtained by solving Ricatti equation 6.5.

$$K = R^{-1} B^T S \tag{6.4}$$

$$A^T S + SA - SBR^{-1} B^T S + Q = 0 \tag{6.5}$$

6.2.4 Command Filters

Commands filters in the controller are designed to be low pass filters in order to shape the command inputs depending on the aircraft dynamic characteristics and capabilities. For especially the transition mode controls these filters are preferred for a smooth transition of command change since this mode has a slow responsive behavior.

6.3 Linear Controller System for Tilt-Duct VTOL UAV

Block diagram of the linear controller model in Figure 6.2 describes the general structure which can be used for all modes of the aircraft. In the inner loop an LQR controller strategy is used as a SAS and feeding back all the states of a longitudinal or a lateral linear system. In the outer loop a PID controller scheme is used feeding back the output depending on the required control mode. The mechanism can be treated as an integral control plus state variable feedback. [7]

Separate block mechanisms for LQR and PID controllers built in MATLAB®-Simulink can be shown as in figures 6.3 and 6.4.

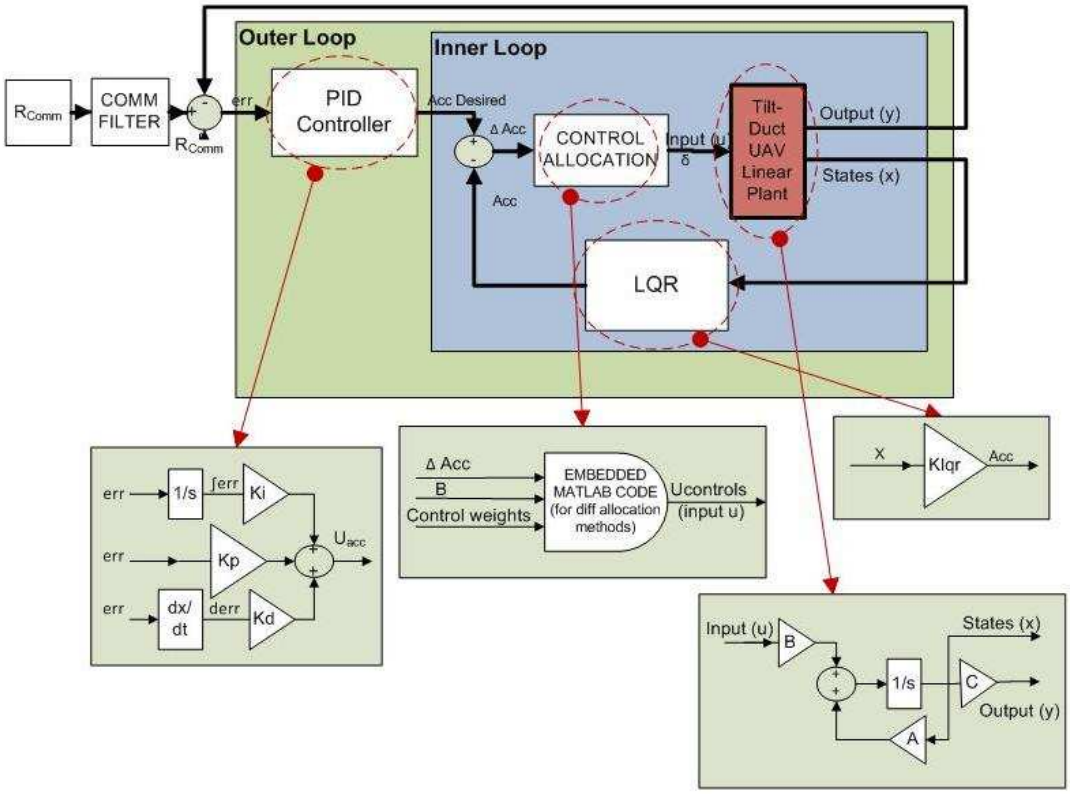

Figure 6.2: General block structure of linear controller

6.3.1 Inner Loop Linear Controller Algorithm

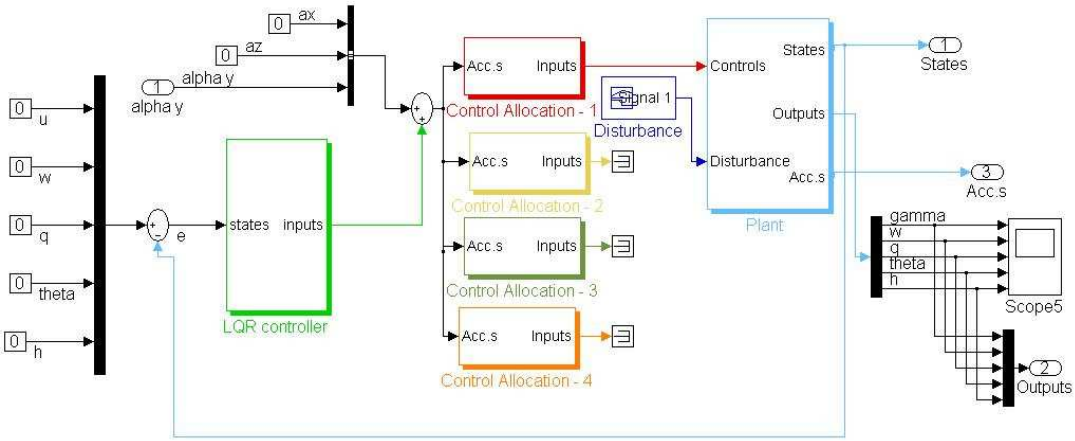

Figure 6.3: Inner loop SAS mechanism of the linear controller in longitudinal

6.3.1.1 LQR Controller and Gains

At each different flight mode, the LQR is solved for a fixed altitude regime (305 m-1000 ft) at different speeds using appropriate linearized system matrices and fixed control input weightings as given in equation 6.6, 6.8, and 6.10. In defining Q weighting the state for `altitude´is also added since the altitude state is also used in the linear control mechanism. The corresponding weights on the regulator are given below.

$$R_{hover,long} = \begin{bmatrix} 0.0001 & 0 & 0 \\ 0 & 0.0001 & 0 \\ 0 & 0 & 0.0001 \end{bmatrix} \quad R_{hover,lat} = \begin{bmatrix} 0.0001 & 0 & 0 \\ 0 & 0.0001 & 0 \\ 0 & 0 & 0.00025 \end{bmatrix} \tag{6.6}$$

$$R_{cruise,long} = \begin{bmatrix} 0.0001 & 0 \\ 0 & 0 \\ 0 & 0.000625 \end{bmatrix} \quad R_{cruise,lat} = \begin{bmatrix} 0.8163 & 0 \\ 0 & 0.4000 \\ 0 & 0 \end{bmatrix} \tag{6.7}$$

$$R_{transition,long} = \begin{bmatrix} 0.0065 & 0 & 0 \\ 0 & 0.0104 & 0 \\ 0 & 0 & 2.7431 \end{bmatrix} \quad R_{transition,lat} = \begin{bmatrix} 0.0866 & 0 & 0 \\ 0 & 0.0089 & 0 \\ 0 & 0 & 0.0801 \end{bmatrix} \tag{6.8}$$

$$Q_{long} = diag(\begin{bmatrix} 0.000025 & 0.000044 & 0.0001 & 0.0002 & 0.01 \end{bmatrix}) \tag{6.9}$$

$$Q_{lat} = diag(\begin{bmatrix} 0.000025 & 0.0002778 & 0.00015625 & 0.0002041 & 0.0025 \end{bmatrix}) \tag{6.10}$$

The solutions are obtained at small speed increments (1 m/s) in order to obtain exact solutions for all speed regime.

LQR Gains for Hover Mode

Table 6.1: Hover mode controller longitudinal LQR gains - altitude 305 m

Control Input	K_{lqru}	K_{lqrw}	K_{lqrq}	$K_{lqr\theta}$	K_{lqrz}
ThrML	-0.2100	-0.9577	29.5215	11.5155	-0.0566
ThrMR	-0.2100	-0.9577	29.5215	11.5155	-0.0566
ThrAlon	0.3995	-1.0277	-67.2354	-22.5761	-0.0600

Table 6.2: Hover mode controller lateral LQR gains - altitude 305 m

Control Input	K_{lqrv}	K_{lqrp}	K_{lqrr}	$K_{lqr\phi}$	$K_{lqr\psi}$
ThrML	-0.3534	-13.4521	-0.7759	-9.7386	-0.0564
ThrMR	-0.3534	-13.4521	-0.7759	-9.7386	-0.0564
ThrAlat	0.0319	3.2746	-62.3350	0.4788	-4.9975

LQR Gains for Cruise and Transition Modes

The gains for the LQR approach for cruise and transition modes are found at various speed values for 305 m (1000 ft) altitude and given in appendix F. Gains at different altitude conditions are also calculated. However it is observed that these gains do not change with altitude.

6.3.2 Outer Loop Linear Controller Algorithm

6.3.3 Structure of the Outer Loop

The controller in the outer loop is composed of a PID controller. The input-output mechanism and general structure of the loop is given in figure 6.4.

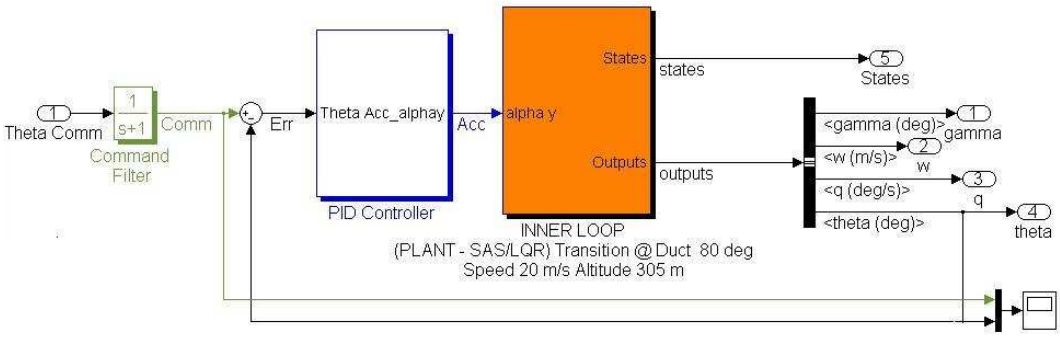

Figure 6.4: Outer loop PID control mechanism of the linear controller in theta-hold mode

6.3.4 PID Controller and Gains

Gain tuning for the PID Controller is done by means of MATLAB© Simulink 'Optimization Technique : Signal Constraint' and trial-error method, considering time response requirements. Due to the modes and conditions of the aircraft, the response characteristics are changing, so there is a need of updating gain tuning analysis for different modes of the aircraft, which means that in different modes, the system PID gains will change.

6.4 Results and Discussion

6.4.1 Hover Flight Mode

The PID gains used in this controller mode are listed in table 6.3.

The pitch-roll-yaw follower mechanisms are designed using the linear PID controller in the outer loop, and LQR controller in the inner loop. Since the system is unstable during hover, inner loop helps as a SAS system and stabilize the aircraft. In the figure 6.5 commanded

Table 6.3: Hover mode PID controller gains - 305 m altitude

	$K_{p\theta/ThML-R}$	$K_{d\theta/ThML-R}$	$K_{i\theta/ThML-R}$	$K_{p\theta/ThA}$	$K_{d\theta/ThA}$	$K_{i\theta/ThA}$
Theta Hold	0.9426	0.3708	3.6250	-182.6581	-364.3349	2.5823
	$K_{p\phi/ThML}$	$K_{d\phi/ThML}$	$K_{i\phi/ThML}$	$K_{p\phi/ThMR}$	$K_{d\phi/ThMR}$	$K_{i\phi/ThMR}$
Phi Hold	-17.3196	-53.1977	-9.0704	21.8965	55.6374	8.9183

	$K_{p\psi/ThMR}$	$K_{d\psi/ThMR}$	$K_{i\psi/ThMR}$
Psi Hold	-1.6910	-9.5460	-0.1055

attitude angles and controller responses are given. The responses of the controls inputs are also given in figure 6.4.1.

Figure 6.5: Commanded pitch-roll-yaw angle and the response in hover mode control

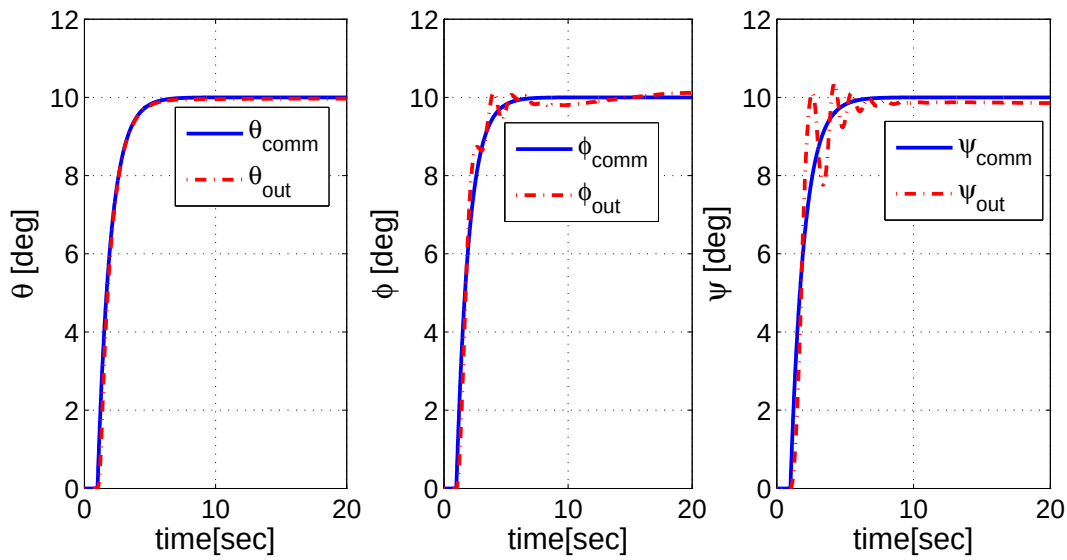

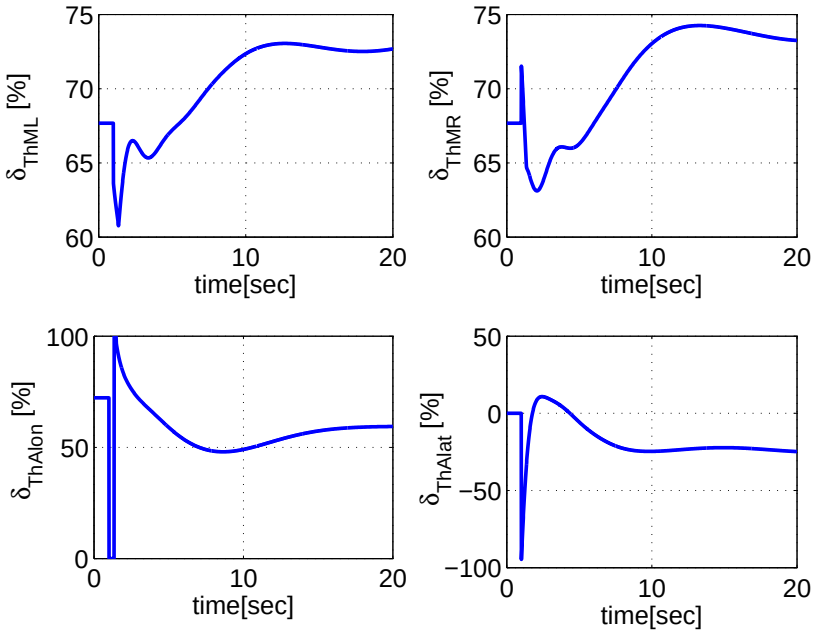

Figure 6.6: Control input response in hover control

The hover control mechanism is used with nonlinear model to test the system in case of horizontal, lateral and vertical gusts as given in figure 6.7. The simulation results are obtained as in figures 6.8, 6.9, and 6.10.

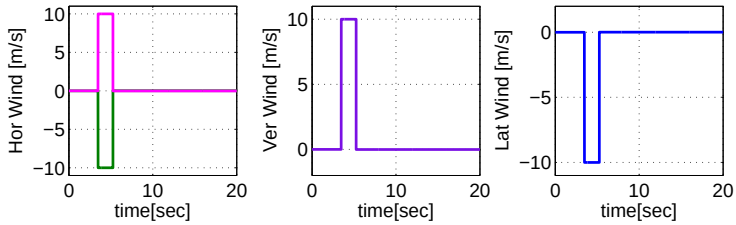

Figure 6.7: Wind gust conditions in hover mode control

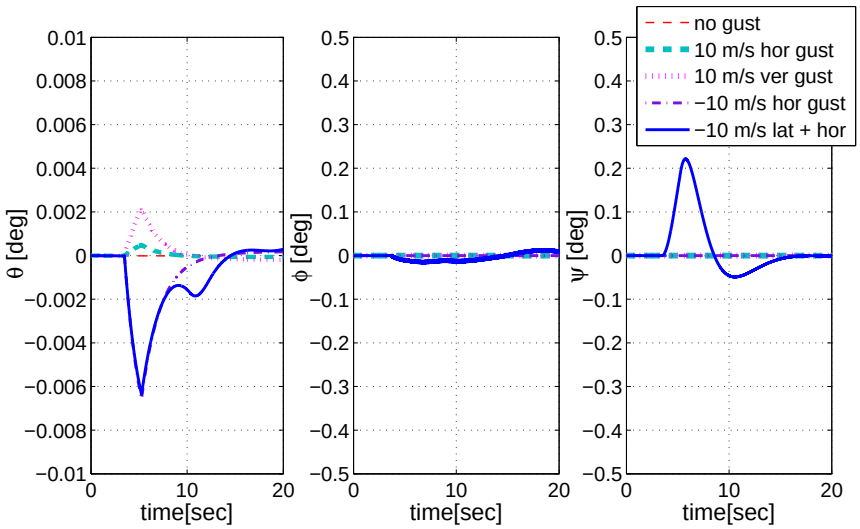

Figure 6.8: Commanded pitch-roll-yaw angle and the response for windy conditions in hover mode

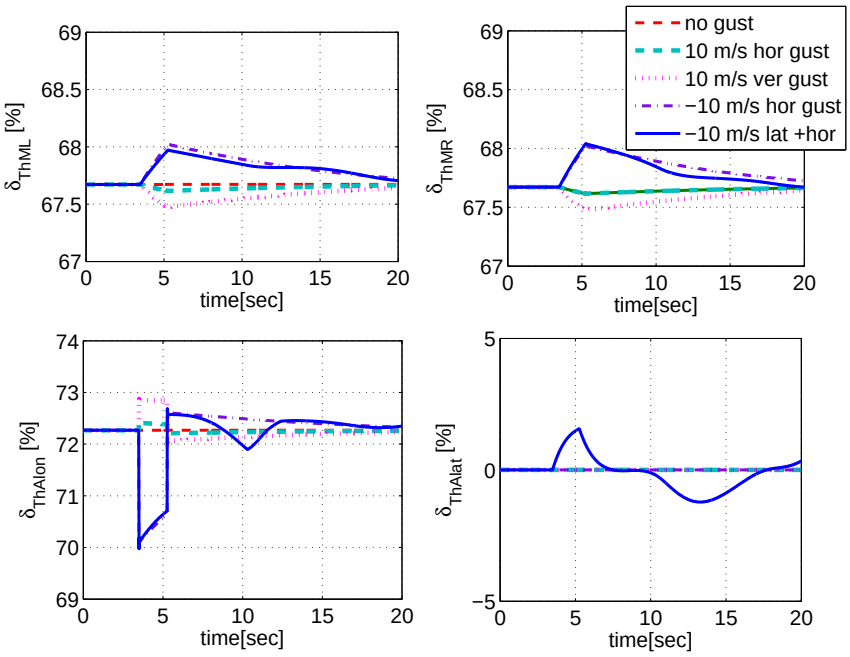

Figure 6.9: Responses as control input for windy conditions in hover mode control

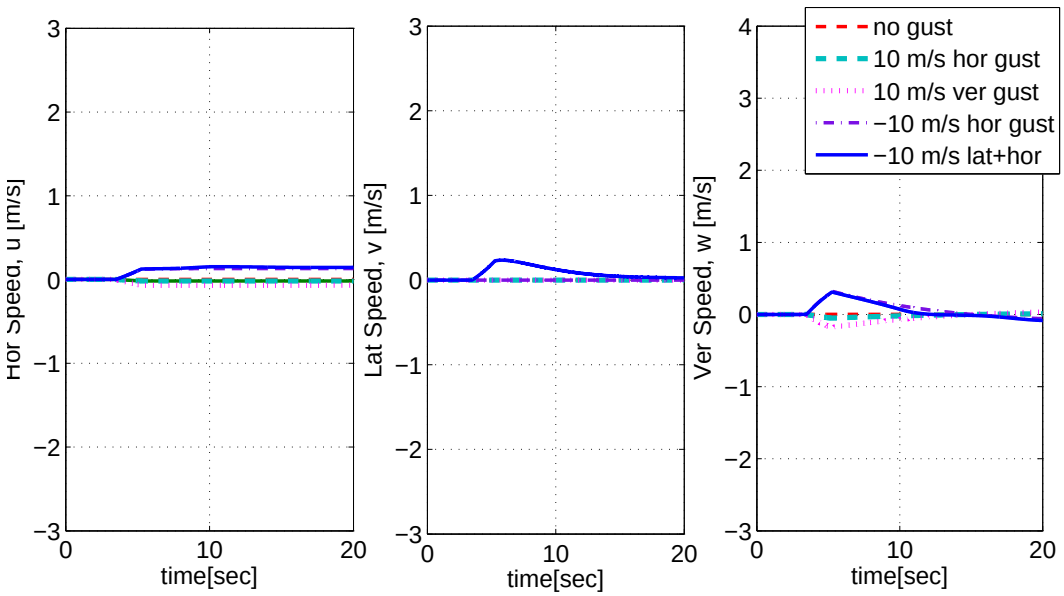

Figure 6.10: Results as speed components for windy conditions in hover mode control

6.4.2 Cruise Flight Mode

The PID gains used in this controller mode are obtained as shown in table 6.4

Table 6.4: Cruise mode controller gains - speed 60 m/s - altitude 305 m

	$K_{p\theta/ThMR}$	$K_{d\theta/ThMR}$	$K_{i\theta/ThMR}$
Theta Hold	-2.1399e+003	-0.0612	623.7996
	$K_{p\psi/Ail}$	$K_{d\psi/Ail}$	$K_{i\psi/Ail}$
Phi Hold	1	1	1
	$K_{p\psi/Rud}$	$K_{d\psi/Rud}$	$K_{i\psi/Rud}$
Psi Hold	0.8260	0.5866	0.2186
	$K_{p\psi/ThrML-R}$	$K_{d\psi/ThrML-R}$	$K_{i\psi/\delta ThrML-R}$
Hor. Speed Hold	47.4456	2.6152	37.5950
	$K_{p\psi/Elev}$	$K_{d\psi/Elev}$	$K_{i\psi/Elev}$
Altitude Hold	-0.6593	-0.2769	-2.0373

The control gains obtained for longitudinal and lateral hold mode in linear controllers are both used to control the nonlinear model, so gain scheduling is done around a cruise condition at 60 m/s speed and 305 m. altitude. Again the associated PID and LQR gains are used. In the cruise mode control the responses for altitude, speed, roll, yaw commands are given in figure 6.11, associated control input responses are also given in figure 6.12, the distances taken in the simulation are also shown in figure 6.13.

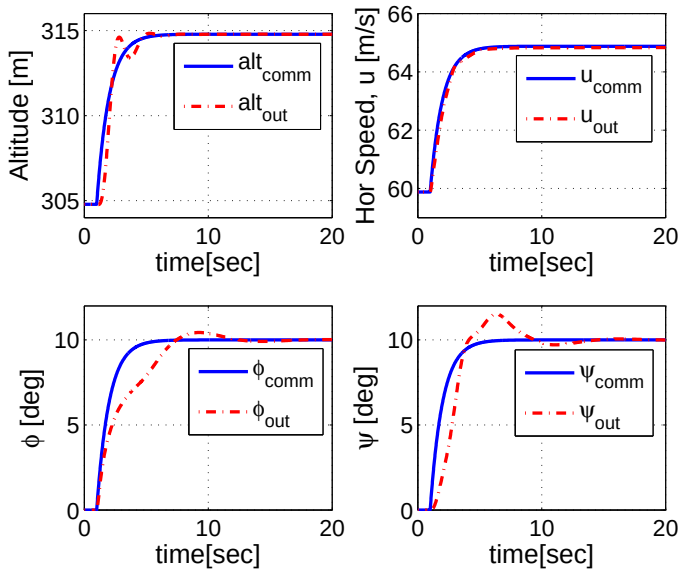

Figure 6.11: Commanded altitude-speed roll-yaw angle and responses in cruise mode control

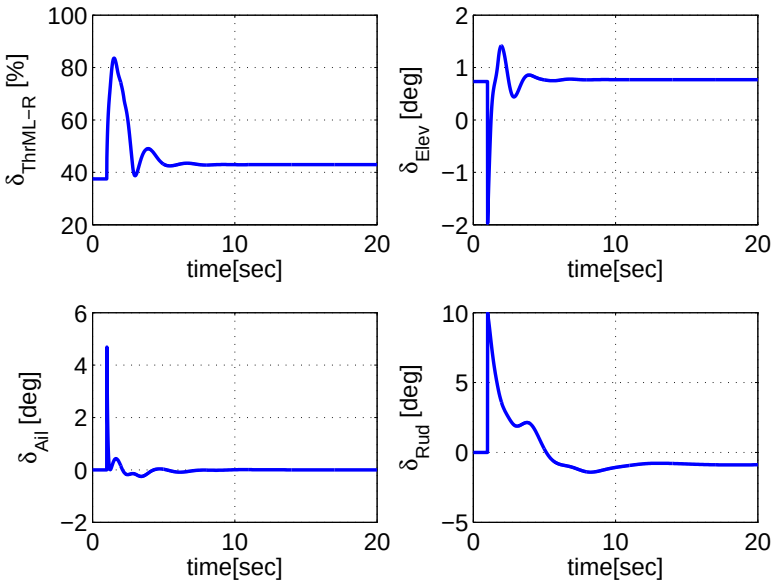

Figure 6.12: Control input responses in cruise mode control

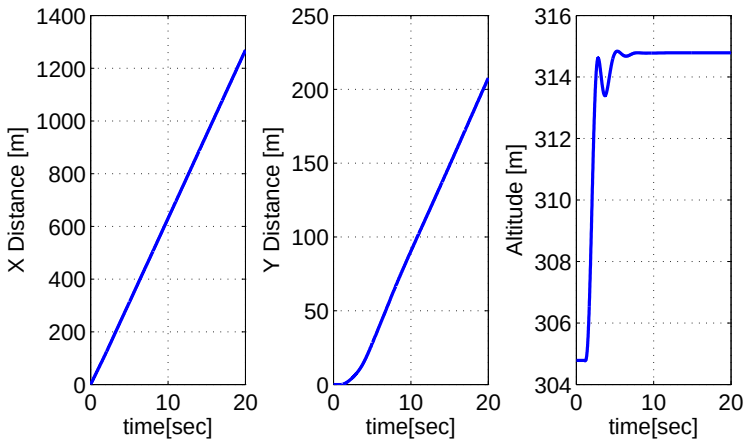

Figure 6.13: Longitudinal-lateral distance results in cruise mode control

6.4.3 Transition Flight Mode

The PID gains used in this controller mode are obtained as in table 6.5.

Table 6.5: Transition mode controller gains for the condition of ducts at 80 degrees, 5 m/s speed, 305 m altitude

	$K_{p\theta/\alpha_y}$	$K_{d\theta/\alpha_y}$	$K_{i\theta/\alpha_y}$
Theta Hold	5.62	1.639	45.02
	$K_{p\phi/\alpha_x}$	$d\phi/\alpha_x$	$K_{i\phi/\alpha_x}$
Phi Hold	1	1	1
	$K_{p\psi/\alpha_z}$	$K_{d\psi/\alpha_z}$	$K_{i\phi/\alpha_z}$
Psi Hold	22.043	7.636	3.5969
	$K_{p\psi/a_x}$	$K_{d\psi/a_x}$	$K_{i\phi/a_x}$
Hor. Speed Hold	10	1	5
	$K_{p\psi/a_z}$	$K_{d\psi/a_z}$	$K_{i\phi/a_z}$
Altitude Hold	30	1	10

6.4.3.1 Pitch Acquire Mode

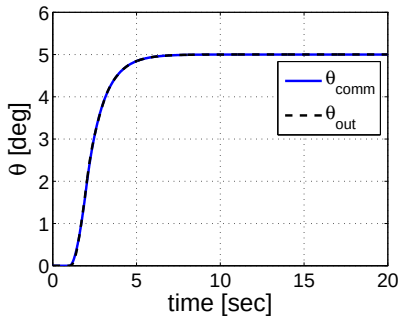

Figure 6.14: Linear controller pitch acquire mode inputs-outputs

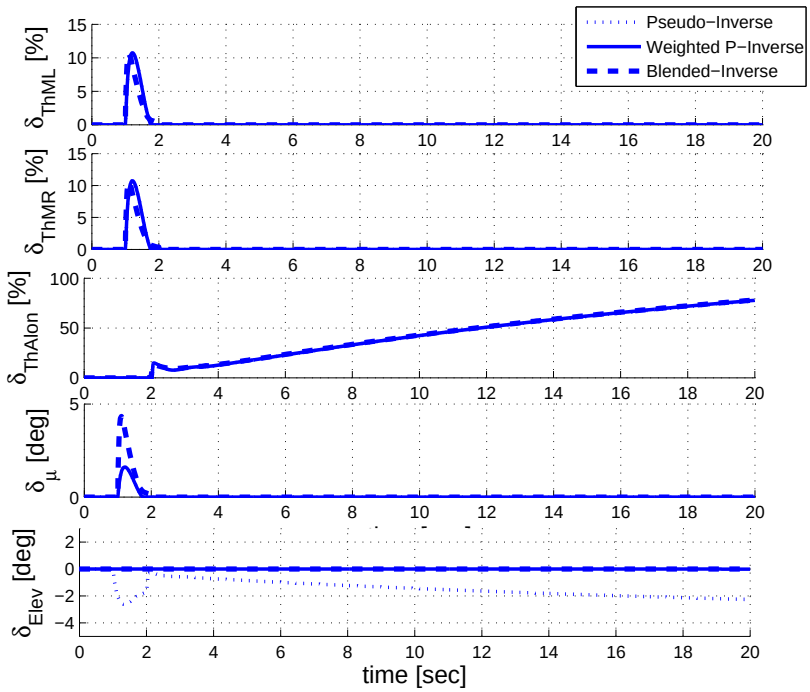

Figure 6.15: Linear controller pitch acquire mode control surfaces

In figure 6.14, the command and response of the controller for pitch acquire mode is given. Since the pitching control is being held in the transition regime very close to hover condition, the elevator input here is not very efficient. Instead the aft throttle shall be the dominant for an effective pitching control. This authority can only be enforced by the allocation methods of `Blended Inverse´, `SR Inverse' and `Weighted Pseudo Inverse´as seen in the control input responses shown in figure 6.15. Here so many weight configurations were tried for the `SR Inverse´and `Weighted Pseudo Inverse´, `Blended Inverse´was the easiest to apply.

6.4.3.2 Roll Acquire Mode

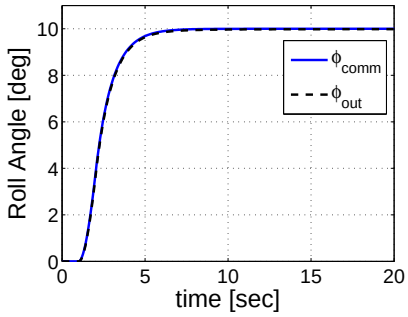

Figure 6.16: Linear controller roll acquire mode inputs-outputs

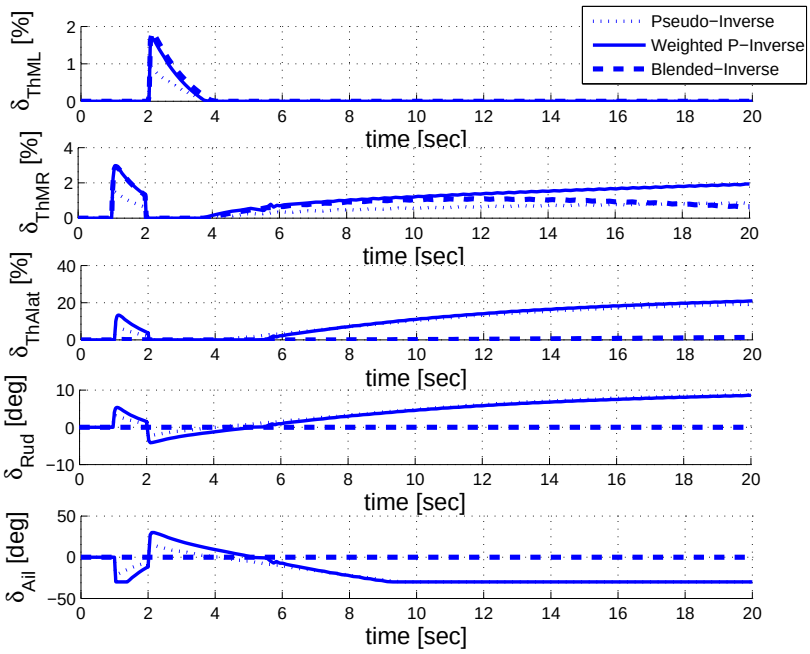

Figure 6.17: Linear controller roll acquire mode control surfaces

In figure 6.16, the command and response of the controller for roll acquire mode is given. Since the rolling control is being held in the transition regime very close to hover condition, the aerodynamic control surfaces here are not expected to be very efficient. Using the ``Blended Inverse´; the control is mainly allocated to the differential thrust instead of aileron as seen in the control input responses shown in figure 6.17.

6.4.3.3 Heading Acquire Mode

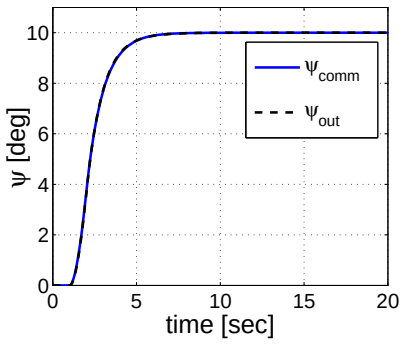

Figure 6.18: Linear controller heading acquire mode inputs-outputs

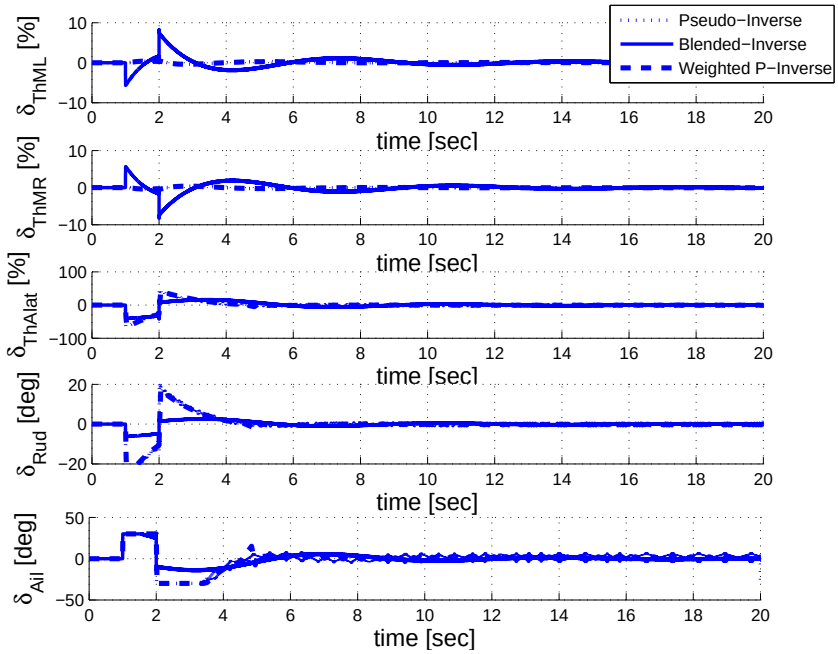

Figure 6.19: Linear controller heading acquire mode control surfaces

In figure 6.18, the command and response of the controller for heading acquire mode is given. In the yawing control, aerodynamic control surface effects can only be minimized by the `Blended Inverse´method. `Weighted Pseudo Inverse´and `MP Inverse´methods give very similar results as seen in the control input responses shown in figure 6.19.

6.4.3.4 Speed Acquire Mode

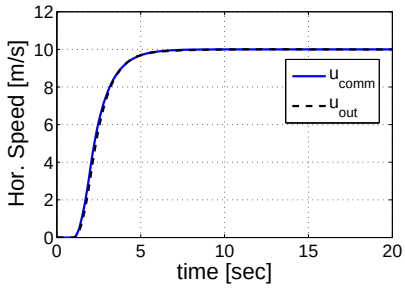

Figure 6.20: Linear controller horizontal speed acquire mode inputs-outputs

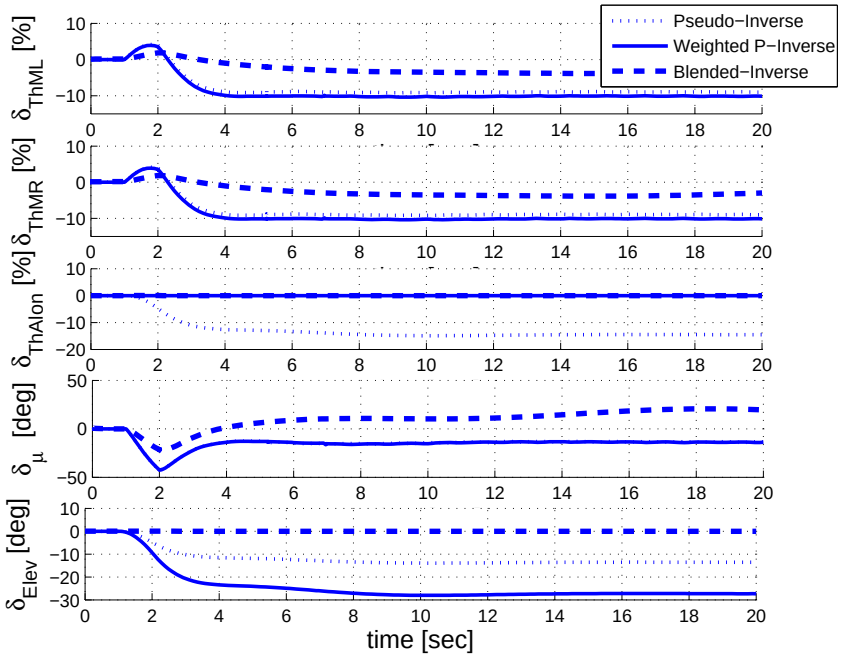

Figure 6.21: Linear controller horizontal speed acquire mode control surfaces

In figure 6.20, the command and response of the controller for speed hold mode is given. Here again with the 'Blended Inverse', elevator is easily excluded and throttle and duct controls can effectively be used as seen in the control input responses shown in figure 6.21.

6.4.3.5 Altitude Hold Mode

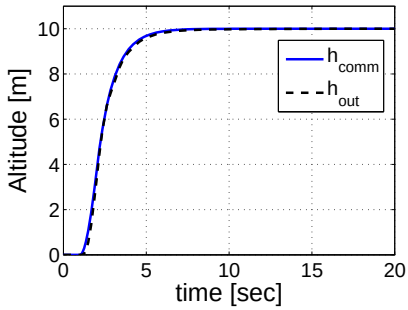

Figure 6.22: Linear controller horizontal altitude-hold mode inputs-outputs

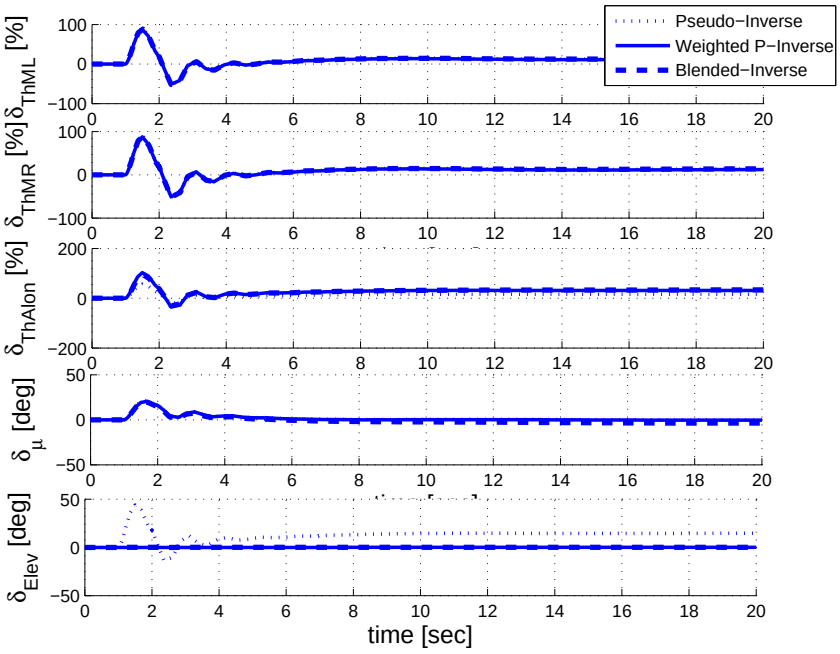

Figure 6.23: Linear controller horizontal altitude-hold mode control surfaces

In figure 6.22, the command and response of the controller for altitude hold mode is given. In altitude hold mode, `Weighted Pseudo Inverse´result showed the same characteristics, whereas the `Blended Inverse´was again effective to exclude aerodynamic control surface as seen in the control input responses shown in figure 6.23.

The results of the linear control trials around a fixed transition condition (with the duct at 80 degrees) has shown that:

- `Pseudo Inverse´method is not a sufficient control allocation method since an authority by weightings or the inputs of desired values cannot be applied.
- `Weighted Pseudo Inverse´method is more acceptable to have a control authority in the expected way, however it requires a weight tuning study which may not be efficient to control all the transition flight conditions of the UAV.
- `Blended Inverse´is the most efficient method to control the over-actuated mechanism in transition mode. In this method, defined in equation 5.5, the desired control input values should be introduced in order to obtain the best results giving the desired control response. Although the desired control responses are given with a general symbolic representations consisting of zeros or ones, the results are over expectations. This method is considered as the most efficient way to control an over-actuated control system and for the rest of the analyses, this method is used.

According to the linear control studies, the following may be concluded:

- In the controller mechanisms, the inputs are smoothed by the command filter and actuator effects are neglected. In some controller modes the response of the system exactly coincides with the input. The main reason of this characteristic is due to these assumptions and the SAS system in the inner loop enhancing the system control characteristics.
- In hover mode, the attitude controllers are used and they are observed to be sufficient for the needed control responses and to supply a necessary hovering characteristics during various severe gust conditions.
- The controller responses are checked in terms of the required military response characteristics [21]. Since responses always show characteristics with at least %20 overshoot and below 1 sec. rise time and 5 sec. settling time, they are defined as acceptable. In cruise mode, the steady errors for lateral attitude controls were late to converge to 0 because of the weakness of the system lateral maneuver capabilities.
- The transition control is made around one unique trim point, with the primary aim to observe and compare the effects of allocation methods in transition control. Due to the comparisons, blended inverse method is defined to be the most efficient method to allocate the controls during transition.

CHAPTER 7

NONLINEAR CONTROLLER DESIGN

7.1 Introduction

Autonomous transition control of VTOL UAV system presents a challenging task, since the system is highly nonlinear as well as unstable. In addition operation under severe wind and gust disturbances adds additional difficulties.

In this thesis, a nonlinear control method is used for the transition mode control, since the linear control approaches are insufficient to deal with the instabilities and nonlinearities during this mode. The linear controller for a system defined around a unique state, using fixed or changing controller gains is hard to develop and is observed to be ineffective to realize stability as well as sufficient performance.

Therefore, a *`State-Dependent Nonlinear Controller´* design of the nonlinear Tilt-Duct UAV is carried out. The controller gains are calculated from the solution of the State-Dependent Riccati Equation (SDRE), with the aim of developing a nonlinear controller algorithm capable of successfully operating transition flight phase and lead to apply solutions for the control allocation problem.

In this chapter, first, the State-Dependent Ricatti Equation (SDRE) based controller methodology is explained in detail with the theory, in the second part the approach of the SDRE method on the control of Tilt Duct UAV is presented. The results are given in the third part for different transition regimes.

7.2 State Dependent Ricatti Equation Controller Method

The main approach of the SDRE technique is manipulating the system dynamic equations into a linear-like and state-dependent coefficient form in which system matrices are given explicitly as a function of the current state as in equation 7.1.

$$\dot{x} = f(x) + B(x)u, \quad x(0) = x_0 \tag{7.1}$$

A direct parameterization is made to bring the nonlinear dynamics of equation 7.1 to the state dependent coefficient (SDC) form by defining equation 7.2. There are many different ways to factor such an SDC matrix form since the states f(x) is assumed to be a continuously differentiable function of x.

$$f(x) = A(x)x \tag{7.2}$$

This approach is alternatively called as `apparent linearization´, `extended linearization´or most recently `state dependent coefficient SDC factorization´.

The technique is like the nonlinear counterpart of LQR based controller, except that the system matrices A(x), B(x) and the weighting matrices Q(x), R(x) are functions of the states. The aim of the controller design is again to find a control u minimizing the performance index in equation 6.2 but in a state dependent form as in equation 7.3 that is subjected to the system as equation 7.1. [36]

$$\bar{J} = \frac{1}{2}\int_0^\infty (x(t)^T Q(x)x(t) + u(t)^T R(x)u(t))dt, \quad Q(x) \geq 0; R(x) > 0 \tag{7.3}$$

In this `nonlinear regulator problem´,the weighting penalties Q(x) and R(x) must be positive-semidefinite and positive-definite respectively.

While defining the SDC parametization, for a valid solution it is important to notice that the pair A(x),B(x) has to be pointwise stabilizable, and detectable in the linear sense for all x in the domain of interest. For scalar systems, the SDC parameterization will be unique for all x≠0 as stated in equation 7.4 [19]. For multivariable problems the f(x)term in equation 7.1 is

also dependent on at least two state components; x_1 and x_2 so the parameterization becomes as a nonlinearity of equation 7.5 as coefficients of x_1 and x_2. Then defining the corresponding SDC matrices as A_1 and A_2, equation 7.6 is also an SDC parameterization for any α showing that there are an infinite family of such representation for a multivariable system.[67]

$$a(x) = \frac{f(x)}{x} \tag{7.4}$$

$$a_{1i}(x) = \frac{f_i(x)}{x_1} \quad a_{2i}(x) = \frac{f_i(x)}{x_2} \tag{7.5}$$

$$A(x, \alpha) = \alpha A_1(x) + (1 - \alpha)A_2(x) \tag{7.6}$$

After obtaining the SDC form, the *Algebraic State Dependent Riccati Equation* (equation 7.7) is solved for P(x) in order to construct the nonlinear feedback controller equation 7.8 and after solving P(x) from the equation 7.7.

$$P(x)A(x) + A^T P(x) - P(x)B(x)R^{-1}(x)B^T(x)P(x) + Q(x) = 0 \quad P(x) \geq 0 \tag{7.7}$$

$$u = -R(x)^{-1}B(x)^T P(x)x \tag{7.8}$$

The greatest advantage of this method is that it provides an effective algorithm for synthesizing nonlinear feedback control that allows nonlinearities in the system states and ´´allows a design flexibility of tuning the system matrices and input weighting matrices, which increases the intuitive on the behavior of the system and also softens the classical state-error vs. input tradeoff´´[39].

The SDRE controlled closed-loop system is known to be locally asymptotically stable. Global stability, as opposed to linear systems, is more difficult to be proven and having stable eigenvalues in the whole state space does not guarantee global asymptotic stability [39]. In addition, with the SDRE approach, system controllability may be lost if the SDC matrices are not properly chosen. This property of the approach can be improved due to flexibility of the SDC matrices as shown in equation 7.6. [24].

7.3 SDRE State Feedback Regulator for Tilt-Duct UAV

7.3.1 Tilt-Duct UAV Nonlinear Controller Structure

Block diagram of the nonlinear state-feedback controller model applicable to the transition mode of the UAV is generally as in the figure 7.1 and a detailed description with inclusion of gravity effects and detailed loop feedback solutions are as seen in the figure 7.2. The system is again composed of inner and outer loops that is designed to improve the controllability of the system. The outer loop defines the needed inputs to the inner loop system as Euler angles defined by the kinematic Euler equations. In the inner loop, the needed control forces and moments are obtained and given through the allocation system, which uses *`Blended Inverse Method´* and computes the needed control inputs which are given to the nonlinear model.

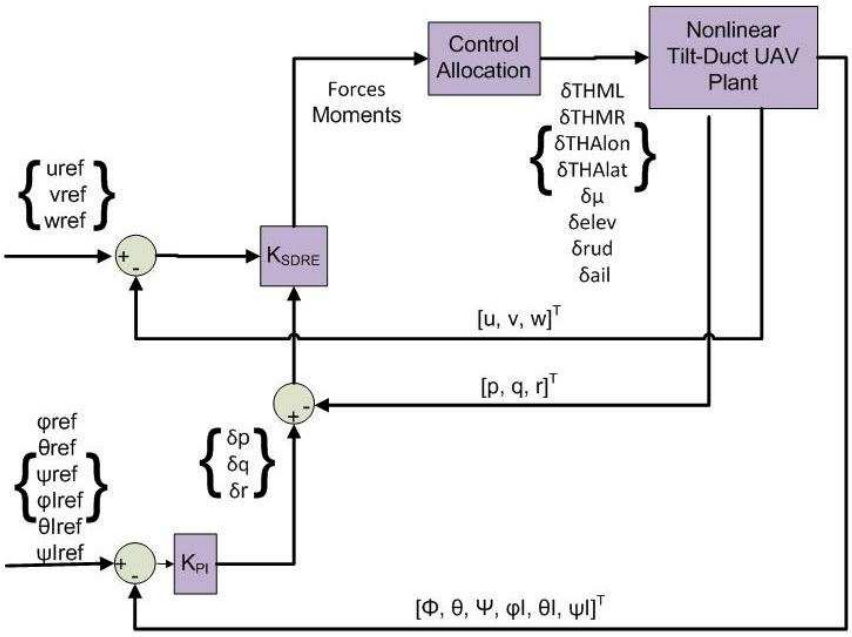

Figure 7.1: General structure of the SDRE controller

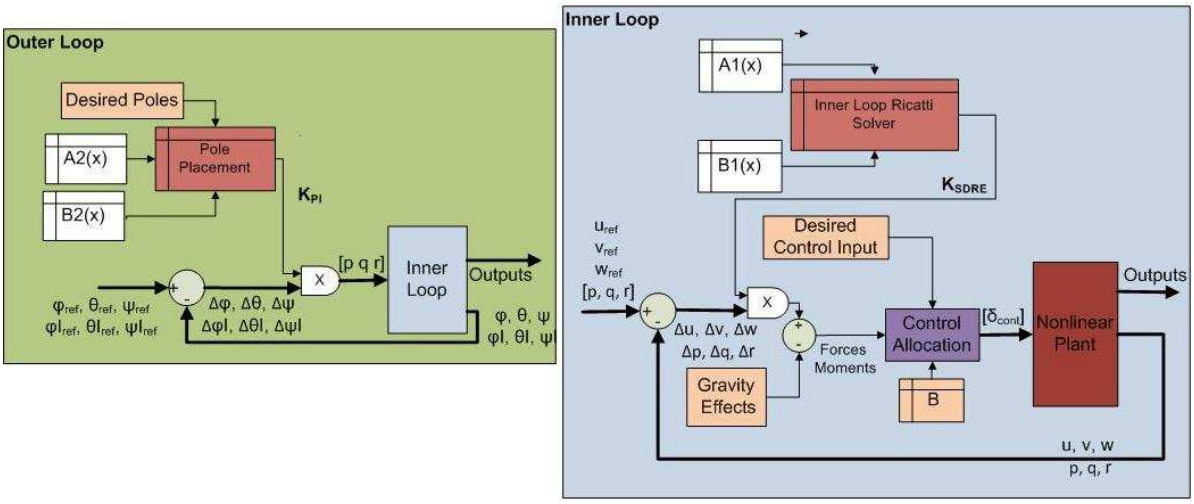

Figure 7.2: Inner loop - outer loop detailed structures

7.3.2 Extended Linearization SDC Matrices

By a general definition of the SDRE method, the state-dependent system can be defined as in equation 7.9.

$$\dot{x} = A(x)x + B(x)u \tag{7.9}$$

The system is divided in two loops which means two different A, B matrices will be defined. Therefore, two different system identifications are done as inner and outer loops defined in 7.10 and 7.11.

$$\dot{x}_{inner} = \dot{x}_1 = A_1(x)x_1 + B_1u_1 \tag{7.10}$$

$$\dot{x}_{outer} = \dot{x}_2 = A_2x_2 + B_2(x)u_2 \tag{7.11}$$

7.3.2.1 Inner Loop Dynamics

The inner loop states and outputs in system (equation 7.10) are designed to be as equations 7.12 and 7.13.

$$x_{inner} = x_1 = \begin{bmatrix} u & v & w & p & q & r \end{bmatrix}^T \tag{7.12}$$

$$u_{inner} = u_1 = \begin{bmatrix} F_x & F_y & F_z & M_x & M_y & M_z \end{bmatrix}^T \tag{7.13}$$

The derivations for the SDC matrices for inner loop are due to the kinematic and dynamical general equations of motion of an aircraft, which yields the resultant equations 7.14 and 7.15 for translational-rotational accelerations.

$$\dot{u} = \frac{X}{-}wq + vr - gsin\theta$$

$$\dot{v} = \frac{Y}{m} - uq + wp + gcos\theta sin\phi$$

$$\dot{w} = \frac{Z}{m} - vp + uq + gcos\theta cos\phi$$

$$\dot{p} = I_1L + I_2N + I_3(qr) + I_4(pq)$$

$$\dot{q} = \frac{M}{I_{yy}} - \frac{(I_{xx} - I_{zz})}{I_{yy}}(pr) + (p^2 - r^2)\frac{I_{xz}}{I_{yy}}$$

$$\dot{r} = I_2 L + I_5 N + I_6(pq) - I_4(qr) \tag{7.14}$$

$$I_1 = \frac{I_{zz}}{I_{num}} \qquad I_4 = \frac{(I_{xx} - I_{yy} + I_{zz})I_{xz}}{I_{num}}$$

$$I_2 = \frac{I_{xz}}{I_{num}} \qquad I_5 = \frac{Ixx}{I_{num}}$$

$$I_3 = \frac{(I_{yy} - I_{zz})I_{zz} - I_{xz}^2}{I_{num}} \qquad I_6 = \frac{(I_{xx} - I_{yy})I_{xx} + I_{xz}^2}{I_{num}}$$

$$I_{num} = I_{xx}I_{zz} - I_{xz}^2 \tag{7.15}$$

The forces defined (7.14) can be expressed as aerodynamic forces and forces due to controls that also includes thrust effects. The simplification in equation 7.16 ignores the small derivative effects (like vertical speed effect on X force).

$$\frac{X}{m} = \frac{X_u}{m}u + \frac{X_w}{m}w + \frac{X_q}{m}q + \frac{X_c}{m} \qquad R = R_u u + R_v v + R_p p + R_r r + R_c$$

$$\frac{Y}{m} = \frac{Y_u}{m}u + \frac{Y_v}{m}v + \frac{Y_p}{m}p + \frac{Y_r}{m}r + \frac{Y_c}{m} \qquad \frac{M}{I_{yy}} = \frac{M_u}{I_{yy}}u + \frac{M_w}{I_{yy}}w + \frac{M_q}{I_{yy}}q + \frac{M_c}{m}$$

$$\frac{Z}{m} = \frac{Z_u}{m}u + \frac{Z_w}{m}w + \frac{Z_q}{m}q + \frac{Z_c}{m} \qquad N = N_u u + N_v v + N_p p + N_r r + N_c \tag{7.16}$$

The mentioned force derivatives in lateral-longitudinal directions are expressed in terms of all the related flight parameters for the SDC inner loop state matrix $A_1(x)$ in equation 7.17.

$$X_u = \frac{C_X \overline{q} S}{2u}, \quad X_w = \frac{C_X \overline{q} S}{2w}, \quad X_q = \frac{C_{Xdyn} \overline{q} S}{q}$$

$$Y_u = \frac{C_Y \overline{q} S}{2u}, \quad Y_v = \frac{C_Y \overline{q} S}{2v}, \quad Y_p = \frac{C_{Ydyn} \overline{q} S}{2p}, \quad Y_r = \frac{C_{Ydyn} \overline{q} S}{2r}$$

$$Z_u = \frac{C_Z \overline{q} S}{2u}, \quad Z_w = \frac{C_Z \overline{q} S}{2w}, \quad Z_q = \frac{C_{Zdyn} \overline{q} S}{q}$$

$$R_u = \frac{C_R \overline{q} S}{3u}, \quad R_v = \frac{C_R \overline{q} S}{3v}, \quad R_p = \frac{C_{Rdyn} \overline{q} S}{2p} \quad R_r = \frac{C_{Rdyn} \overline{q} S}{2r}$$

$$M_u = \frac{C_M \overline{q} S}{2u}, \quad M_w = \frac{C_M \overline{q} S}{2w}, \quad M_q = \frac{C_{Mdyn} \overline{q} S}{q}$$

$$N_u = \frac{C_N \overline{q} S}{2u}, \quad N_v = \frac{C_N \overline{q} S}{2v}, \quad N_p = \frac{C_{Ndyn} \overline{q} S}{2p}, \quad N_r = \frac{C_{Ndyn} \overline{q} S}{2r} \tag{7.17}$$

Resultant $A_1(x)$ and B_1 inner loop system matrices are summarized in equations 7.18 and 7.19.

$$A_1(x) = \begin{bmatrix} \frac{X_u}{m} & \frac{r}{2} & \frac{X_w}{m} + \frac{q}{2} & 0 & \frac{X_q}{m} - \frac{w}{2} & \frac{v}{2} \\ \frac{Y_u}{m} - \frac{q}{2} & \frac{Y_v}{m} & -\frac{u}{2} & \frac{Y_p}{m} + \frac{w}{2} & \frac{p}{2} & \frac{Y_r}{m} \\ \frac{Z_u}{m} + \frac{q}{2} & -\frac{p}{2} & \frac{Z_w}{m} & -\frac{v}{2} & \frac{Z}{m} + \frac{u}{2} & 0 \\ I_1R_u + I_2N_u & I_3\frac{r}{2} + I_4\frac{p}{2} & 0 & I_1R_p + I_2N_p + I_4\frac{q}{2} & I_1R_v + I_2N_v & I_1R_r + I_2N_r + I_3\frac{q}{2} \\ \frac{M_u}{Iyy} & 0 & \frac{M_w}{Iyy} & \frac{(Izz-Ixx)}{Iyy}p + \frac{Ixz}{Iyy}r & \frac{M}{Iyyq} & \frac{(Izz-Ixx)}{Iyy}p - \frac{Ixz}{Iyy}r \\ I_5N_u + I_2R_u & I_6\frac{p}{2} - I_4\frac{r}{2} & 0 & I_5N_p + I_2R_p + I_6\frac{q}{2} & I_5N_v + I_2R_v & I_5N_r + I_2R_r - I_4\frac{q}{2} \end{bmatrix} \tag{7.18}$$

$$B_1 = \begin{bmatrix} \frac{1}{mass} & 0 & 0 & 0 & 0 & 0 \\ 0 & \frac{1}{mass} & 0 & 0 & 0 & 0 \\ 0 & 0 & \frac{1}{mass} & 0 & 0 & 0 \\ 0 & 0 & 0 & I_1 & 0 & I_2 \\ 0 & 0 & 0 & 0 & \frac{1}{Iyy} & 0 \\ 0 & 0 & 0 & I_2 & 0 & I_5 \end{bmatrix} \tag{7.19}$$

The inertia parameters are defined in equation 7.15.

7.3.2.2 Outer Loop Dynamics

The outer loop states and outputs are designed to be as in equations 7.20 and 7.21. Since this loop is controlled with a simple pole-placement method, the integral states are also added to prevent steady-state error.

$$x_{outer} = x_2 = \begin{bmatrix} \phi & \theta & \psi & \phi_I & \theta_I & \psi_I \end{bmatrix}^T \tag{7.20}$$

$$u_{outer} = u_2 = \begin{bmatrix} p & q & r \end{bmatrix}^T \tag{7.21}$$

The outerloop system can be rewritten as in equation 7.11. As explained previously, since the SDRE is not applied to the outer loop, A_2 matrix is not written in terms of the states, instead, B_2 matrix is state-dependent and created due to the Euler angle kinematic relations given in equation 3.46. The derivation of the SDC matrices in the outer loop is done as in equation 7.22. Since pitch attitude (θ) is not expected to reach 90 degree, the formulation will be useful throughout the transition mode.

$$\begin{Bmatrix} \dot{\phi} \\ \dot{\theta} \\ \dot{\psi} \\ \dot{\phi}_I \\ \dot{\theta}_I \\ \dot{\psi}_I \end{Bmatrix} = \begin{bmatrix} 0 & 0 & 0 & 0 & 0 & 0 \\ 0 & 0 & 0 & 0 & 0 & 0 \\ 0 & 0 & 0 & 0 & 0 & 0 \\ 1 & 0 & 0 & 0 & 0 & 0 \\ 0 & 1 & 0 & 0 & 0 & 0 \\ 0 & 0 & 1 & 0 & 0 & 0 \end{bmatrix} \begin{Bmatrix} \phi \\ \theta \\ \psi \\ \phi_I \\ \theta_I \\ \psi_I \end{Bmatrix} + \frac{1}{cos\theta} \begin{bmatrix} cos\theta & sin\theta sin\phi & sin\theta cos\phi \\ 0 & cos\theta cos\phi & -cos\theta sin\phi \\ 0 & sin\phi & cos\phi \\ 0 & 0 & 0 \\ 0 & 0 & 0 \\ 0 & 0 & 0 \end{bmatrix} \begin{Bmatrix} p \\ q \\ r \end{Bmatrix} \tag{7.22}$$

7.3.3 Control Allocation in SDRE State Feedback Regulator

Control Allocation approach is done in SDRE Controller as described in chapter 4. However according to the results of linear control analysis the most effective `Blended Inverse Method´is used. The allocation method uses the control forces, desired control inputs and the actual B matrix which can also be obtained online. This control matrix is calculated by using the linearization equation in 7.24 for matrix B at each time step. The control vector is defined as in equation 7.23 in order to avoid singularities due to the duct angle values.

$$u = \begin{bmatrix} \delta_{ThMLlon} & \delta_{ThMRlon} & \delta_{ThMLlat} & \delta_{ThMRlat} & \delta_{ThAlon} & \delta_{ThAlat} & \delta_{Elev} & \delta_{Ail} & \delta_{Rud} \end{bmatrix}^T \tag{7.23}$$

$$
\left[\begin{array}{cccccccccc}
\frac{T_{mperc}}{m} & \frac{T_{mperc}}{m} & 0 & 0 & 0 & 0 & \frac{\rho u^2 S}{2m} C_{X_{elev}} & \ldots & 0 & 0 \\
0 & 0 & 0 & 0 & 0 & -\frac{T_{aperc}}{m} & 0 & \ldots & 0 & 0 \\
0 & 0 & \frac{T_{mperc}}{m} & \frac{T_{mperc}}{m} & \frac{T_{aperc}}{m} & 0 & \frac{\rho u^2 S}{2m} C_{Z_{elev}} & \ldots & 0 & \frac{\rho u^2 S}{2m} C_{Y_{rud}} \\
-I_1 Lxcg_{Thm} T_{mperc} & I_1 Lxcg_{Thm} T_{mperc} & I_2 Lycg_{ThmL} T_{mperc} & I_2 Lycg_{ThmR} T_{mperc} & 0 & -I_2 Lxcg_{Tha} T_{aperc} & 0 & \ldots & 0 & 0 \\
0 & 0 & Lxcg_{Thm} \frac{T_{mperc}}{I_{yy}} & Lxcg_{Thm} \frac{T_{mperc}}{I_{yy}} & -Lxcg_{Tha} \frac{T_{aperc}}{I_{yy}} & 0 & \frac{\rho u^2 S c}{2 I_{yy}} C_{My_{elev}} & \ldots & 0 & I_1 \frac{\rho u^2 S b}{2} (C_{Mz_{ail}}) + I_2 \frac{\rho u^2 S b}{2} (C_{Mx_{ail}}) \\
I_2 Lxcg_{Thm} T_{mperc} & I_2 Lxcg_{Thm} T_{mperc} & I_5 Lycg_{ThmL} T_{mperc} & I_5 Lycg_{ThmR} T_{mperc} & 0 & -I_5 Lxcg_{Tha} T_{aperc} & 0 & \ldots & 0 & I_1 \frac{\rho u^2 S b}{2} (C_{Mx_{rud}}) + I_2 \frac{\rho u^2 S b}{2} (C_{Mz_{rud}}) \\
0 & 0 & 0 & 0 & 0 & 0 & 0 & \ldots & 0 & 0 \\
0 & 0 & 0 & 0 & 0 & 0 & 0 & \ldots & 0 & I_5 \frac{\rho u^2 S b}{2} (C_{Mx_{ail}}) + I_2 \frac{\rho u^2 S b}{2} (C_{Mz_{ail}}) \\
0 & 0 & 0 & 0 & 0 & 0 & 0 & \ldots & 0 & I_5 \frac{\rho u^2 S b}{2} (C_{Mz_{rud}}) + I_2 \frac{\rho u^2 S b}{2} (C_{Mx_{rud}})
\end{array}\right]
\tag{7.24}
$$

In the control matrix, the inertia parameters and reference lengths are as defined before in equation 7.15 and table A.9. The aerodynamic coefficient due to control surfaces are those transformed values as defined in equations 3.36 and 3.37.

7.3.4 Control Weightings and System Poles

The Q(x) and R(x) weighting in the SDRE control can be defined as functions of states, and can lead a flexibility on the designer to choose the best intuitive over the controls. For example, if Q(x) increases and R(x) decreases as x increases it can lead to saving on control effort near the origin. Far from the origin, system can be driven to its equilibrium [39]. However in the thesis the weightings are taken as constants as in equations 7.25 and 7.26. The main consideration while choosing the best penalties is to soften the state-error vs. input tradeoff.

$$Q = diag(\begin{bmatrix} 12.3 & 0.1 & 62.5 & 0.1 & 1.2x10^4 & 0.1 \end{bmatrix}) \tag{7.25}$$

$$R = diag(\begin{bmatrix} 0.61x10^{-6} & 0.16x10^{-4} & 0.61x10^{-6} & 0.12x10^{-6} & 0.504x10^{-5} & 0.12x10^{-6} \end{bmatrix}) \tag{7.26}$$

In the outer loop, the poles that are assigned are given below.

$$\begin{bmatrix} -0.5 & -0.9 & -0.3 & -1.7 & -0.8 & -2 \end{bmatrix} \tag{7.27}$$

7.3.5 Results and Discussion

The transition control results are obtained for two transition flight scenarios that are described in chapter 4. According to two transition scenarios, the controller inputs to be tracked are determined from the trim conditions as in figures 7.3 and 7.4. The trim conditions are the same with the previously obtained results in trim analyses and shown in figures 4.3 and 4.8. These inputs are given to the system by a look-up table with time dependency, and the transition is required to last about 45 sec. up to the cruise condition at 42 m/s by using closed loop SDRE control system.

In this transition study, the aerodynamic controls are switched off at low speed regions (about 11-13 m/s) and aft throttle is switched off at high speed regions. The defined intermediate speed is chosen where in scenerio -1 aft throttle is not sufficient to satisfy the nose up moment and for scenerio-2 according to the value of required elevator deflections.

The allocation process is done by using the trim results of the required control input values. They are also given to the system as shown in figures 4.3 and 4.8 and by using look up table which takes the speed as reference. The external horizontal gust effect is also considered in the responses as given in figures 7.5 and 7.15.

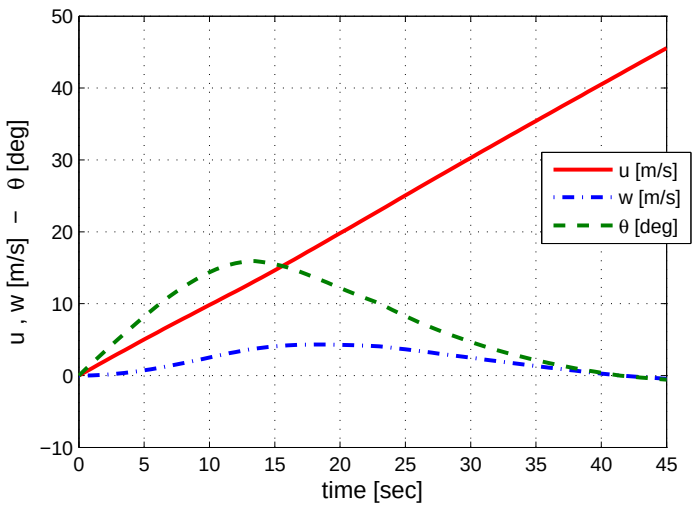

Figure 7.3: Input commands for control due to transition scenario-1

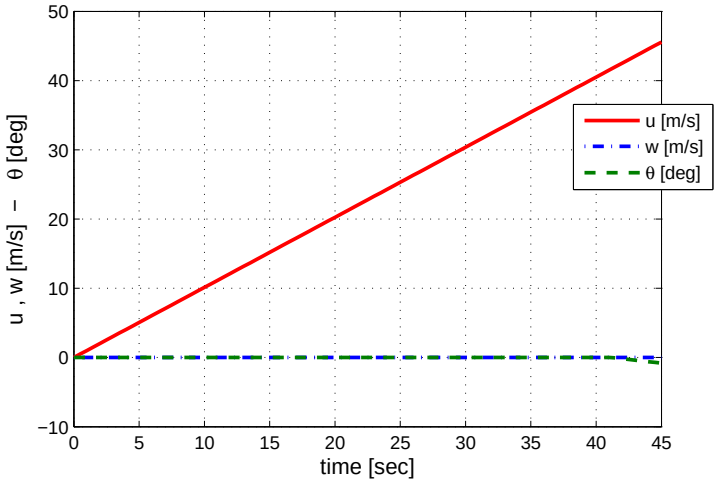

Figure 7.4: Input commands for control due to transition scenario-2

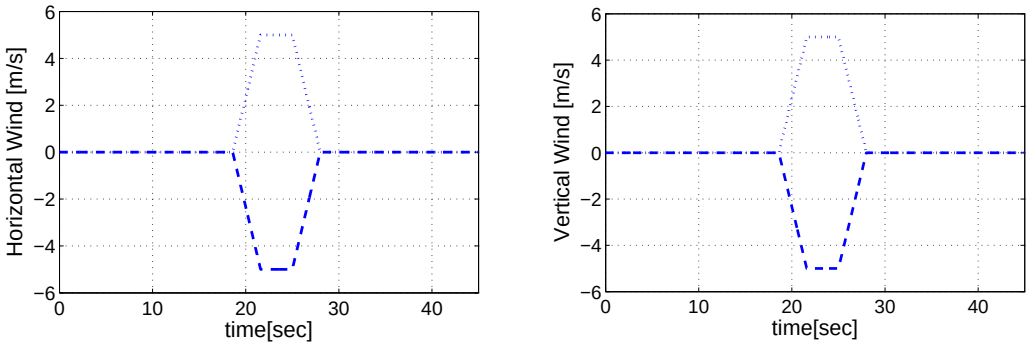

Figure 7.5: Horizontal - vertical gust during transition scenario-1

7.3.5.1 Transition Scenario-1 Controller Responses

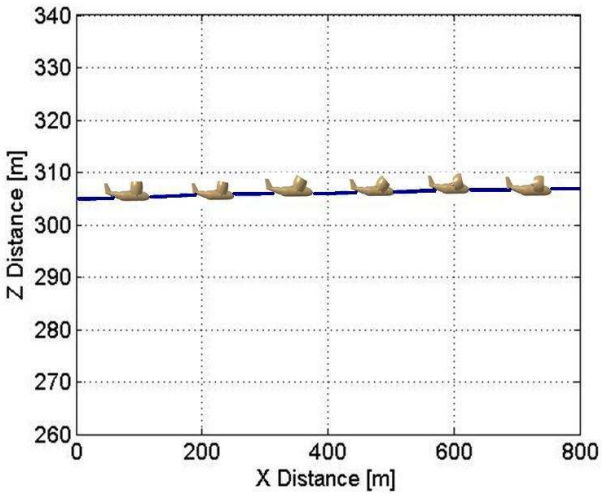

Figure 7.6: Trajectory followed by controller for transition scenario-1

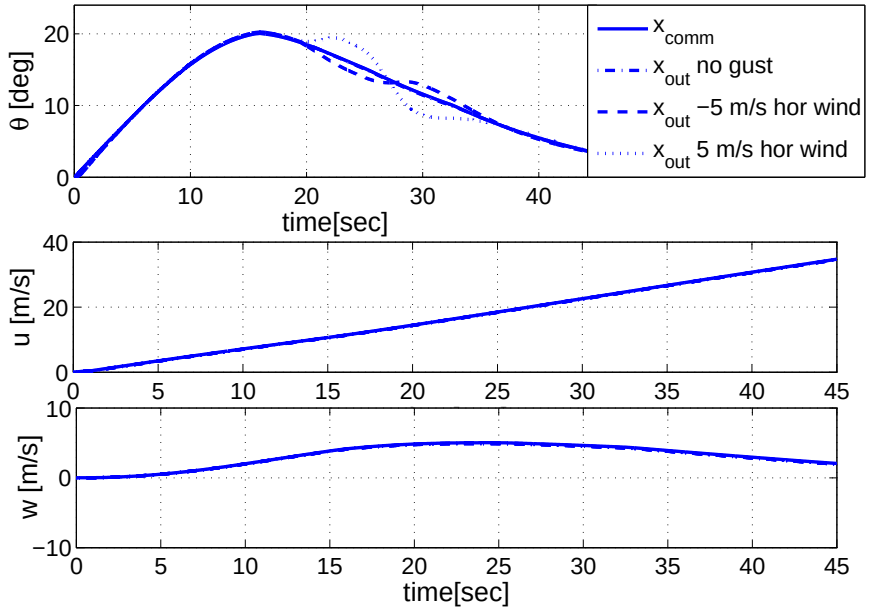

Figure 7.7: Controler commands and responses in horizontal gust for transition Scenario-1

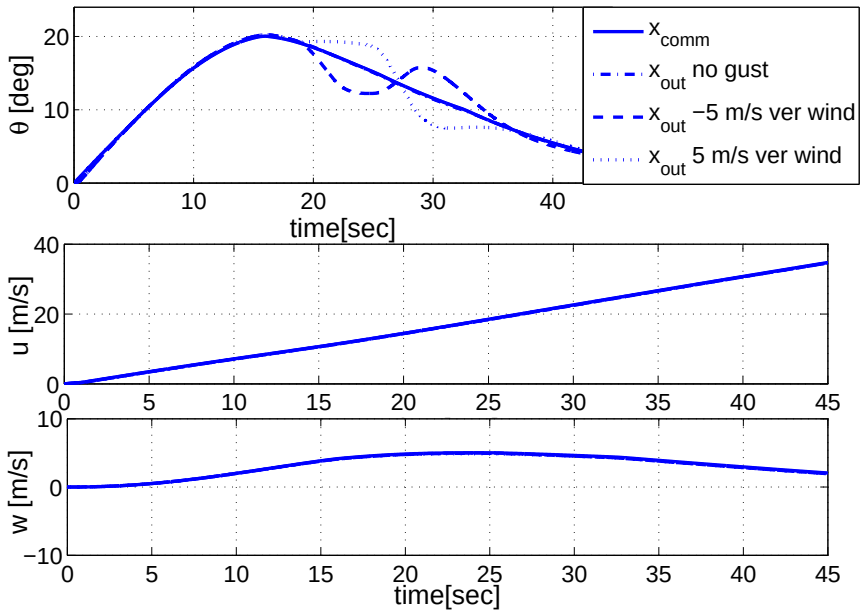

Figure 7.8: Controler commands and responses in vertical gust for transition scenario-1

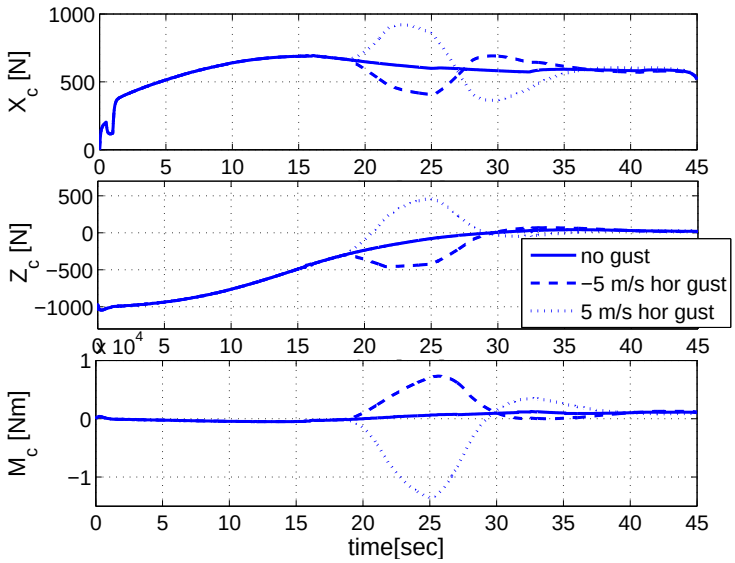

Figure 7.9: Forces and moments required from control surfaces in horizontal gust for transition scenario-1

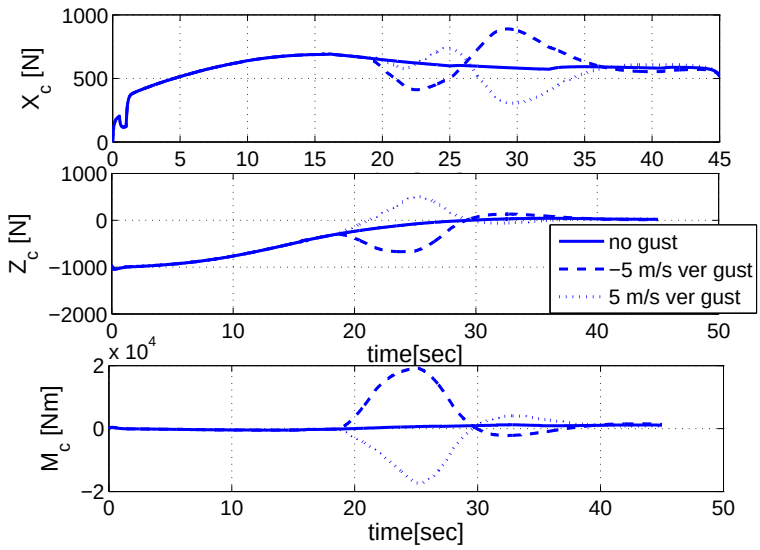

Figure 7.10: Forces and moments required from control surfaces in vertical gust for transition scenario-1

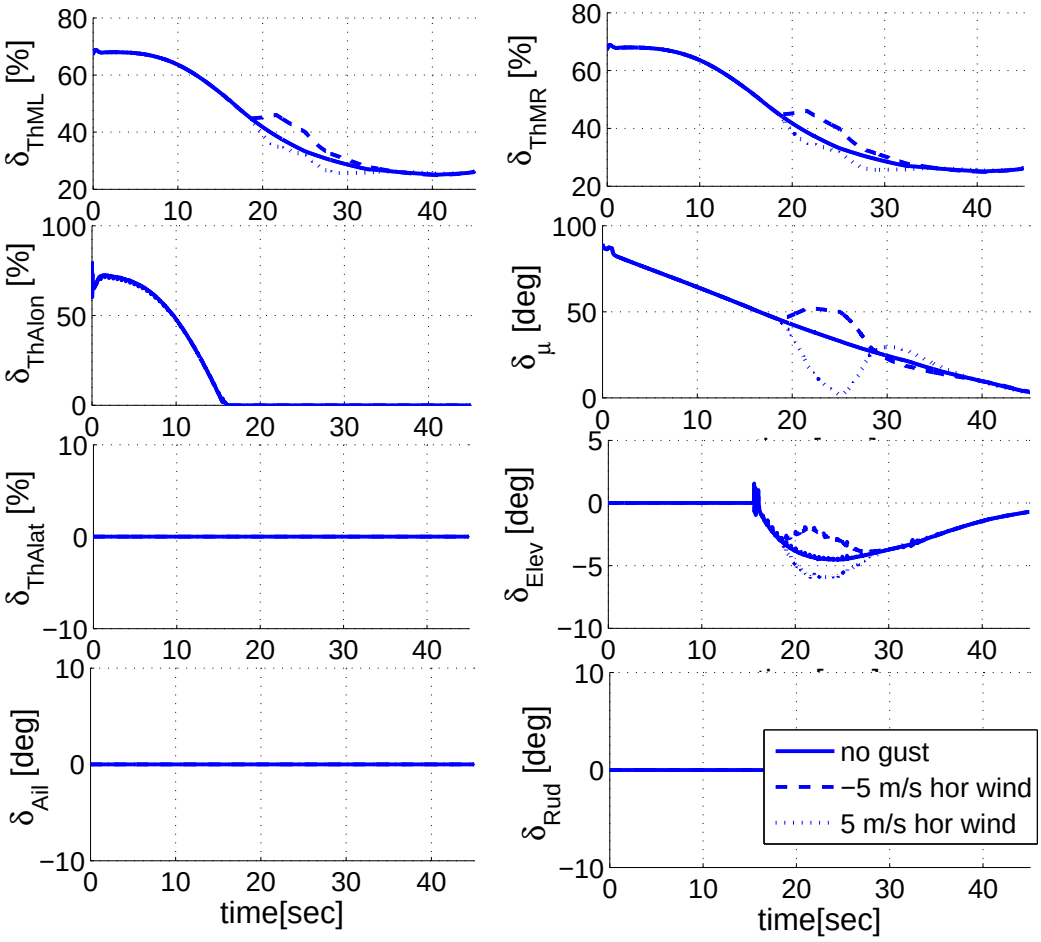

Figure 7.11: Controls after allocation in horizontal gust for transition scenario-1

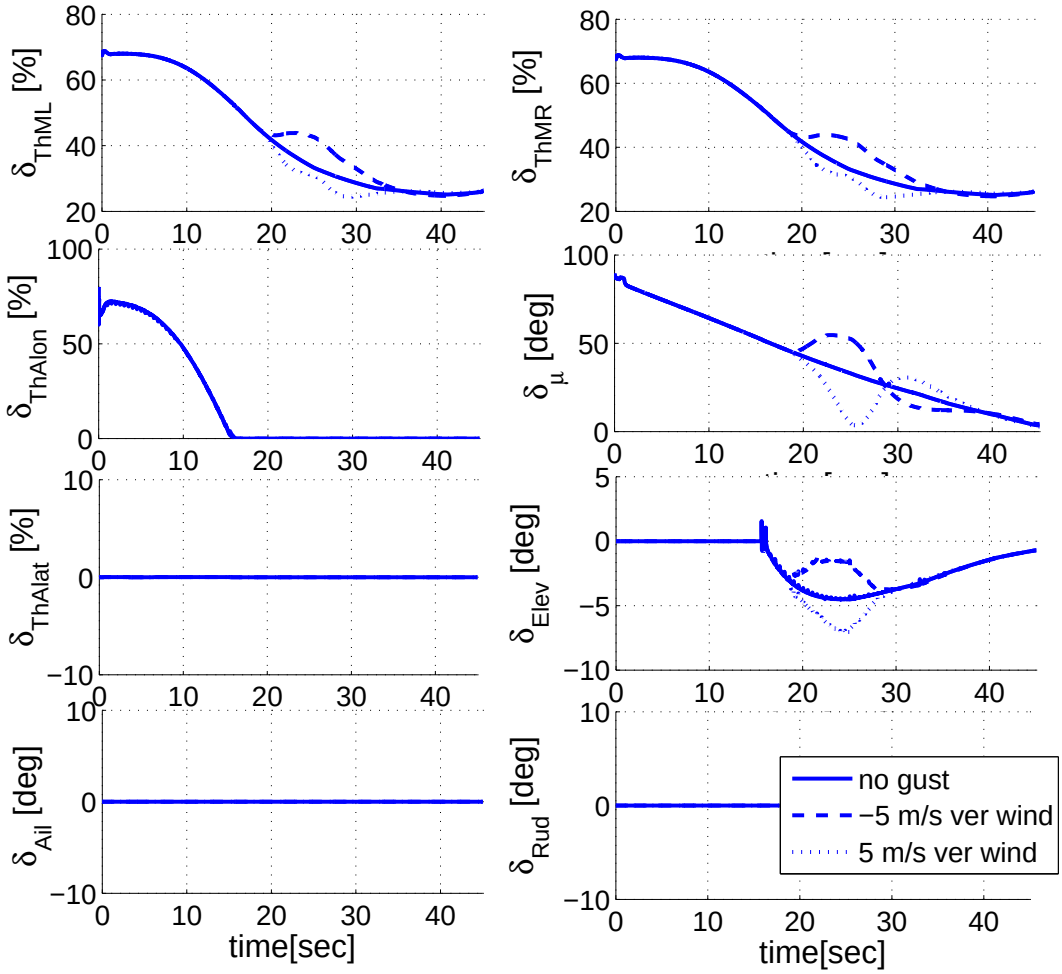

Figure 7.12: Controls after allocation in vertical gust for transition scenario-1

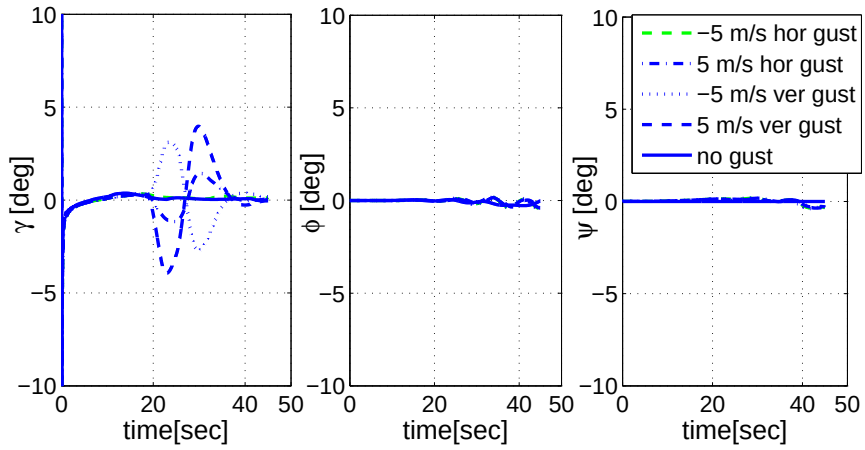

Figure 7.13: Simulation results of flight path-bank-heading angle for transition scenario-1

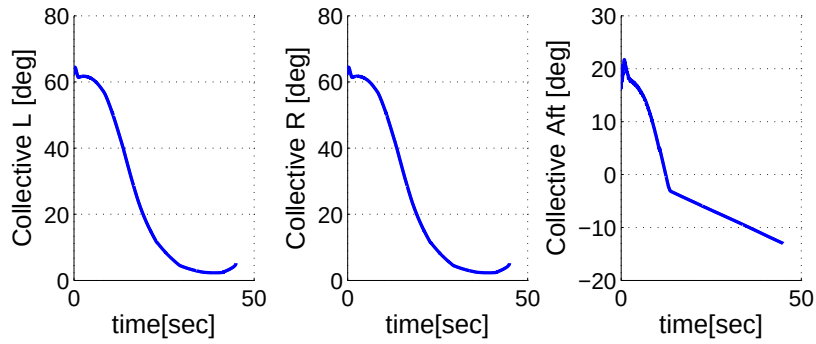

Figure 7.14: Collective inputs needed during transition scenario-1

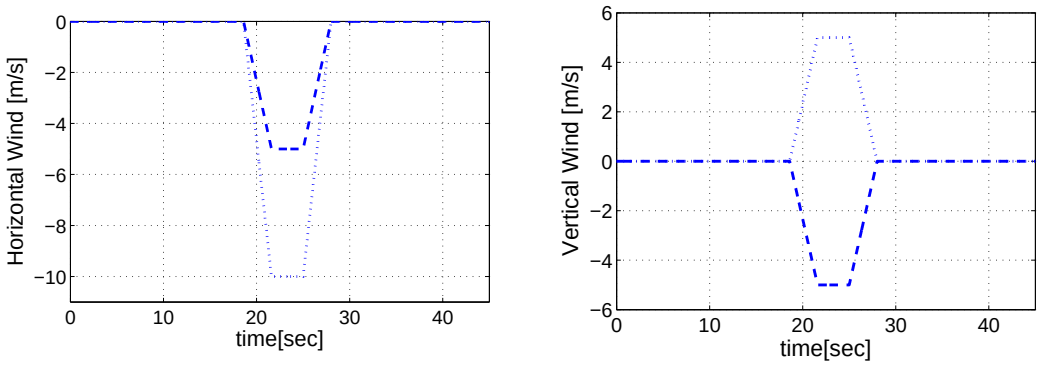

Figure 7.15: Horizontal - vertical gust during transition scenario-2

7.3.5.2 Transition Scenario-2 Controller Responses

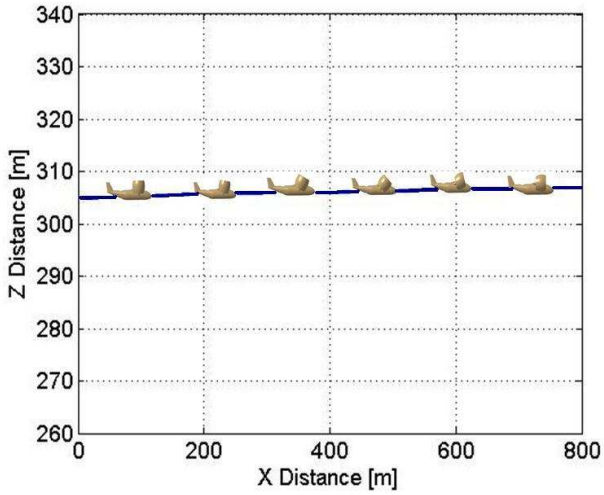

Figure 7.16: Trajectory followed by controller in transition scenario-2

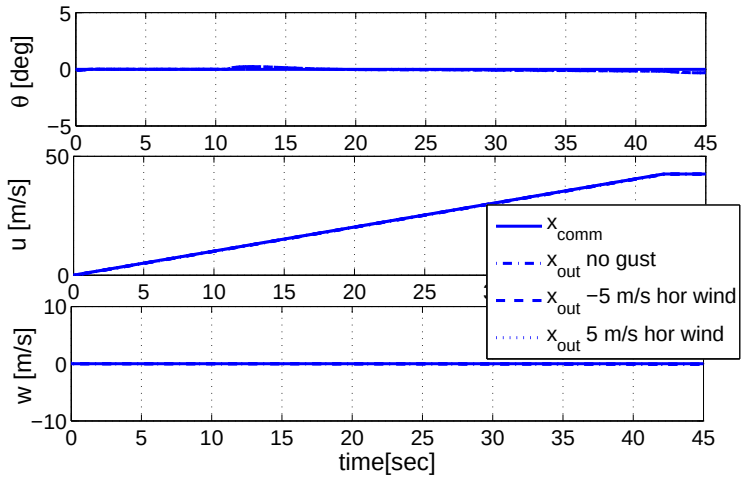

Figure 7.17: Controler commands and responses in horizonal gust for transition scenario-2

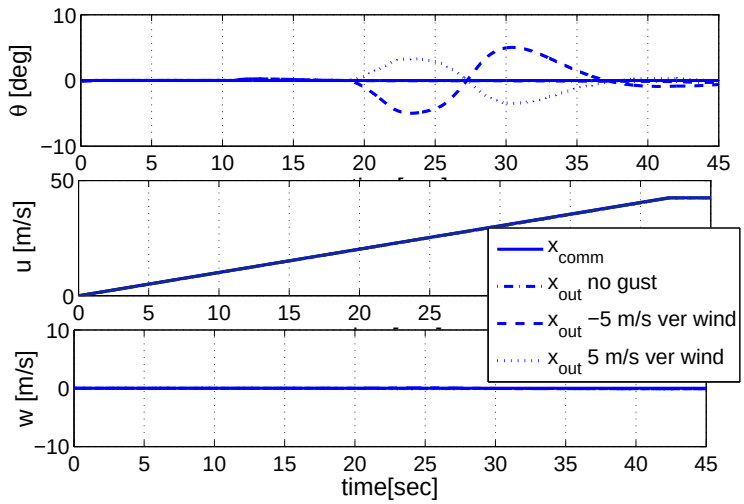

Figure 7.18: Controler commands and responses in vertical gust for transition scenario-2

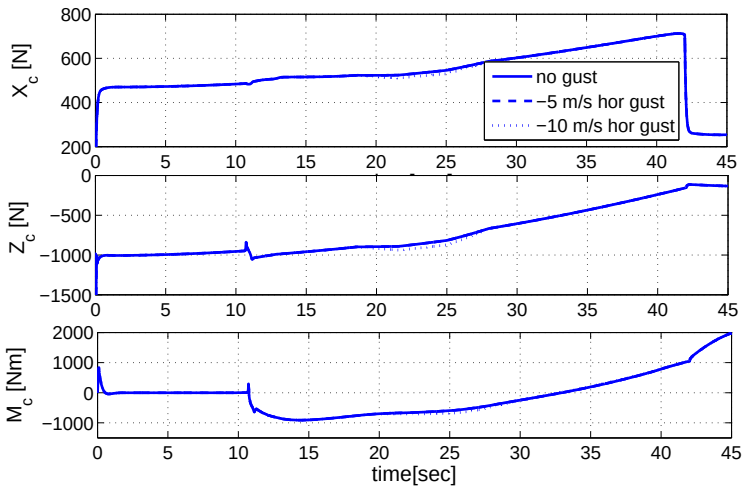

Figure 7.19: Forces and moments required from control surfaces in horizontal gust for transition scenario-2

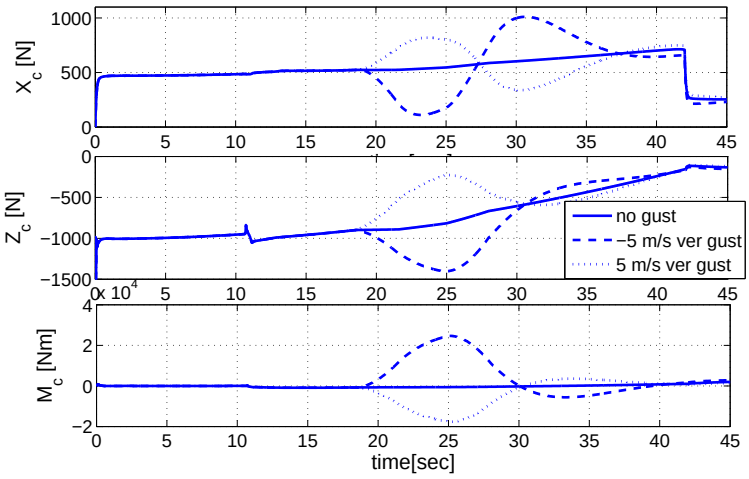

Figure 7.20: Forces and moments required from control surfaces in vertical gust for transition scenario-2

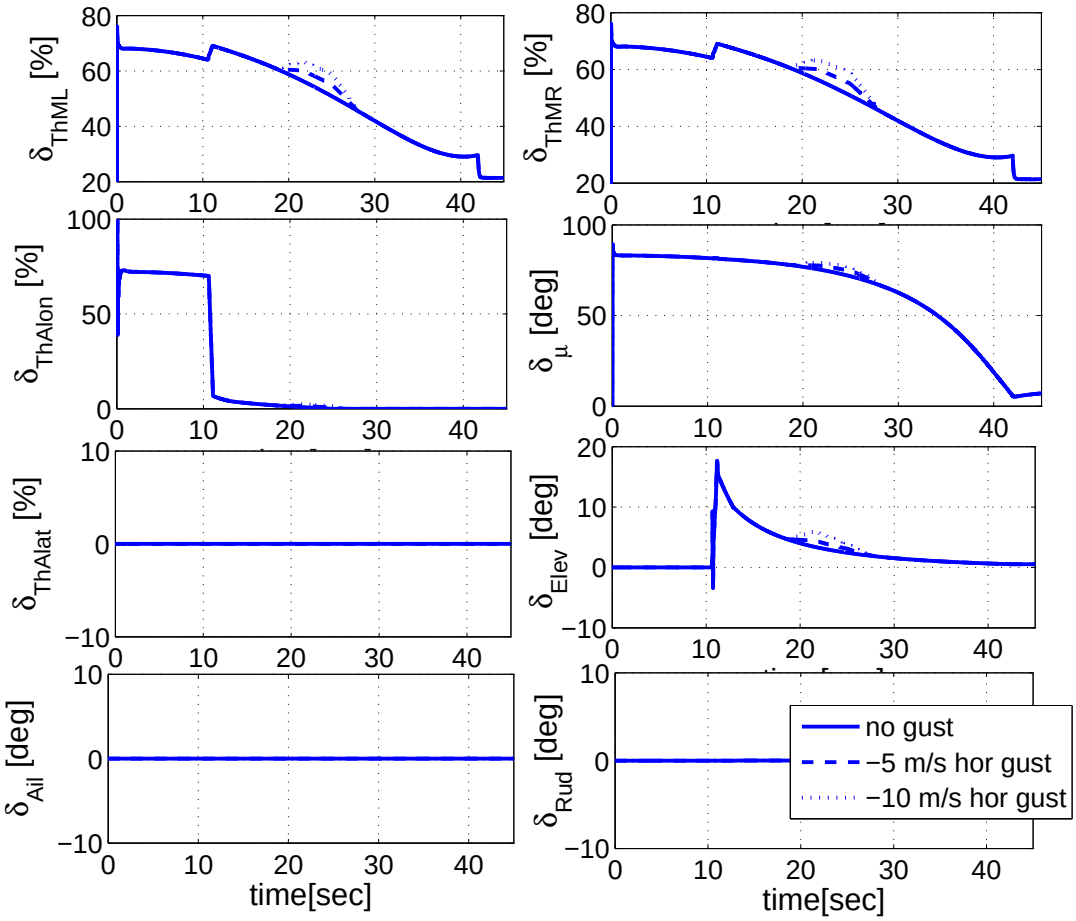

Figure 7.21: Controls after allocation in horizontal gust for transition scenario-2

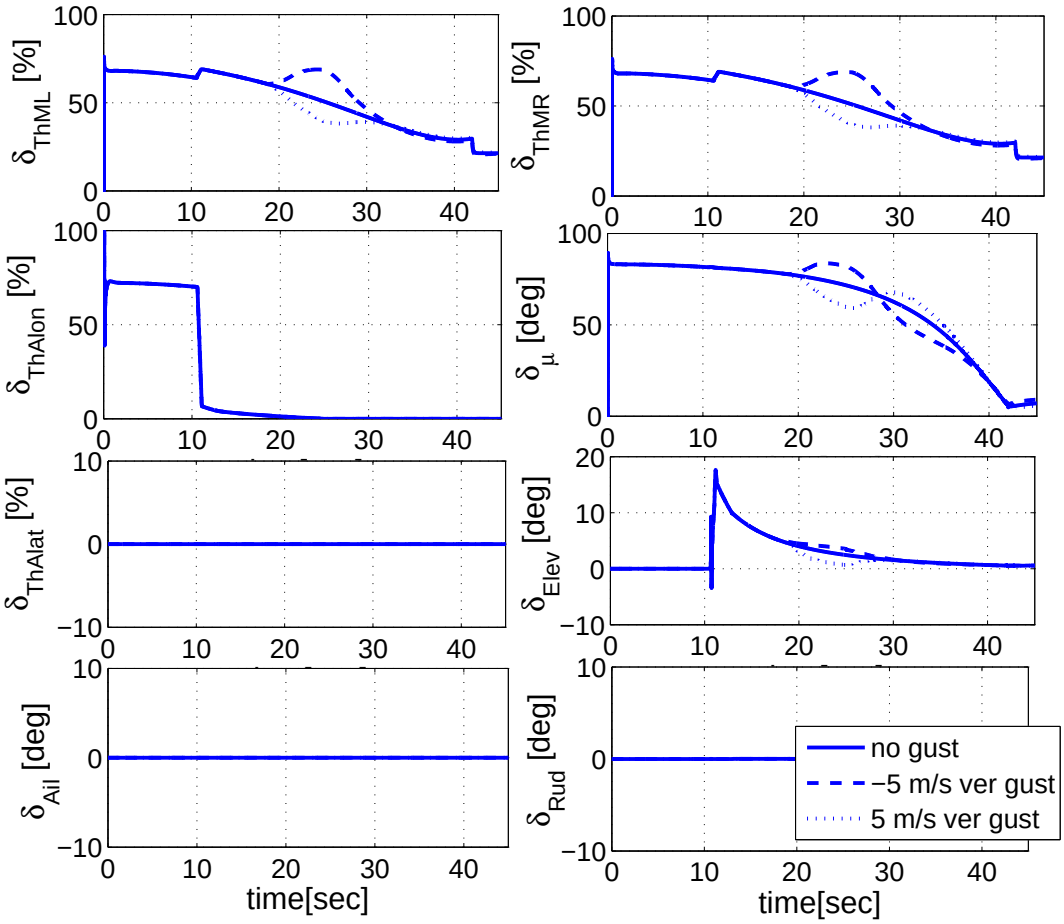

Figure 7.22: Controls after allocation in vertical gust for transition scenario-2

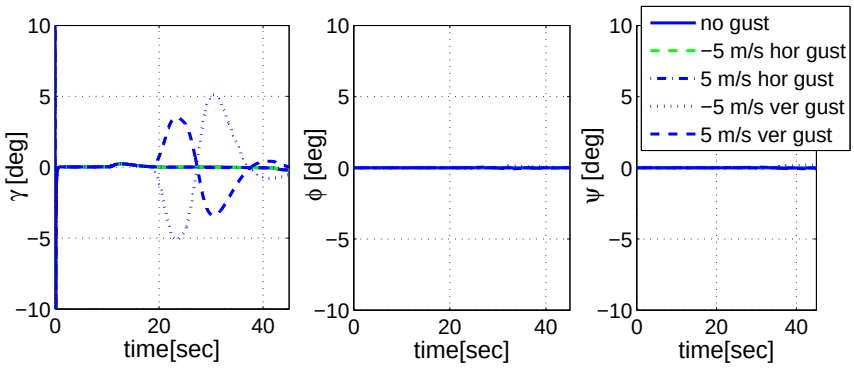

Figure 7.23: Simulation results of flight path-bank-heading angle for transition scenario-2

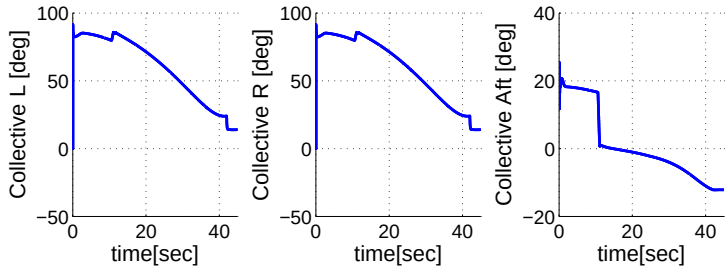

Figure 7.24: Collective inputs needed during transition scenario-2

As seen from the responses of the SDRE controller approach, the transition is done for both scenarios as seen in figures 7.6 and 7.16, required trajectory is tracked as in figures 7.7, 7.8, 7.17 and 7.18, expected control inputs are obtained (in figures 7.11, 7.12, 7.21 and 7.22) which correspond to the required control forces (in figures 7.9, 7.10, 7.19 and 7.20), although there are many redundancies in the control system. The system is tested for severe gust conditions in horizontal and vertical directions and the tracking ability is proved to be true. The control forces which are the main outputs of the controller are also tried to be given directly to the nonlinear plant and validated to track the commands.

In addition, the simulation results of flight path , bank, and heading angle as control system responses are given in figures 7.13 and 7.23 which are around 0 as expected. The collective inputs needed for the corresponding main left- right and aft throttle input are obtained as shown in 7.14 and 7.24.

The allocation approach is fed by the `B matrix´obtained at each time step and the control inputs found by trim analyses, in order to obtain the best authority on the controls to obtain

the required control input responses according to the transition scenario trim results. Actuator effects are neglected, saturations are used for control input limits and all the nonlinearities due to the model and controller are included in this control study.

The controller can also be used to control the other flight modes of the aircraft. In this case, the control input requirements shall be defined correctly.

The main contribution of defining such a control method is to allow to obtain an on-line `B matrix´that allows the user to allocate the controls in case of an over-actuated system. The other contribution is to obtain a control system without the need for gain scheduling or re-design of the controller for different flight conditions since there exists a self-state-dependency.

CHAPTER 8

CONCLUSIONS

In this thesis, an automatic flight control system is designed for a tilt duct UAV. For this purpose, a nonlinear simulation code is developed in the Matlab®-Simulink environment. Nonlinear aerodynamic database, 6-DOF equations of motion, axes transformations, environmental and geodetic frame effects, dynamic modeling of the rotors and control actuators, wind gust models are implemented to this mathematical model.

Linear model analyses are done by trimming and linearizing the mathematical model for various flight modes of the UAV. These linear analyses are mainly used for the linear controller studies done for the hover and cruise modes and also transition mode around a unique trim condition. The allocation methods for over-actuated UAV system in transition mode are tested. The blended inverse, control allocation method, parameters are tuned through simulations.

Gain schedule approach is observed not to be satisfactory for the transition mode since the system is highly nonlinear and the allocation methods in static sense cannot be implemented unless a continuously updated control matrix, B is obtained. Due to the nonlinearities of this mode together with the instability near the hover flight condition, a state-dependent controller design is used. Two-loop state feedback control approach is implemented and adapted to the nonlinear model of the UAV, together with extended linearization. In the inner state feedback loop, SDRE method is used to find feedback gains for controlling the translational speed and rotational rates. In the outer loop, UAV attitude and their integrals are controlled. In both cases extended linearization is applied. In the outer loop, eigenvalue assignment is used. The controls are allocated using blended inverse algorithm.

In the future some further improvements shall be carried out as;

- Detailed aerodynamics of the propellers.
- Inclusion of the dynamic models such as gyroscopic moments to the simulation code and examination of their effects to the flight control system.
- Inclusion of the actuator effects.
- Addition of flight path control modes to the outer loop.

In conclusion, a detailed control analysis on a Tilt-Duct VTOL UAV is done concerning especially the over-actuated transition mode of the aircraft. Nonlinear modeling is done, trim conditions are obtained for many flight conditions especially for the linear controller combining classical control and optimal control approaches. It is shown that Blended Inverse control allocation method as well as the two loop nonlinear state dependent feedback scheme including SDRE technique is quite effective to stabilize and effectively control the transition phase of the aircraft.

REFERENCES

[1] Abbott, I. H. , Von Doenhoff A. E. "*Theory of Wing Sections: Including a Summary of Airfoil Data*",Dover Publications Inc., New York, 1959.

[2] Kalman R.E., Y. C. Ho, K.S. Narenda "*Controllability of Linear Dynamical Systems in Contributions to Differential Equations*", Vol.1 New York : John Wiley & Sons , Inc., 1962.

[3] Pearson, J. D. "*Approximation Methods in Optimal Control*", *Journal of Electronics and Control* Vol. 13 No. 5 pp. 453–465, 1962.

[4] Hoerner F. "*Fluid Dynamic Drag: Practical Information on Aerodynamic Drag and Hydrodynamic Resistance*", Hoerner Fluid Dynamics, June, 1965.

[5] Burghart, J. A. "*A Technique for Suboptimal Control of Nonlinear Systems*", *In Proceedings of the IEEE Transactions on Automatic Control* Vol. 14 No. 5 pp. 530–533, 1969.

[6] Doland E. Kirk "*Optimal Control Theory : An Introduction*", Englewood Cliffs, N.J. : Prentice Hall, 1970.

[7] Kwakernaak H., Sivan R. "*Linear Optimal Control Systems*", John Wiley & Sons, Inc., 1972.

[8] Wernli, A. and Cook, G. "*Suboptimal Control for the Nonlinear Quadratic Regulator Problem*", Automatica Vol. 11 No. 1 pp. 75–84, 1975.

[9] U.S. Government Printing Office "*U.S. Standard Atmosphere*", Washington, D.C, 1976.

[10] McDonnell Douglas Corporation "*United States Air Force (USAF) Stability and Control DATCOM*", Douglas Aircraft Division and Flight Control Division, Wright-Patterson Air Force Base, OH, April 1978.

[11] Nazareth Sarkis Bedrossian "*Steering Laws for Control Moment Gyroscope Systems Used in Spacecraft Attitude Control*", MS Thesis, Mechanical Engineering Department, MIT, August 1987.

[12] Ehrler, D. and Vadali, S. R. "*Examination of the Optimal Nonlinear Regulator Problem*", *In Proceedings of the AIAA Guidance, Navigation, and Control Conference*", Minneapolis MN, August 1988.

[13] Hefley, R. K., Mnich, M. A. "*Minimum-Complexity Helicopter Simulation Math Model*", NASA Contractor Report 177476 USAAVSCOM Technical Report 87-A-7, 1988.

[14] McLean, D. "*Automatic Flight Control Systems*", Prentice Hall, 1990.

[15] Franklin, G. F., Emami–Naeini, A., and Powell, J. D. "*Feedback Control of Dynamic Systems*", 3rd. Addison–Wesley Longman Publishing Co., Inc, 1993.

[16] Riccardo M., Patrizio T. "*Nonlinear Control Design: Geometric, Adaptive and Robust*", Prentice Hall International (UK) Limited, Rome, 1995.

[17] W. Blake "*USAF Stability and Control Digital DATCOM*" McDonnell Douglas Corporation, Wright Laboratories, WL/FIGC, January 1996.

[18] Qu, Z., Cloutier, J. R., and Mracek, C. P. "*A New Sub-optimal Nonlinear Control Design Technique-SDARE*", *In Proceedings of the 13th IFAC World Congress* pp. 365–370, San Francisco CA, July 1996.

[19] Cloutier J.R., D'Souza C. N., Mracek Ridgely C.P. "*Nonlinear Regulation and Nonlinear H_∞ Control via State-Dependent Ricatti Equation Technique*", *In Proceedings of the First International Conference on Nonlinear Problems in Aviation and Aerospace* 117–141, Daytona Beach FL, 1996.

[20] Friedland, Bernard "*Advanced Control System Design*", Prentice-Hall Inc., Englewood Cliffs New Jersey, 1996.

[21] Navy-AS. "*Military Specification MIL-F-8785C*", NOTICE 2, 1996.

[22] Etkin B., Reid L.D. "*Dynamics of Flight, Stability and Control,3rd Edition*", John Wiley & Sons, Inc., 1996.

[23] Titterton D.H. and Weston J.L. "*Strapdown Inertial Navigation Technology*", Peter Peregrinus Ltd., on behalf of the Institution of electrical engineers, London, UK, 1997.

[24] Hammet K. D., Hall C. D., Ridgely D. B. "*Controllability Issues In Nonlinear State-Dependent Ricatti Equation Control*", Air Force Institute of Technology, *Journal of Guidance,Control and Dynamics* Vol 21 No. 5, OH, September October 1998

[25] A. J. Calise, R. T. Rysdyk "*Nonlinear Adaptive Flight Control Using Neural Networks*", IEEE Controls Systems Magazine, 1998.

[26] Pamadi, B. N. "*Performance, Stability, Dynamics, and Control of Airplanes*", AIAA Education Series, 1998.

[27] Limbach Flugmotoren Coorp. "*http://www.limflug.de*", Last update 1999.

[28] Kuo, Benjamin C.,"*Automatic Control Systems*" , Prentice Hall Englewood Cliffs, New Jersey, 1999.

[29] National Imagery and Mapping Agency NIMA "*Department of Defense World Geodetic System WGS 84, Its Definition and Relationships with Local Geodetic Systems*", TR8350.2 Third Edition Amendment, January, 2000.

[30] Okan, A. "*Modeling and Control of a Tilt-Duct VTOL UAV*", Master of Science Thesis, Department of Aerospace Engineering of METU, Ankara, Turkey, December 2000.

[31] Armutcuoglu, O. "*The Conceptual Design of a Tilt-Duct VTOL UAV*", Master of Science Thesis, Department of Aerospace Engineering of METU, Ankara, Turkey, December 2000.

[32] Goodwin, G. C., Graebe, S. F., Salgado, M. E. "*Control System Design*", 1st. Prentice Hall PTR, 2000.

[33] Stone R.H., Clarke G., "*Optimization of Transition Maneuvers for a Tail-Sitter Unmanned Air Vehicle (UAV)*" , *In Proceedings of the Australian International Aerospace Congress*" Paper 105, Canberra, March 2001.

[34] Marc Rauw, "*FDC 1.2 - A Simulink Toolbox for Flight Dynamics and Control Analysis*", 2nd edition, May 2001.

[35] Cycon, J. P., Scott, Mark W., Dewitt, C. W. "*Unmanned aerial vehicle with counter-rotating ducted rotors and shrouded pusher-prop United States Patent 6270038*",http://www.freepatentsonline.com/6270038.html, Stratford, CT, June 2001.

[36] Cloutier J. R., Stansbery D. T. "*Nonlineaar, Hybrid Bank-to-Turn/Skid-to-Turn Missile Autopilot Design*", *In Proceedings of the AIAA Guidance, Navigation and Control Conference* 01–5929, Montreal Canada, August 2001.

[37] J. Yu, A. Jadbabaie, J. Primbs and Y. Huang, "*Comparison of Nonlinear Control Design Techniques on a Model of the Caltech Ducted Fan*", Automatica, vol. 37, pp. 1971-1978, 2001.

[38] Roskam J. "*Airplane Flight Dynamics and Automatic Flight Controls*", Part 1, DARcorporation, 2001.

[39] E. Bilge Erdem "*Analysis and Real-Time Implementation of State-Dependent Ricatti Equation Controlled Systems*", PhD Thesis, Mechanical Engineering Department, University of Illinois at Urbana-Champaign, Illinois, 2001.

[40] The MathWorks "*Aerospace Blockset Users Guide, For Use with Simulink®*", The MathWorks Inc., July, 2002.

[41] Roger E. Beck "*Application of Control Allocation Methods to Linear Systems with Four or More Objectives*", PHD Thesis, Faculty of the Virginia Polytechnic Institute and State University, Blacksburg Virginia, June 2002.

[42] M. Bodson "*Evaluation of optimization methods for control allocation*", *Journal of Guidance, Control, and Dynamics*, 25(4):703-711, 2002.

[43] Carmichael R.L. "*The Hydrostatic Equations*", January 23, 2003.

[44] Yedavalli R. K., Shankar P., Doman David B. "*Combining State Dependent Ricatti Equation Approach with Dynamic Inversion : Application to Control of Flight Vehicles*", Air Force Institute of Technology, OH, February 2003.

[45] E. Yavuzoglu "*Steering Laws for Control Moment Gyroscope Systems Used in Spacecraft Attitude Control*", MS Thesis, Aerospace Engineering Department, METU, November 2003.

[46] Harkegard 0. "*Efficient Active Set Algorithms for Solving Constrained Least Squares Problems in Aircraft Control Allocation*", Department of Electrical Engineering Linkoping University, Linkoping Sweden, 2003.

[47] David G. Hull "*Optimal Control Theory for Applications*", Springer–Verlag New York Inc, 2003.

[48] Harkegard 0. "*Backstepping and Control Allocation with Applications to Flight Control*", PHD Thesis, Department of Electrical Engineering Linkoping University, Linkoping Sweden, 2003.

[49] Harkegard 0. "*Dynamic Control Allocation Using Constrained Quadratic Programming*", *Journal of Guidance, Control, and Dynamics*, 0731-5090 vol.27 no.6 (1028-1034), 2004.

[50] Harkegard, 0., Glad, T. S. "*Resolving actuator redundancy : optimal control vs. control allocation*", Division of Automatic Control, Department of Electrical Engineering, Linköping University, Linköping Sweden, October 2004.

[51] Morris K., Navasca C. "*Iterative Solution of Algebraic Ricatti Equations using a Modified Newton-Kleinman Method*", Department of Mathematics, University of Waterloo, Canada 2004.

[52] Tekinalp, O., and E. Yavuzoglu "*A New Steering Law for Redundant Control Moment Gyroscope Clusters*", *In Proceedings of the Aerospace Science and Technology* Vol. 9 No. 7 pp. 626-634, October 2005.

[53] A. Altay "*Steering of Redundant Robotic Manipulators and Spacecraft Integrated Power and Attitude Control - Control Moment Gyroscopes*", MS Thesis, Aerospace Engineering Department, METU, January 2006.

[54] GlobalSecurity, "*Vertical and Short Takeoff and Landing Aircraft V/STOL*", http://www.globalsecurity.org/military/systems/aircraft/vstol.htm, last update on March 2006.

[55] Green, W.E., Oh P.Y., "*Autonomous Hovering of a Fixed-Wing Micro Air Vehicle*",*In Proceedings of the IEEE International Conference of Robotics and Automation (ICRA)* pp. 2164-2169, Orlando FL, May 2006.

[56] GlobalSecurity, "*Tiltrotor*", http://www.globalsecurity.org/military/systems/aircraft/vstol.htm, last update on August 2006.

[57] Johnson E. N., Turbe M. A. "*Modeling, Control, and Flight Testing of a Small Ducted Fan Aircraft*", *In Proceedings of the AIAA Journal of Guidance, Control and Dynamics*, 2006.

[58] OPAL-RT Technologies Inc. "*RT-LAB manuals*", Montreal, Canada, 2006.

[59] Boo-Min Kim, Kwangchan Choi, Byoung Soo Kim, "*Trajectory Tracking Controller Design Using Neural Networks For Tiltrotor UAV*" *In Proceedings of the AIAA Guidance, Navigation and Control Conference and Exhibit*, South Carolina, August 2007.

[60] Andy Ko A., Osgar John Ohanian O.J., Gelhausen P. , "*Ducted Fan UAV Modeling and Simulation in Preliminary Design*" ,*In Proceedings of the AIAA Modeling and Simulation Technologies Conference and Exhibit*", South Carolina, August 2007.

[61] Osborne S.R., "*Transitions Between Hover and Level Flight for a Tailsitter UAV*" , Master of Science Thesis, Department of Electrical and Computer Engineering Brigham Young University, Provo Utah, December 2007.

[62] Pathfield G. D. "*Helicopter flight dynamics:The Theory and Application of Flying Qualities and Simulation Modelling*", Blackwell Publishing, 2nd Edition, Washington DC, 2007.

[63] Aurora Flight Sciences, "*Ducted-Fan Unmanned Aircraft Systems*" , *http://www.darpa.mil/SBIR/pdf_files/Aurora_Flight_08_17_07_low_res.pdf*, last updated on 2007.

[64] Geering H. P. "*Optimal Control with Engineering Applications*", Springer–Verlag Berlin Heidelberg, 2007.

[65] Johnson E. N., Wu A., Neidhoefer J. C., Kannan S. K., Turbe M. A. "*Flight-Test Results of Autonomous Airplane Transitions Between Steady-Level and Hovering Flight*", *In Proceedings of the AIAA Journal of Guidance, Control and Dynamics* Vol. 31 No. 2, March April 2008.

[66] Brandon, John "*Altitude and altimeters*", Recreational Aviation Australia Inc., http://www.auf.asn.au/groundschool/umodule3, May 2008.

[67] Çimen T. "*State-Dependent Ricatti Equation (SDRE) Control : A Survey*", *In Proceedings of the International Federation of Automatic Control*, Seoul Korea, July 2008.

[68] Benner P., Li J., Li R., Penzl T. "*Iterative Solution of Algebraic Ricatti Equations Using a Modified Newton-Kleinman Method*", *In Proceedings of the Numerical Linear Algebra with Applications*, TU Chemnitz, Germany, 15:755–777, 2008.

[69] Xili Y., Yong F., Jihong Z. "*Transition Flight Control of Two Vertical/Short Takeoff and Landing Aircraft*", Tsinghua University, Beijing CHINE *Journal of guidance, control, and dynamics*", ISSN 0731-5090, 2008.

[70] Kahraman, O., and O. Tekinalp "*Satellite Attitude Control Using Dissimilar Redundant Actuators*", *In Proceedings of the 19th AIAA/AAS Space Flight Mechanics Meeting*, AAS 09-252, Savannah GA, February 2009.

[71] Zaccarian, L., "*Dynamic allocation for input redundant control systems*", Dipartimento di Informatica, Sistemi e Produzione, University of Rome, Rome, Italy, March 2009.

Appendix A

TILT-DUCT UAV GEOMETRY

A.1 Aircraft Technical Drawings

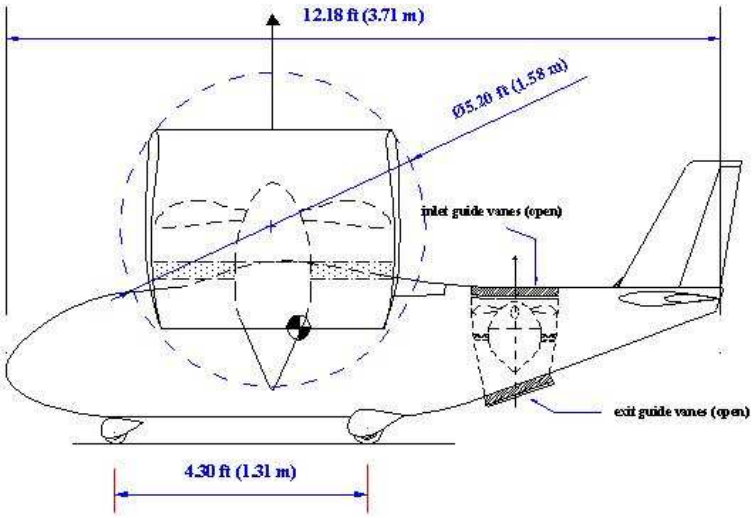

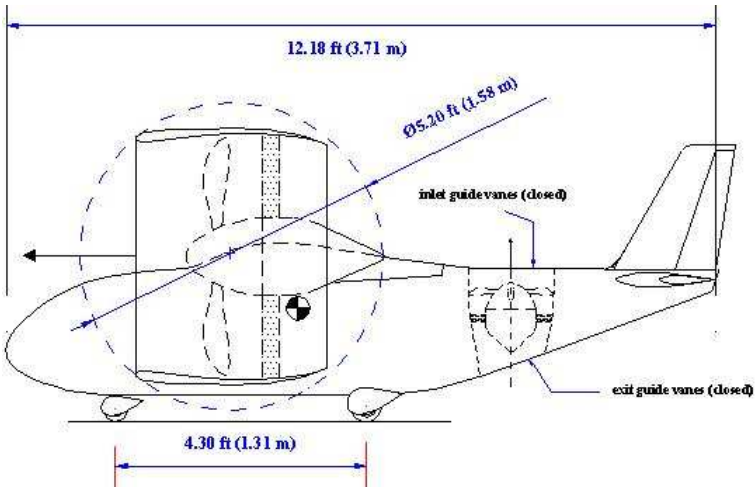

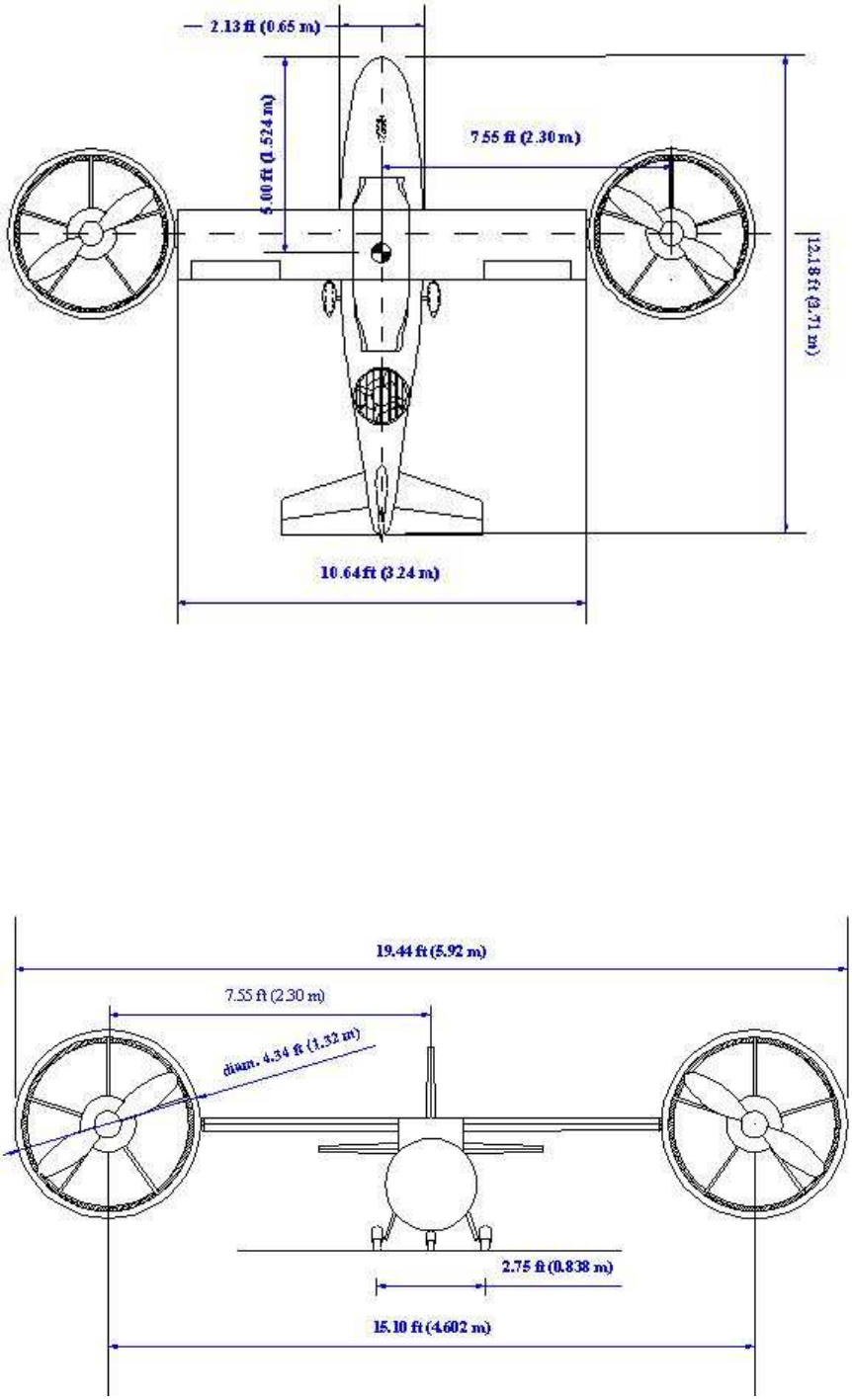

Figure A.1: Tilt-Duct VTOL UAV design

A.2 Aircraft Geometric Parameters

A.2.1 Wing Geometry

Table A.1: Geometric parameters for wing

Parameter	Acronym	Value	Unit
Area	S_w	1.754	m^2
Span	b_w	3.24	m
Chord	c_w	0.541	m
Exposed Area	S_{exp}	1.75	m^2
Exposed Span	b_{exp}	3.2348	m
Wetted Area	S_{wet}	3.62	m^2
	y	0.81	m
Volume	V	0.07	m^3
Wing Leading Edge Point	X_w	1.438	m
Aircraft Center of Gravity	X_{cg}	2.82*0.541=1.5256	m
Sweep Angle		0	
Taper Ratio	λ	0	
Dihedral	Λ	0	
Airfoil Section		Eppler E-583	
Airfoil for Datcom		Naca 7-74-A-415	

A.2.2 Fuselage Geometry

Table A.2: Geometric parameters for fuselage

Parameter	Acronym	Value	Unit
Length	L_{fus}	3.71	m
Diameter	D_{fus}	0.65	m
Volume	Vol	2.65	m^3
Exposed Area (Top)	S_{exp} (top)	1.79	m^2
Wetted Area (Side)	S_{wet} (side)	1.97	m^2
Aft Sweep	Aft Sweep	19.76	deg
Fineness Ratio	Fineness R.	5.718	

A.2.3 Horizontal Tail Parameters

Table A.3: Geometric parameters for horizontal tail

Parameter	Acronym	Value	Unit
Moment Arm	L_{HT}	1.93	m
Chord	C_{HT}	1.29	m
Area	S_{HT}	0.63	m^2
Span	b_{HT}	1.59	m
Root Chord	c_r	0.53	m
Tip Chord	c_t	0.26	m
Mean Aerodynamic Chord	%mac	0.41	m
	y	0.35	m
Tail Leading Edge Point	X_{ht}	3.2686	m
Sweep Angle		14.3	deg
Taper ratio	λ	0.5	
Airfoil Section		Eppler E-5831	
Airfoil for Datcom		Naca 0015	

A.2.4 Vertical Tail Geometry

Table A.4: Geometric parameters for vertical tail

Parameter	Acronym	Value	Unit
Moment Arm	L_{VT}	2	m
Chord	C_{VT}	0.09	m
Area	S_{VT}	0.25	m^2
Span	b_{VT}	0.64	m
Root Chord	c_r	0.53	m
Tip Chord	c_t	0.27	m
Mean Aerodynamic Chord	%mac	0.41	m
	y	0.28 m	
Sweep Angle	Sweep	22.1	deg
Taper ratio	λ	0.5	
Tail Leading Edge Point	X_{VT}	3.5042	m
Airfoil Section		Eppler E-5831	
Airfoil for Datcom		Naca 0015	

A.2.5 Nacelle Parameters

Table A.5: Geometric parameters for nacelles

Parameter	Acronym	Value	Unit
Exposed Area (Side)	S_{exp} (side)	0.6	m^2
Exposed Area (Top)	S_{exp} (top)	1.37	m^2
Wetted Area	S_{wet}	8.1	m^2
Volume	Vol	1.38	m^3

A.2.6 Aileron Geometry

Table A.6: Geometric parameters for aileron

Parameter	Acronym	Value	Unit
Area	S_{ail}	0.19	m^2
Span	b_{ail}	1.394	m
Mean Chord	c_{ail}	0.13	m
Ratio to Wing Area	S_{ail}/S_w	% 10.7	
Inboard Span	bi_{ail}	0.823	
Outboard Span	bo_{ail}	1.52	

A.2.7 Elevator Geometry

Table A.7: Geometric parameters for elevator

Parameter	Acronym	Value	Unit
Area	S_{elev}	0.25	m^2
Span	b_{elev}	1.59	m
Root Chord	c_r	0.212	m
Tip Chord	c_t	0.106	m
Ratio to Horizontal Tail Area	S_{ail}/S_{HT}	% 40	

A.2.8 Rudder Geometry

Table A.8: Geometric parameters for rudder

Parameter	Acronym	Value	Unit
Hingeline	c_b/c_c	%8.9	% chord
Thickness ratio @ hinge line	t/c	%3.37	% chord
Area	S_{rud}	0.1	m^2
Span	b_{rud}	0.61	m
Root Chord	c_r	0.21	m
Tip Chord	c_t	0.11	m
Ratio to Horizontal Tail Area	$S_{(}rud)/S_{(}VT)$	% 40	

A.2.9 Main Duct and Aft Fan Geometry

Table A.9: Distances of ducts and aft fan from CG

Parameter	Acronym	Value	Unit
Duct Side length		1	m
Duct Side width		1.32	m
Left Duct Distance to cg in y axis	$Lycg_{ThmL}$	-2.3	m
Right Duct Distance to cg in y axis	$Lycg_{ThmR}$	2.3	m
Left - Right Duct Distance to cg in x axis	$Lxcg_{Thm}$	0.178	m
Aft Fan Distance to cg in x axis	$Lxcg_{Tha}$	-1.0874	m

A.2.10 Aircraft Exposed Area

Table A.10: Aircraft exposed ares in different modes

Parameter	Acronym	Value	Unit
Exposed Area in Hover (Side)	S_{exp} (side) Hover	2.83	m^2
Exposed Area in Cruise (Side)	S_{exp} (side) Cruise	2.81	m^2
Exposed Area in Hover (Top)	S_{exp} (top) Hover	5.54	m^2
Exposed Area in Cruise (Top)	S_{exp}(top) Cruise	5.47	m^2
Wetted Area	S_{wet}	14.39	m^2

A.3 Weight and Balance Parameters

Table A.11: Inertia of mass parameters

Total Mass (kg)	I_{xx}	I_{yy}	I_{zz}	I_{xz}
110	277.17	297.79	829.24	44.42

Table A.12: Weight and balance parameters

Item	Weight (N)	Location (x/mac)	Location (m)
Wing	57.5	2.703	-0.137
Hor tail	9.2	6.144	5.966
Ver tail	5.1	6.587	6.751
Fuselage	131.4	3.253	0.839
Main LG	86.7	3.486	1.252
Node LGs	21	1.056	-3.057
Main Engine	304.4 x2	2.491	-0.513
Aft Engine	85.2	4.83	3.635
Camera	78.5	0	-4.930
TOTAL	1083.8	2.78	1.479

Appendix B

AERODYNAMIC CHARACTERISTICS

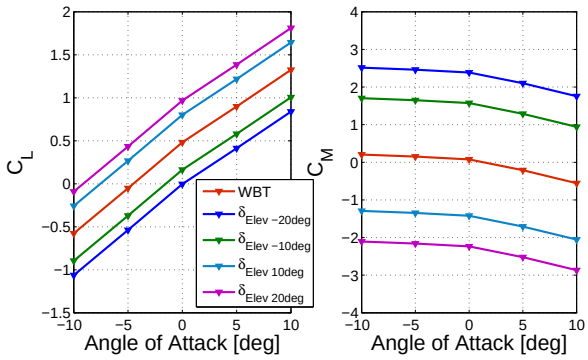

Figure B.1: Tilt-Duct UAV WBT lift-pitching moment coeffieicnts (.25 mac) with elevator effect

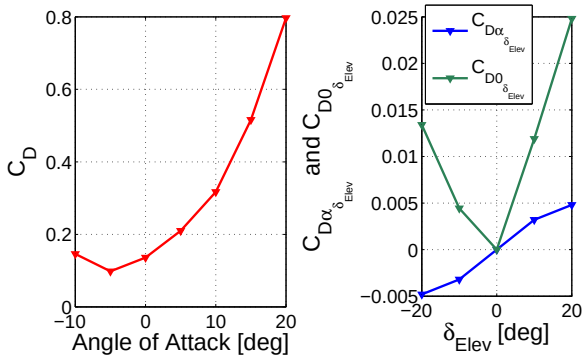

Figure B.2: Tilt-Duct UAV drag coefficient data, with elevator incremental effect

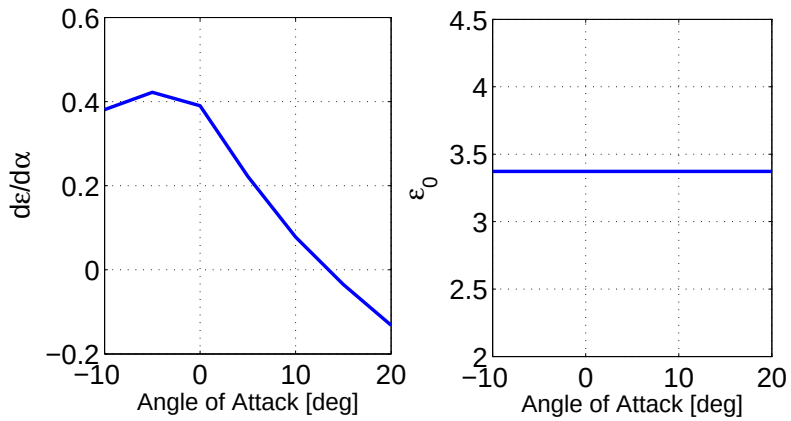

Figure B.3: Tilt-Duct UAV downwash effect on horizontal tail

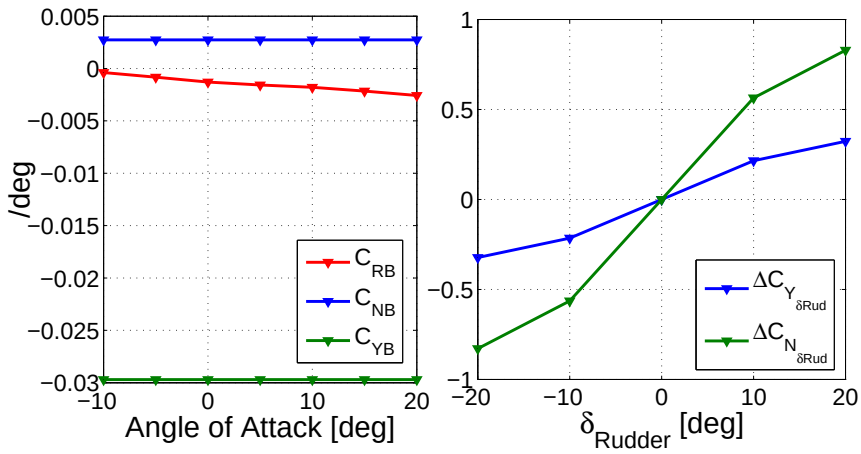

Figure B.4: Tilt-Duct UAV lateral-directional static coefficients and rudder effect on CY - CN coefficients

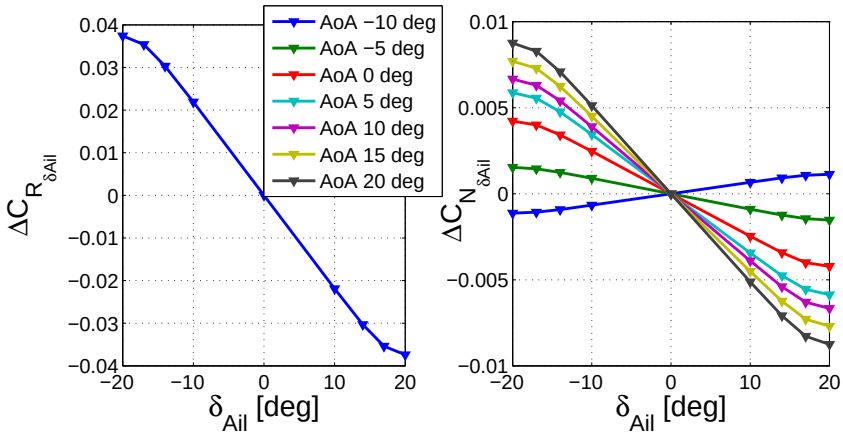

Figure B.5: Tilt-Duct UAV aileron effect on CR - CN coefficients

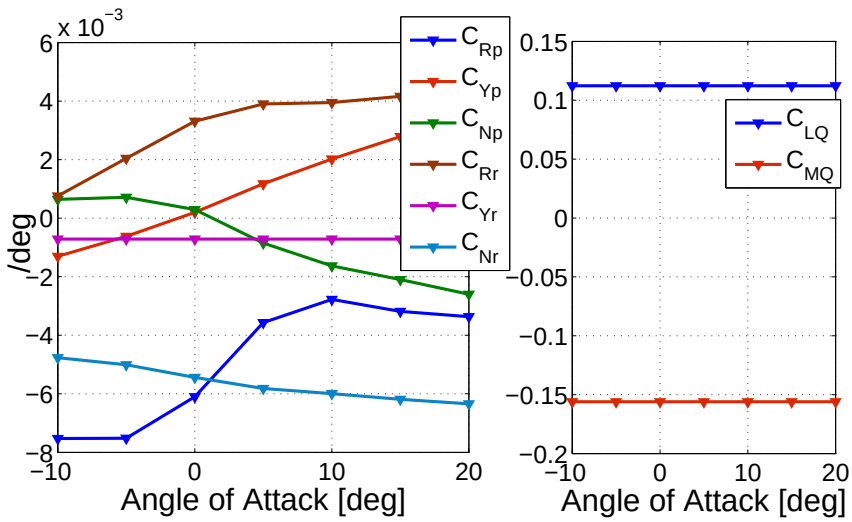

Figure B.6: Tilt-Duct UAV longitudinal and lateral dynamic derivatives

Appendix C

SIMULATION MODEL SUBSYSTEMS

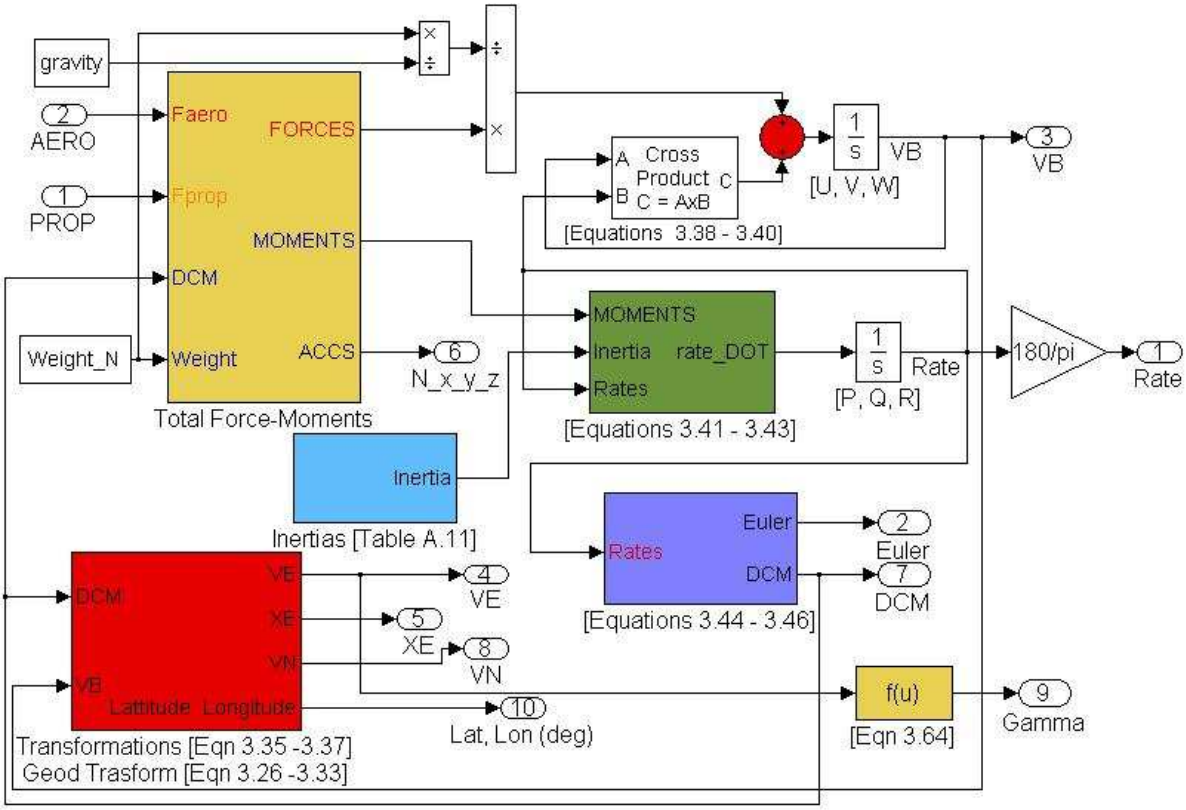

Figure C.1: 6-DOF Equations of Motion Subsystem Model

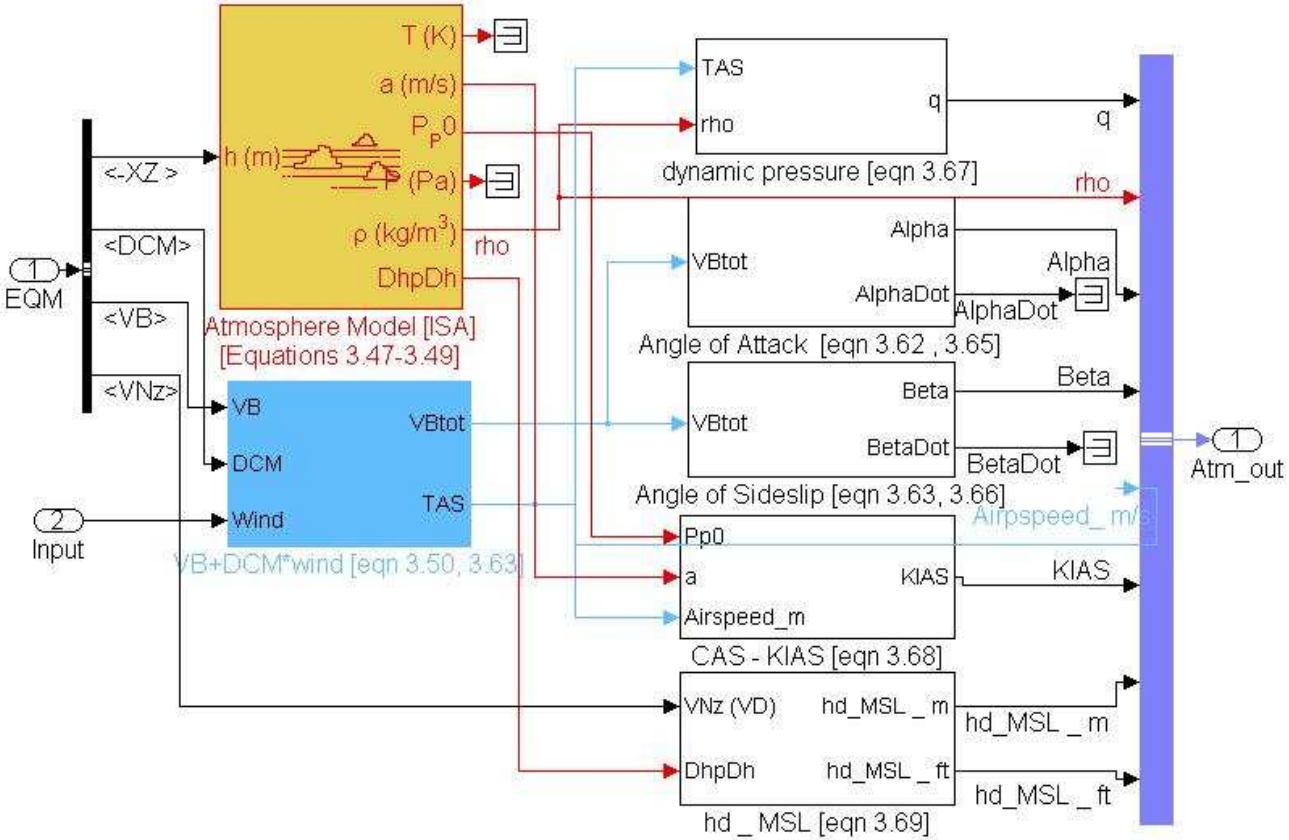

Figure C.2: Atmosphere - Environment Subsystem Model

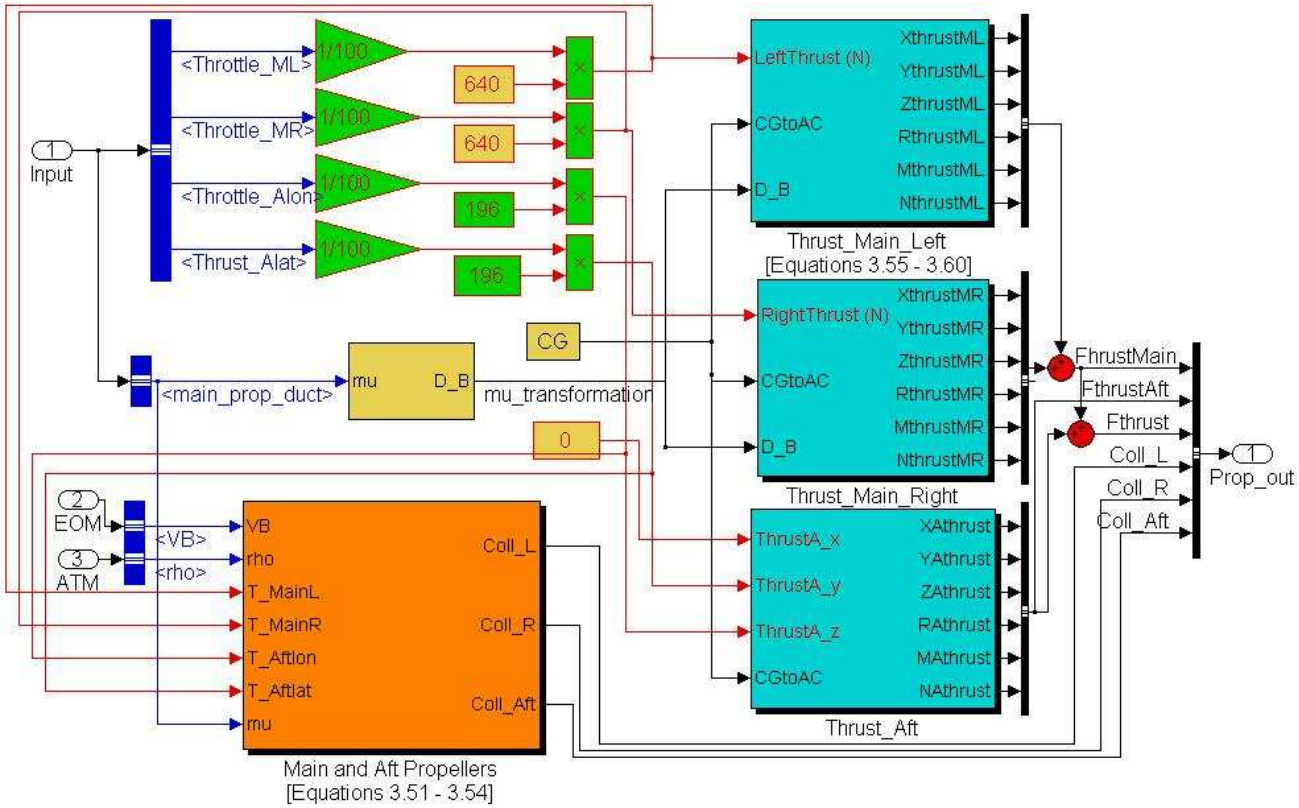

Figure C.3: Propulsion-Thrust Subsystem Model

Appendix D

LINEARIZED SYSTEM MATRICES

$$A_{cruiselon} = \begin{bmatrix} -0.1559 & -0.1511 & 1.4170 & -9.8020 \\ -0.4710 & -3.50545 & 2.1589 & 0.2667 \\ -0.0025 & -0.0908 & -0.0044 & 0 \\ 0 & 0 & 1 & 0 \end{bmatrix} \tag{D.1}$$

$$B_{cruiselon} = \begin{bmatrix} 0.0623 & 0.0623 & 0 & -0.001 & -0.0705 \\ 0 & 0 & -0.0191 & -0.0645 & -0.937 \\ 0 & 0 & -0.0072 & 0.004 & -0.8223 \\ 0 & 0 & 0 & 0 & 0 \end{bmatrix} \tag{D.2}$$

$$C_{cruiselon} = \begin{bmatrix} -0.0298 & -1.0973 & 0 & 57.2958 \\ 0 & 1 & 57.2958 & 0 \\ 0 & 0 & 0 & 0 \\ 0 & 0 & 0 & 57.2958 \end{bmatrix} \tag{D.3}$$

$$\lambda = \begin{bmatrix} -1.7892 \pm 1.2836i \\ -0.0436 \pm 0.2604i \end{bmatrix} \tag{D.4}$$

$$A_{cruiselat} = \begin{bmatrix} -0.9592 & -1.4176 & -52.1767 & 9.802 \\ -0.0386 & -0.0081 & 0.0031 & 0 \\ 0.0361 & -0.0002 & -0.0021 & 0 \\ 0 & 1 & -0.0272 & 0 \end{bmatrix} \tag{D.5}$$

$$B_{cruiselat} = \begin{bmatrix} 0 & 0 & 0.0191 & 0 & 0.6326 \\ -0.0029 & 0.0029 & -0.0004 & 0.1648 & 0 \\ -0.0179 & 0.0179 & -0.0026 & 0.0023 & 0 \\ 0 & 0 & 0 & 0 & 0 \end{bmatrix} \tag{D.6}$$

$$C_{cruiselat} = \begin{bmatrix} 1 & 0 & 0 & 0 \\ 0 & 57.2958 & 0 & 0 \\ 0 & 0 & 57.2958 & 0 \\ 0 & 0 & 0 & 57.2958 \end{bmatrix} \tag{D.7}$$

$$\lambda = \begin{bmatrix} 0 \\ 0.0006 \\ -0.2436 \\ -0.3632 \pm 1.2362i \end{bmatrix} \tag{D.8}$$

$$A_{translon_{\mu 40}} = \begin{bmatrix} -0.1422 & -0.1644 & 1.5151 & -9.8005 \\ -0.4159 & -3.1514 & 46.9368 & 0.3167 \\ -0.0091 & -0.0815 & -0.0040 & 0 \\ 0 & 0 & 1.0000 & 0 \end{bmatrix} \tag{D.9}$$

$$B_{translon_{\mu 40}} = \begin{bmatrix} 0.0477 & 0.0477 & 0 & -0.0430 & -0.0597 \\ -0.0400 & -0.0400 & -0.0191 & -0.0506 & -0.7587 \\ 0.0025 & 0.0025 & -0.0072 & 0.0031 & -0.666 \\ 0 & 0 & 0 & 0 & 0 \end{bmatrix} \tag{D.10}$$

$$C_{translon_{\mu 40}} = \begin{bmatrix} -0.0394 & -1.2190 & 0 & 57.2958 \\ 0 & 1.0000 & 0 & 0 \\ 0 & 0 & 57.2958 & 0 \\ 0 & 0 & 0 & 57.2958 \end{bmatrix} \tag{D.11}$$

$$\lambda = \begin{bmatrix} -1.6030 \pm 1.1640i \\ -0.0458 \pm 0.1082i \end{bmatrix} \tag{D.12}$$

$$A_{translat_{\mu 40}} = \begin{bmatrix} -0.8633 & -1.5157 & -46.9528 & 9.8005 & 0 \\ -0.0332 & -0.0074 & 0.0027 & 0 & 0 \\ 0.0326 & -0.0001 & -0.0019 & 0 & 0 \\ 0 & 1.0000 & -0.0323 & 0 & 0 \\ 0 & 0 & 1.0005 & 0 & 0 \end{bmatrix} \tag{D.13}$$

$$B_{translat_{\mu 40}} = \begin{bmatrix} 0 & 0 & 0.0191 & 0 & 0.5124 \\ -0.0366 & 0.0366 & -0.0004 & 0.1334 & 0 \\ -0.0156 & 0.0156 & -0.0026 & 0.0019 & 0 \\ 0 & 0 & 0 & 0 & 0 \\ 0 & 0 & 0 & 0 & 0 \end{bmatrix} \tag{D.14}$$

$$C_{translat_{\mu 40}} = \begin{bmatrix} 1.0000 & 0 & 0 & 0 & 0 \\ 0 & 57.2958 & 0 & 0 & 0 \\ 0 & 0 & 57.2958 & 0 & 0 \\ 0 & 0 & 0 & 57.2958 & 0 \\ 0 & 0 & 0 & 0 & 57.2958 \end{bmatrix} \tag{D.15}$$

$$\lambda = \begin{bmatrix} 0 \\ 0.0005 \\ -0.2617 \\ -0.3057 \pm 1.1113i \end{bmatrix} \tag{D.16}$$

$$A_{hoverlon_{\mu 40}} = \begin{bmatrix} 0 & 0 & 0 & -9.8056 & 0 \\ 0 & 0 & 0 & 0 & 0 \\ 0 & 0 & 0 & 0 & 0 \\ 0 & 0 & 1 & 0 & 0 \end{bmatrix} \tag{D.17}$$

$$B_{hoverlon_{\mu 40}} = \begin{bmatrix} 0 & 0 & 0 \\ -0.0623 & -0.0623 & -0.0191 \\ 0.0038 & 0.0038 & -0.0072 \\ 0 & 0 & 0 \end{bmatrix} \tag{D.18}$$

$$C_{hoverlon_{\mu 40}} = \begin{bmatrix} 0 & -6.0000 & 0 & 0 & 0 \\ 0 & 0.001 & 0 & 0 & 0 \\ 0 & 0 & 57.2958 & 0 & 0 \\ 0 & 0 & 0 & 57.2958 & 0 \end{bmatrix} \tag{D.19}$$

$$\lambda = \begin{bmatrix} -0.05630.0281 \pm 0.0488i \\ 0 \pm 0.0000i \end{bmatrix} \tag{D.20}$$

$$A_{hoverlat_{\mu 40}} = \begin{bmatrix} 0 & 0 & 0 & 9.8056 & 0 \\ 0 & 0 & 0 & 0 & 0 \\ 0 & 0 & 0 & 0 & 0 \\ 0 & 1 & 0 & 0 & 0 \\ 0 & 0 & 1 & 0 & 0 \end{bmatrix} \tag{D.21}$$

$$B_{hoverlat_{\mu 40}} = \begin{bmatrix} 0 & 0 & 0.0191 \\ -0.0536 & -0.0536 & -0.0004 \\ -0.0029 & -0.0029 & -0.0026 \\ 0 & 0 & 0 \\ 0 & 0 & 0 \end{bmatrix} \tag{D.22}$$

$$C_{hoverlat_{\mu 40}} = \begin{bmatrix} 1.0000 & 0 & 0 & 0 & 0 \\ 0 & 57.2958 & 0 & 0 & 0 \\ 0 & 0 & 57.2958 & 0 & 0 \\ 0 & 0 & 0 & 57.2958 & 0 \\ 0 & 0 & 0 & 0 & 57.2958 \end{bmatrix} \tag{D.23}$$

$$\lambda = \begin{bmatrix} 0 \\ 0 \\ 0 \\ -0.0000014 \\ -0.000000433 \end{bmatrix} \tag{D.24}$$

Appendix E

TABULATED TRIM RESULTS

Table E.1: Transition trim results for scenario-1 up to cruise speed at 305 m altitude

$V(TAS)[m/s]$	$u[m/s]$	$w[m/s]$	$\theta[deg]$	$\alpha[deg]$	$Duct[deg]$	$\delta_{ThM}[\%]$	$\delta_{ThA}[\%]$	$\delta_{elev}[deg]$
0.51	0.51	0.01	0.86	0.86	89	67.66	72.25	0
1.01	1.01	0.03	1.71	1.71	88	67.64	72.18	0
3.04	3.03	0.27	5.04	5.04	84	67.22	70.84	0
5.06	5.01	0.72	8.20	8.20	80	66.10	66.40	0
6.08	5.99	1.02	9.70	9.70	78	65.20	62.53	0
7.09	6.96	1.36	11.07	11.07	76	63.92	57.42	0
9.11	8.87	2.12	13.42	13.42	72	60.31	43.29	0
10.13	9.81	2.51	14.37	14.37	70	57.99	34.32	0
11.14	10.75	2.91	15.13	15.13	68	55.38	24.35	0
12.15	11.70	3.27	15.62	15.62	66	52.54	13.90	0
13.16	12.66	3.61	15.91	15.91	64	49.57	2.99	0
14.18	13.64	3.86	15.82	15.82	62	46.28	0	-0.92
16.20	15.65	4.20	15.04	15.04	58	39.89	0	-2.53
18.23	17.71	4.31	13.69	13.69	54	34.66	0	-3.10
20.25	19.80	4.28	12.19	12.19	50	30.41	0	-3.18
22.28	21.89	4.15	10.74	10.74	46	26.91	0	-3.03
24.30	24.00	3.86	9.14	9.14	42	24.28	0	-2.63
26.33	26.11	3.41	7.45	7.45	38	22.53	0	-2.03
30.38	30.28	2.48	4.69	4.69	30	20.15	0	-1.01
34.43	34.40	1.54	2.57	2.57	22	19.82	0	-0.32
38.48	38.47	0.68	1.01	1.01	14	20.18	0	0.20
42.02	42.02	-0.01	-0.02	-0.02	7	21.06	0	0.54
45.57	45.57	-0.46	-0.57	-0.57	0	23.76	0	0.56

Table E.2: Transition trim results for scenario-2 up to cruise speed at 305 m altitude

$V(TAS)[m/s]$	$u[m/s]$	$w[m/s]$	$\theta[deg]$	$\alpha[deg]$	$Duct[deg]$	$\delta_{ThM}[\%]$	$\delta_{ThA}[\%]$	$\delta_{elev}[deg]$
0.51	0.51	0	0	0	90.00	67.66	72.26	0
2.03	2.03	0	0	0	89.96	67.51	72.19	0
4.05	4.05	0	0	0	89.83	67.04	71.94	0
8.10	8.10	0	0	0	89.31	65.14	70.94	0
12.15	12.15	0	0	0	88.07	67.27	5.10	12.24
14.18	14.18	0	0	0	87.66	65.26	3.41	8.32
16.20	16.20	0	0	0	86.90	62.88	2.54	6.33
18.23	18.23	0	0	0	85.96	60.18	1.84	4.95
20.25	20.25	0	0	0	84.82	57.18	1.21	3.95
23.29	23.29	0	0	0	82.57	52.11	0.40	2.90
25.32	25.32	0	0	0	80.59	48.39	0	2.39
26.33	26.33	0	0	0	79.41	46.44	0	2.18
28.35	28.35	0	0	0	76.55	42.37	0	1.81
29.37	29.37	0	0	0	74.81	40.26	0	1.66
30.38	30.38	0	0	0	72.81	38.13	0	1.52
31.39	31.39	0	0	0	70.50	35.97	0	1.39
31.90	31.90	0	0	0	69.20	34.89	0	1.33
32.40	32.40	0	0	0	67.80	33.81	0	1.27
33.42	33.42	0	0	0	64.64	31.67	0	1.17
34.43	34.43	0	0	0	60.92	29.57	0	1.07
35.44	35.44	0	0	0	56.52	27.57	0	0.98
36.46	36.46	0	0	0	51.30	25.69	0	0.90
36.96	36.96	0	0	0	48.35	24.82	0	0.86
37.47	37.47	0	0	0	45.16	24.02	0	0.82
38.48	38.48	0	0	0	37.99	22.62	0	0.75
39.49	39.49	0	0	0	29.81	21.59	0	0.68
40.51	40.51	0	0	0	20.69	21.01	0	0.62
41.01	41.01	0	0	0	16.02	20.3	0	0.59
41.52	41.52	0	0	0	11.30	20.99	0	0.57
42.02	42.02	0	0	0	6.51	21.20	0	0.54
42.53	42.53	0	0	0	1.80	21.55	0	0.52

Table E.3: Forward flight trim results at 305 m altitude

$V(TAS)[m/s]$	$u[m/s]$	$w[m/s]$	$\theta[deg]$	$\alpha[deg]$	$\delta_{ThM}[\%]$	$\delta_{elev}[deg]$
31.32	31.16	3.11	5.70	5.70	19.27	-1.73
33.93	33.85	2.31	3.90	3.90	19.47	-0.99
36.54	36.51	1.56	2.45	2.45	20.05	-0.44
39.15	39.14	0.87	1.28	1.28	20.64	0.01
41.76	41.76	0.23	0.31	0.31	21.31	0.38
44.37	44.37	-0.27	-0.35	-0.35	22.82	0.53
46.98	46.97	-0.67	-0.82	-0.82	24.89	0.58
49.59	49.57	-1.05	-1.22	-1.22	27.08	0.62
52.20	52.18	-1.42	-1.56	-1.56	29.39	0.66
54.80	54.78	-1.77	-1.85	-1.85	31.81	0.68
57.41	57.37	-2.11	-2.10	-2.10	34.35	0.71
60.02	59.97	-2.44	-2.33	-2.33	37.01	0.73
62.63	62.57	-2.76	-2.52	-2.52	39.79	0.75
65.24	65.17	-3.07	-2.69	-2.69	42.68	0.77
67.85	67.77	-3.37	-2.85	-2.85	45.69	0.79
70.46	70.36	-3.67	-2.98	-2.98	48.82	0.80
73.07	72.96	-3.96	-3.11	-3.11	52.07	0.81
75.67	75.56	-4.24	-3.22	-3.22	55.44	0.82
78.28	78.15	-4.53	-3.31	-3.31	58.92	0.83
80.89	80.75	-4.80	-3.40	-3.40	2.52	0.84
83.50	83.34	-5.08	-3.49	-3.49	66.24	0.85
86.11	85.94	-5.35	-3.56	-3.56	70.07	0.86
88.71	88.54	-5.61	-3.63	-3.63	74.02	0.86
91.32	91.13	-5.88	-3.69	-3.69	78.10	0.87
93.93	93.73	-6.14	-3.75	-3.75	82.28	0.88

Appendix F

LINEAR QUADRATIC REGULATOR GAINS

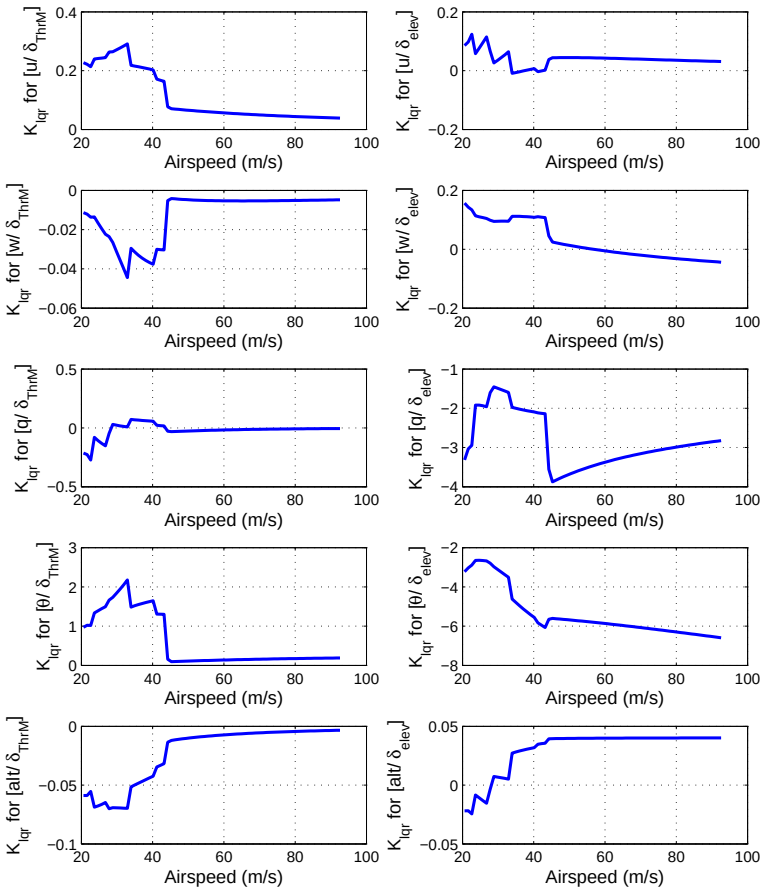

Figure F.1: LQR gains in longitudinal for cruise from 20 to 90 m/s airspeed at 305 m altitude

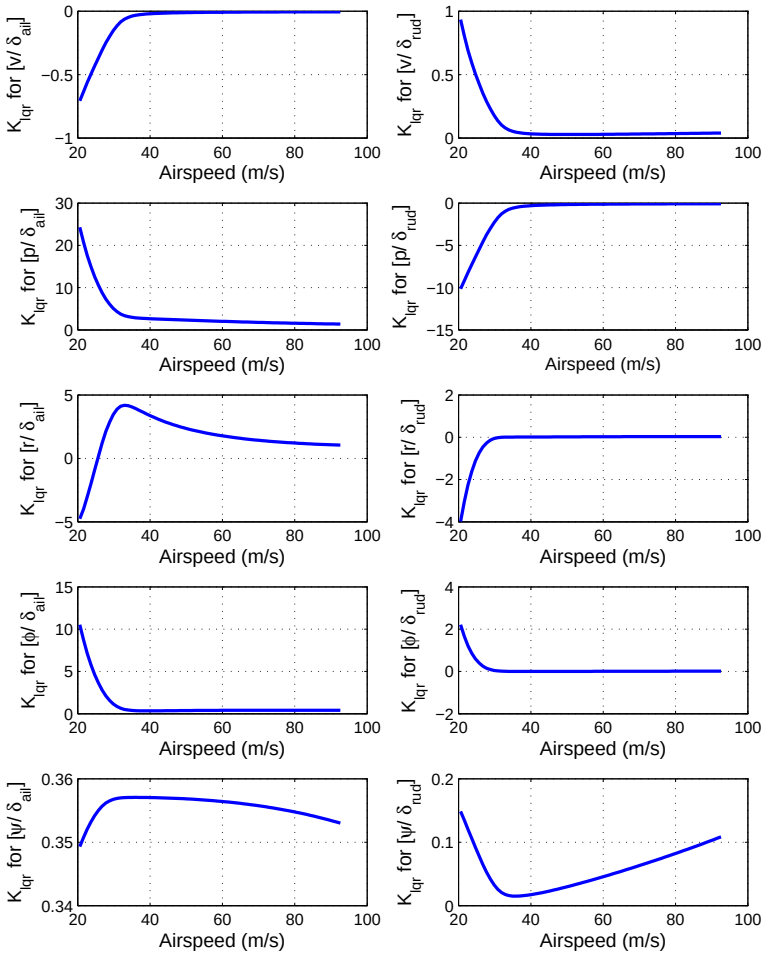

Figure F.2: LQR gains in lateral-directional for cruise from 0 to 90 m/s airspeed at 305 m altitude

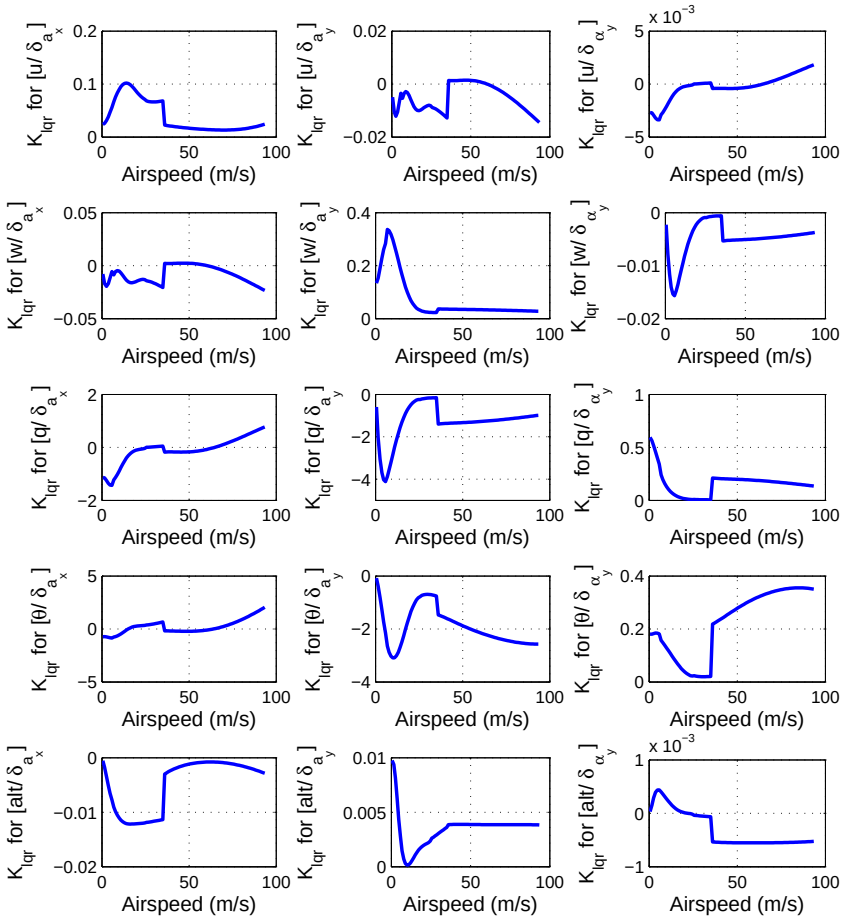

Figure F.3: LQR gains in longitudinal for transition scenario 1 from 0 to 90 m/s airspeed at 305 m altitude

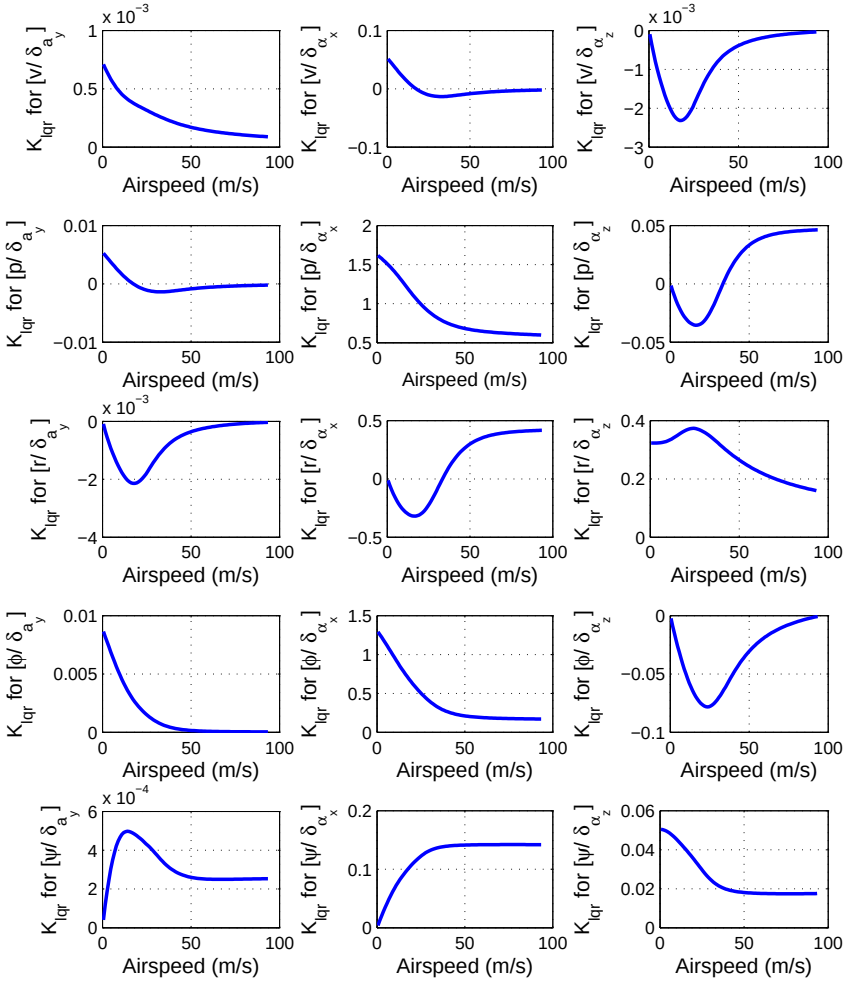

Figure F.4: LQR gains in lateral-directional for transition scenario 1 from 0 to 90 m/s airspeed at 305 m altitude

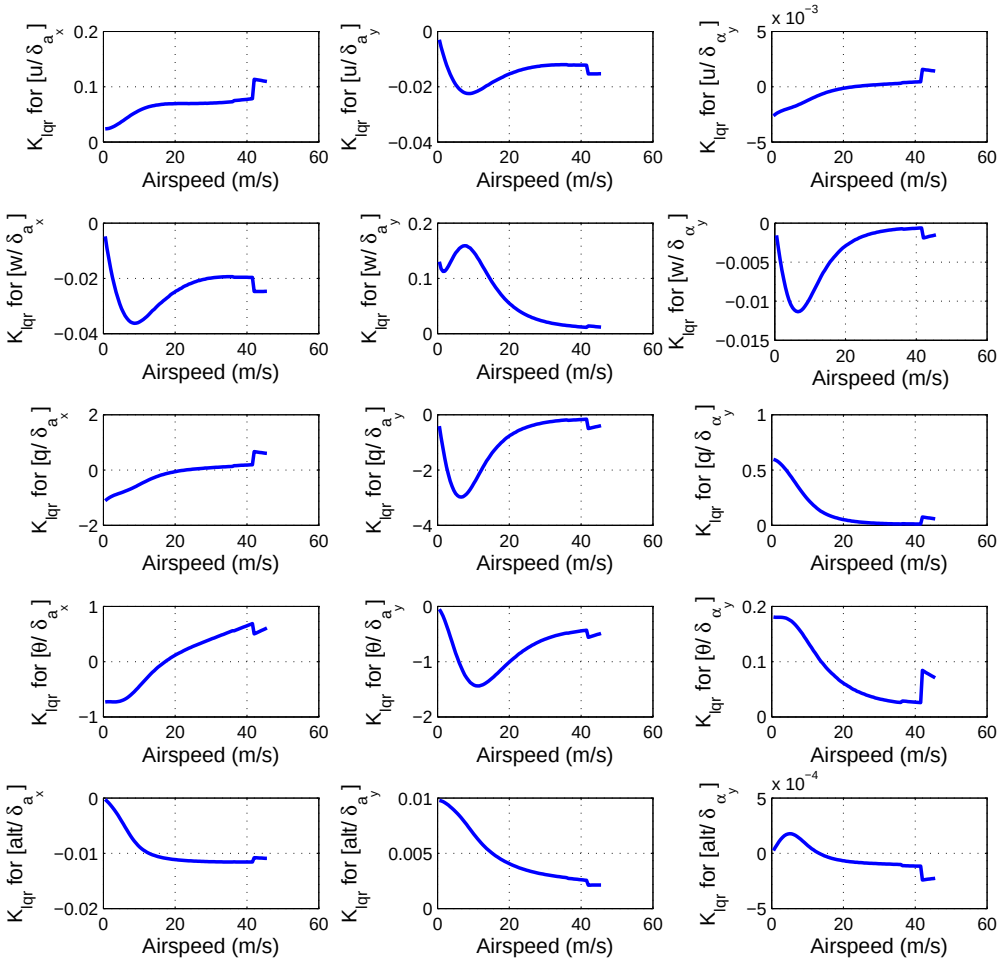

Figure F.5: LQR gains in longitudinal for transition scenario 2 from 0 to 90 m/s airspeed at 305 m altitude

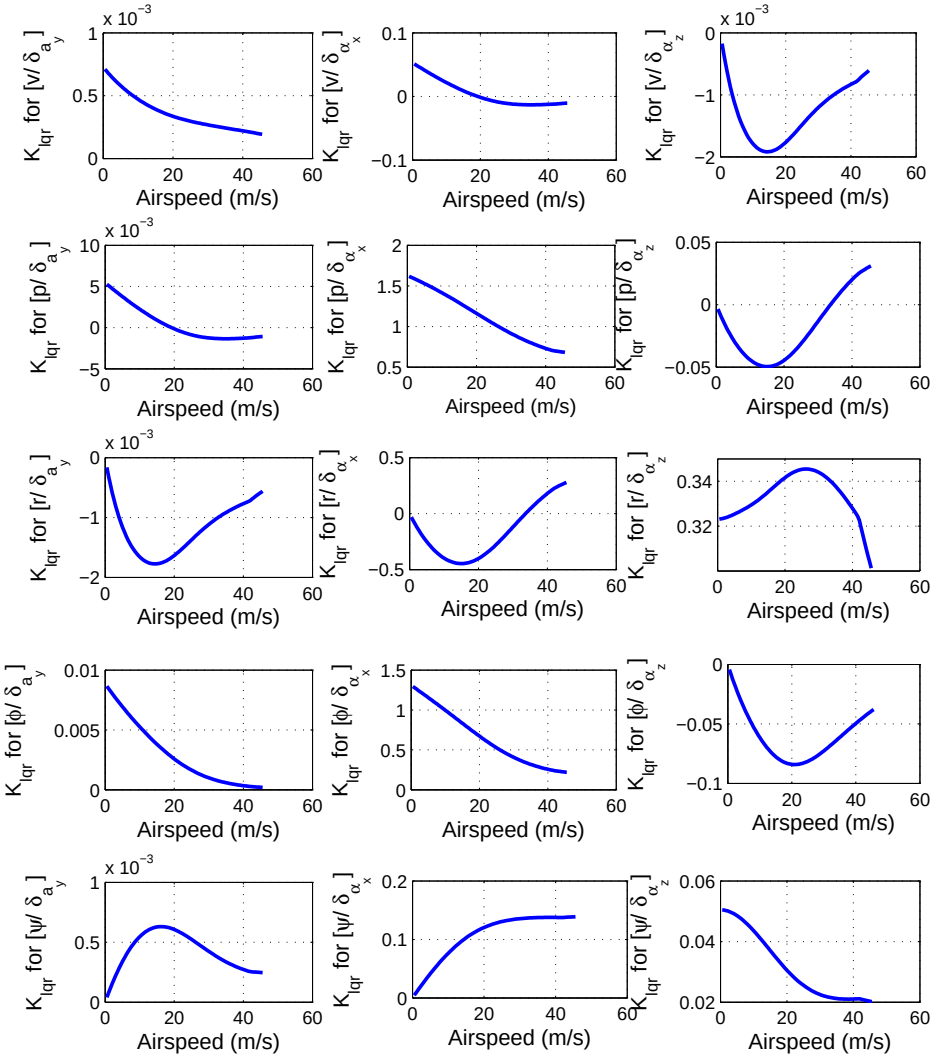

Figure F.6: LQR gains in lateral-directional for transition scenario 2 from 0 to 90 m/s airspeed at 305 m altitude